University of Nottingham
UK | CHINA | MALAYSIA

Molecular Dynamics Simulation of NASH and its Composites

Xiwen GUAN

Thesis submitted to

the University of Nottingham for

the degree of Doctor of Philosophy

13th December 2022

Content

Acknowledgements

Firstly, I would like to express my sincere appreciation and deepest gratitude to my supervisors, Dr Hainam Do and Dr Bo Li, for their kind support. For my research, they have provided patient guidance and significant advice from different perspectives of computational chemistry and civil engineering materials. It helps me to enter a new research field and complete my PhD study successfully. Their brilliant ideas always inspire me. It is a great pleasure to work with you both. The same goes for my co-supervisor, Dr Alvaro Garcia Hernandez. Besides, I would also thank my examiners, Dr Dongshuai Hou and Dr Yong Sun, who have paid efforts to review my work and provided valuable comments on my research.

Secondly, I would also like to thank my co-workers and friends, Dr Ding Fan, Dr Ling Jiang, Jia-Qi Wu and Wenjie Luo, who gave me valuable suggestions on my research work and theoretical study; their experience also helped me to overcome significant technical difficulties. It has been a great pleasure working with them for the past three years. I wish to thank all my colleagues and friends at the lab and office, including Zhixuan Li, Hanwen Chen, Allen Rosette ASABA, Weixin Zhang, Zhanhui Lu, Zongxuan Liu, Jie Jiang, Weiwei Chen, Xinyu Shen, Yuan Jiang, Xinyan Liu, Rui Huang, and Mingwei Feng.

I am grateful for access to the University of Nottingham High-Performance Computing Facility in Ningbo China. I thank the Faculty of Science and Engineering at University of Nottingham Ningbo China for a PhD scholarship.

Finally and significantly, I would like to give my love and appreciation to my family, my parents, my wife and my son. Their endless love always supports and encourages me. Life just won’t be the same without you.

List of Publications

The following peer-reviewed journal articles have been published or are in preparation to be published as a result of the work undertaken as part of this thesis:

1. **Guan, X.**, Jiang, L., Fan, D., Hernandez, A. G., Li, B.* & Do, H.* (2022). "Molecular simulations of the structure-property relationships of NASH gels." *Construction and Building Materials*, 329, 127166.

2. **Guan, X.**, Wu, J.-Q., Hernandez, A. G., Li, B.* & Do, H.* (2022). "Molecular dynamic simulations of interfacial interaction mechanism between the NASH gels and the polyethene fibre." *Construction and Building Materials*, 349, 128769.

3. **Guan, X.**, Xu, M., Li, B.* & Do, H.* (2023). "Molecular dynamic study of interaction between amorphous silica and sodium alumino-silicate hydrate gels." *The Journal of Physical Chemistry C*, Under review.

The following peer-reviewed journal articles have been published or are in preparation to be published, but not as part of this thesis:

4. Luo, W., Liu, S., Jiang, Y., **Guan, X.**, Hu, Y., Hu, D. & Li, B.* (2021). "Utilisation of dewatered extracted soil in concrete blocks produced with Portland cement or alkali-activated slag: Engineering properties and sustainability." *Case Studies in Construction Materials*, 15, e00760.

5. Lu, J, Ali, H. A., Jiang, Y., **Guan, X.**, Shen, P., Chen, P. & Poon, C. S.* (2022). "A novel high-performance lightweight concrete prepared with glass-UHPC and lightweight microspheres: Towards energy conservation in buildings." *Composites Part B: Engineering*, 247, 110295.

6. **Guan, X.**, Luo, W., Liu, S.*, Hernandez, A. G., Li, B. & Do, H. (2023). "Ultra-high early strength fly ash-based geopolymer paste cured by microwave radiation." *Developments in the Built Environment*, Under review.

List of Figures

List of Tables

List of Abbreviations

ASH	alumino-silicate-hydrate
BO	bond order
CNT	carbon nanotube
ECC	engineered cementitious composite
EEM	electron equilibration method
EFF	empirical force field
FA	fly ash
FRGC	fibre-reinforced geopolymer composite
FTIR	Fourier transform infrared spectroscopy
GCMC	grand canonical Monte Carlo
GGBS	ground granulated blast-furnace slag
GO	graphene oxide
ITZ	interfacial transition zone
LAMMPS	large-scale atomic/molecular massively parallel simulator
MD	molecular dynamics
MK	metakaolin
MSD	mean square displacement
NAS	sodium-alumino-silicate
NASH	sodium-aluminate-silicate-hydrate
NMR	nuclear magnetic resonance
NPT	isothermal-isobaric ensemble
NVE	micro-canonical ensemble

NVT	canonical ensemble
OPC	ordinary Portland cement
PAA	polyacrylic acid
PE	polyethene
PEG	polyethene glycol
PP	polypropylene
PVA	polyvinyl alcohol
QC	quantum chemical
RDF	radial distribution function
RHA	rice husk ash
SEM	scanning electron microscopy
UTS	uniaxial tensile strength
vdW	van der Waal
XRD	X-ray diffraction

Abstract

Geopolymer, as an environmentally friendly substitute material for ordinary Portland cement (OPC), possesses attractive engineering properties. In the past decades, efforts have been devoted to improving geopolymer's sustainability and performances, investigating the reaction mechanism, and exploring its practical applications. However, due to its complicated amorphous constituents, the understanding of geopolymer gel structure is still insufficient. A comprehensive understanding of it at the molecular level is needed to provide insights into the nature of geopolymerisation reaction and further suggestions for material design. Thus, this thesis utilizes molecular dynamics (MD) simulation to investigate the sodium-alumino-silicate-hydrate (NASH) gel and its composites from a theoretical and computational point of view.

First of all, the geopolymerisation reaction has been mimicked based on a realistic bottom-up modelling method. By employing seven types of experimentally characterized oligomers, the reactive MD simulation reveals the poly-condensation reaction and the formation of 3D cross-linked network structure of NASH gels. The effects of Si/Al ratio and oligomers' configuration in the system on the reaction degree, structure complexity, skeleton bond angle distribution, and water mobility are evaluated. In the MD simulation, the skeleton chains breakage and hydrolysis reaction during the uniaxial tensile test are observed. More broken Al-O than Si-O bonds are found, indicating a weaker Al-O bond strength. Apart from the structure-property relationship, the interactions between NASH gels and other inorganic or organic materials are investigated based on the developed NASH gel models.

Nano-silica modification has been an effective approach to improve the mechanical property and durability of geopolymers. This thesis provides an insight into the interaction between amorphous nano-silica and NASH gel

at the atomic level by MD simulation. Geopolymerisation reaction between these two parts in the composite is observed from the density distribution function and RDF results, with an interfacial transition zone (ITZ) of an average thickness of ~10 Å. Adding amorphous silica increases the reaction degree, bridge oxygen percentage, and enhances the stability of NASH gel. Mechanical strengths in various phases are found in the order of ITZ > NASH-s > neat NASH gel. The tensile strength of NASH gels is consequently improved by 10~40%, particularly for those with low Si/Al ratios. In addition, the enhancement of NASH gels by nano-silica is confirmed at the molecular level.

Moreover, NASH/polyethene (PE) composite models have been built with the developed NASH gel models to simulate the interface between NASH gel and PE fibre. It reveals the fibre-reinforced mechanism in the matrix at the molecular level. Based on the structure analysis, energy and dynamics characterization, and pull-out simulation, the adhesion mechanism and bonding performances have been explored. The adhesive bonding between NASH gel and PE mainly depends on the interfacial interaction (i.e. atomic pair interaction and the van der Waals force (vdW)) and mechanical interlocking (i.e. derived from the surface roughness). The weak H-bond is found between PE and NASH, which provides the dominant Coulombic interaction. A larger Si/Al ratio increases the bonding by mainly enhancing the vdW interaction energy. The optimum pull-out shear bonding strength of 0.43 GPa is achieved at a Si/Al ratio of 2.5. In addition, increasing the internal moisture in NASH gels increases adhesion properties, by providing more H-bonds at the interface. At the Si/Al ratio of 2.5, the bonding strength of a dry structure is calculated as only 70% of that of a full water one.

In conclusion, this thesis proposes a reliable reactive modelling approach for NASH gels. It also provides insights into structural information and the interaction mechanism of geopolymers and its composites at the microscopic level, which is crucial for further materials study and design.

Chapter 1

Introduction

1.1 Synopsis

This chapter begins with the background introduction to geopolymer which is an environmentally friendly substitution for ordinary Portland cement (OPC). It gives an overview of the green features of geopolymer, as well as its advantages compared to OPC, including the mechanical properties, durability, and thermal and chemical resistance. Afterwards, the chapter briefly introduces the reaction mechanism of geopolymerisation, followed by highlighting the challenges in developing geopolymers. The chapter ends by providing the aims and objectives as well as the outline of the thesis.

1.2 Geopolymer: A Green Cementitious Material

Geopolymer has attracted increasing interest in recent decades in its formulation optimization, performance improvement, reaction mechanism exploration, and microstructure characterization, etc. However, it is also facing some challenges and issues that must be tackled before it can be widely used in the construction industry.

1.2.1 Introduction of geopolymer

Concrete, whose production volume globally in 2020 was as high as 14.0 billion m^3, is the second most consumed material in the world, only after water (Monteiro et al. 2017). It is a composite material consisting of fine and coarse aggregates bonded by the binder that hardens over time. It is widely adopted for infrastructural construction, including reinforced concrete buildings, pavements, foundations, bridges, and sewage systems, etc. One of the key ingredients of concrete is the binder, which is often known as cement or OPC. Globally, the production of OPC was over 4.4 billion metric tons in 2021 and keeps increasing (Garside 2022). Thus, OPC is believed to be one of the most significant manufactured materials in the world. However, this results in a number of environmental issues. Most notably, due to the grinding and calcination processes, OPC production leads to around 8% of global greenhouse gas emissions (Lehne and Preston 2018). Given the effort to reduce CO_2 emissions alongside the ever-increasing demand for cement, cutting down greenhouse gas emissions from cement production becomes a significant challenge. Therefore, the decarbonization of cement production has attracted much attention and is becoming a more prominent issue for the traditional OPC industry. This is listed in several official reports, including the World Business Council for Sustainable Development International Agency (IEA) Cement Roadmap (2009), the Industrial Decarbonization & Energy Efficiency Roadmaps to 2050, and the British Cement Association (BCA73 Carbon Strategy 2005).

To reduce carbon emissions, alternative fuels have been proposed to replace fossil fuels in the OPC production. However, this cannot be a long-term solution due to the high demand for cement, the low efficiency, and the high cost of alternative fuels. The use of waste materials or industrial by-products to partially replace clinker used in cement systems has recently been introduced. These materials include incineration fly ash, husk ash, and other hazardous wastes (Kajaste and Hurme 2016). The cement produced with the incorporation of waste materials or by-products should possess comparable properties in comparison with OPC. However, it is still challenging to control the properties

of the alternative cement due to the variation of additional raw materials. Thus, the quest for a "greener" cement is still underway.

Amongst the emerging technologies, novel binders such as geopolymers or alkali-activated aluminosilicate cement have attracted much interest due to a much lower environmental carbon footprint than OPC. The term "geopolymer" was first raised by Joseph Davidovits (1991). This class of binders are inorganic solids synthesized from alkali silicate solution and aluminosilicate source powders, including industrial by-products (e.g. ground granulated blast-furnace slag (GGBS), fly ash (FA)), minerals clays (e.g. metakaolin (MK)), and agricultural waste (e.g. rice husk ash (RHA)). The reaction can happen spontaneously and result in a fast hardened material that exhibits exceptional hardness and mechanical strength. In this respect, geopolymers are similar to OPC (Nicholson et al. 2005).

As the geopolymer uses a large number of waste materials as the precursor and avoids the "two grinding and one burning" process in the OPC production, it emits approximately 44-64% fewer greenhouse gases (McLellan et al. 2011) and consumes up to 90% less energy than the OPC (Zhao et al. 2021). Moreover, compared to the OPC concrete, geopolymers exhibit various advantages, including high compressive strength (Khan et al. 2016), rapid controllable hardening time (Chindaprasirt et al. 2012), excellent fire resistance (Kong and Sanjayan 2010), high chemical resistance (e.g. acids and salts solutions) (Palomo et al. 1999), and low shrinkage (Duxson et al. 2006b). In addition, it can be used to immobilise and store hazardous heavy metal-containing and radioactive materials (Rasaki et al. 2019). Therefore, extensive studies have been conducted on the reaction mechanism and material performances of geopolymers in recent decades.

1.2.2 Geopolymerisation reaction

Geopolymer is synthesized from aluminosilicate powders and alkali solution. Specifically, the alkaline utilized is usually alkali silicate solution (e.g. sodium or potassium ion-based silicate solution) which is also called "water glass", and the aluminosilicate powders are fine reactive powders with a large number of

amorphous aluminosilicate phases. The geopolymerisation process can be divided into three stages: (1) dissolution of the solid aluminosilicate materials; (2) formation of the aluminosilicate oligomers by the dissolved reactive aluminate and silicate monomers; (3) condensation of the aluminosilicate oligomers to form the geopolymeric gel with 3D cross-linked networks structure (Duxson et al. 2006a; J.Davidovits 1989).

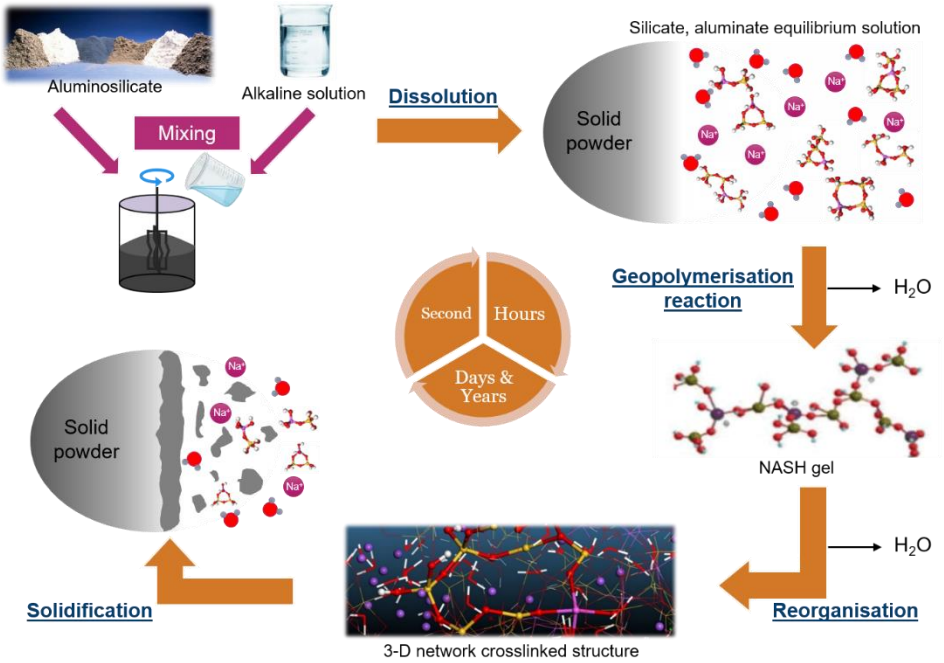

Figure 1.1 Diagram of the geopolymerisation reaction procedures

Taking the sodium-based geopolymer as an example, as shown in **Figure 1.1**, the aluminate and silicate monomers are dissolved from the solid precursors in a high-alkaline aqueous solution (e.g. sodium silicate and sodium hydroxide mixtures) in the first stage. The Si-O-Al and Si-O-Si bonds are broken at a high pH (Pacheco-Torgal 2015). As illustrated by Equation (1-1), the $\equiv Si-OH$ and $\equiv Si-O^-$ species are released into the solution as the result of ions attack to the Si-O-Si bonds. Negative charges of the $\equiv Si-O^-$ species are compensated by alkaline cations, as shown in Equation (1-2). The dissolution of amorphous aluminosilicates is rapid at a high pH solution. Besides, the Si-O-Al bonds in the solid precursor are broken in a similar way, as shown in Equations (1-3). The 5- and 6-coordinated Al in the solid precursor are mainly converted to the 4-coordinated Al during the dissolution process to form the $Al(OH)_4$ species.

$$\equiv Si - O - Si \equiv \; + \; OH^- \; \rightarrow \; \equiv \underset{\underset{OH^-}{|}}{Si} - O - Si \equiv \rightarrow \equiv Si - OH \; + \; \equiv Si - O^- \quad (1\text{-}1)$$

$$\equiv Si - O^- \xrightarrow{Na^+} \equiv Si - O - Na \quad (1\text{-}2)$$

$$\equiv Al - O - Si \equiv \; + \; OH^- \; \rightarrow \; \equiv \underset{\underset{OH^-}{|}}{Al} - O - Si \equiv \rightarrow \equiv Al - OH \; + \; \equiv Si - O^- \quad (1\text{-}3)$$

In the second stage, the concentrations of the released aluminium and silicon species in the solution increase as time elapses. The aluminosilicate oligomers would form when the silicon and aluminium species are in contact with each other (Dimas et al. 2009). Moreover, the poly-condensation reaction occurs between the aluminosilicate oligomers in the created supersaturated aluminosilicate solution. This results in the formation of a gel structure built with polymeric Si-O-Al bonds and simultaneously releases the water molecules. In addition, the alkali metal cations also take part in the reaction as a component to balance the negative charge of the aluminium tetrahedrons (Davidovits 1991).

In the last stage, the continuous gelation process forms an amorphous 3-D cross-linked network structure which is further rearranged and reorganized during the geopolymerisation reaction. The mechanical properties of the geopolymer material can be improved with the development of the network structure.

The above three stages exist almost simultaneously during the geopolymerisation process. The water molecules can form clusters and reside within pores in the gels. The final amorphous product is consistently named sodium-aluminate-silicate-hydrate (NASH) gel. Moreover, the geopolymerisation process and the NASH gel are affected by the various contents of the aluminosilicate source powders, the chemical composition of the alkaline solutions, and the synthesis conditions (Ahmed et al. 2022).

1.2.3 Development and challenges of geopolymers

Many studies have been conducted on the material's performances and the reaction mechanism of geopolymers in the past decades. Firstly, various aluminosilicate sources have been used as precursor for synthesizing geopolymer in a more environmentally friendly manner, particularly those by-

products and waste materials, e.g. GGBS, FA, red mud, RHA, etc. Secondly, some studies focus on improving the fresh properties, mechanical performance, and durability of geopolymers by adjusting the receipt (i.e. the precursor combinations and alkaline solution concentrations), the curing regime, and the functional additives. In addition, other studies concern the features and application scenarios of geopolymer concrete, e.g. performances of geopolymer concrete with various densities, compatibility of geopolymers with numerous kinds of fillers and aggregates, 3D printing geopolymer concrete, and developing chemical and fire resistance of geopolymers. Moreover, some studies investigate the microstructure of the gelation products by microscopic techniques. The microscopic features characterize the reaction degree, gel structure, moisture content, ions diffusion, and pore distribution, etc., which can be correlated to the mechanical properties (Amran et al. 2020; Ng et al. 2018).

However, as a relatively new developed material, there are still some critical challenges for geopolymer to be further widely employed in the construction industry. Firstly, numerous types of precursors and a lack of selection standards restrict the broad application of geopolymer as a green binder. It is essential to improve the characterization of raw materials that are appropriate for geopolymerisation (Majidi 2009). Secondly, there is a lack of knowledge on the long-term behaviours of geopolymers, which tends to be a potential risk for structural applications. It is time-consuming to conduct long-term durability tests on geopolymer. More importantly, geopolymer gel is an amorphous structure; due to the limited resolution of the individual sites in characterization, the understanding of geopolymer gel structure is insufficient (Duxson et al. 2006a). It is significant to reveal the microstructure, nanostructure, and even molecular structure of the geopolymerisation products, which can provide insights into the nature of geopolymerisation and further suggestions for material design.

Various characterization techniques have been utilized to observe the reaction product and analyse its structures at a micro-scale. However, the geopolymerisation mechanism cannot be fully revealed by the microstructural analysis (Xu et al. 2021a). Meanwhile, nano-modification has been made on

geopolymer to improve its mechanical properties and disabilities. Thus, the research of geopolymers at the molecular or atomic scale has attracted increasing attention, aiming to enhance the properties of geopolymers. Recently, several studies explored the molecular structure and behaviours of geopolymer gel by utilizing computational techniques to simulate the NASH gel structures. With the development of computing power and methodology, molecular dynamics (MD) simulations have become an indispensable tool for material modelling and can provide a possible way to understand geopolymer at an atomic level.

1.3 Aims and Objectives

In this thesis, MD simulation is utilized to investigate the NASH gel, which is the main reaction product of geopolymer materials at the nanoscale. It aims to provide a more comprehensive understanding of the molecular structure of NASH gel, give insights into the better material design of geopolymer and its composites, and further promote carbon emission reduction in the construction industry. The main objectives of this thesis include:

(1) Developing realistic models for NASH gels to characterise the structure and properties of geopolymers. These models are created by mimicking the geopolymerisation reaction. The compositions of the models are designed to be adjustable to represent the class of geopolymer materials.
(2) Structural-property relationship analysis. Based on the NASH gel models, structural-property relationships are explored to understand the mechanical performances of geopolymers at the atomic level. The effects of compositions of NASH gels on the mechanical performances can then be explained, which is valuable for the materials design on a macro-scale.
(3) Modelling of NASH gel composites. Apart from studying the atomic nature and properties of NASH gel, MD simulation can provide the interaction information of composite materials. This study also aims to build composite models of NASH gel by incorporating inorganic reactive amorphous silica

and organic nonreactive polyethene fibres. Moreover, the interaction and chemistry behaviours at the interface of the composites can be analysed.

(4) Interaction analysis between amorphous silica and NASH gel. For the silica-NASH composites, the reactive MD simulation is employed to investigate the interaction and influences of amorphous silica on the performance of NASH gels. Based on the composite model, the atomic structure, dynamic properties and mechanical performances at the interface are characterized. The interaction between the two phases can be illustrated, and the effect of amorphous silica on geopolymerisation reaction can be explored by comparing the original neat NASH gel with NASH gel generated on the silica substrate.

(5) Interfacial characterization between PE and NASH gel. Based on the developed NASH gel models, the PE molecular model is employed as an interlayer of the NASH gel structures to build the composite models. The atomic structures, energy calculation and mechanical pull-out behaviours at the interface between geopolymer and PE fibres can be explored at a molecular level to explain the bonding mechanism. In addition, the NASH gel compositions' effects on the bonding can also be explored.

Based on the MD simulation of NASH gels, it is expected that more comprehensive knowledge of geopolymers at the molecular level can be obtained, which will benefit to the understanding and design of geopolymers and their composites in engineering practices.

1.4 Outline of Thesis

This thesis is organized into the following seven chapters:

Chapter 1 briefly introduces the background and development of geopolymer materials. The reaction mechanism of geopolymerisation, enhancement strategy for geopolymer materials, and engineering application are also presented. Afterwards, the research gaps, objectives and significance of the proposed study are highlighted.

Chapter 2 reviews the existing studies of MD simulation of NASH gels regarding structural properties, dynamics, and mechanical behaviours. This chapter also reviews the development of CSH and NASH gel composite models, followed by the introduction of challenges and barriers in the MD simulation of NASH composite materials.

Chapter 3 describes the theoretical background and methodology utilized in this thesis. It starts with the concept of MD simulation, which involves the basic functions of molecular mechanics, ensembles, and the simulation algorithm in this study. It then specified the force fields employed for the simulation of NASH gels, e.g. ReaxFF, ClayFF and OPLS force fields. Afterwards, the modelling construction procedures and analysis approaches for trajectories and properties are illustrated and discussed.

Chapter 4 develops the molecular models for NASH gels based on aluminosilicate oligomers with different Si/Al ratios and configurations. By mimicking the geopolymerisation process, the model is compared and validified by experimental results. From the discussion of the structure-properties relationships, the microscopic structures, reaction process, and mechanical properties are studied. Moreover, the optimum Si/Al ratio has been explored.

Chapter 5 provides an insight into the interaction between amorphous nano-silica and NASH gel at the atomic level by MD simulation. It first introduces the existing experimental studies on nano-modified geopolymers, followed by the introduction of computational details. Afterwards, with various Si/Al ratios, the atomic structure, geopolymerisation reaction degree, dynamic properties and mechanical performances are compared to investigate the effect of amorphous silica in NASH gels. Moreover, the reaction between the two phases is observed in the interfacial transition zone (ITZ), and the tensile simulation reveals the strengthening mechanism of nano-silica to the geopolymer binder.

Chapter 6 employs the developed models to investigate the interfacial interaction mechanism between NASH gels and polyethene (PE) fibre. It starts with an overview of the fibre-reinforced geopolymer composite (FRGC) and the computational details in this chapter. Apart from the structure and energy

analysis of the interface, the dynamic pull-out simulation of PE from NASH gel substrate is simulated. Afterwards, the interfacial adhesion mechanism between PE fibre and NASH gels is revealed by calculating atomic and van der Waals (vdW) interactions. Moreover, the effects of mechanical interlocking and internal moisture content on the bonding behaviours are analysed.

Finally, Chapter 7 summarises the main findings based on the MD simulation of NASH gels and their composites. Afterwards, the major contributions of this thesis are highlighted, followed by potential developing extensions and future research interests.

Chapter 2

Literature Review

2.1 Synopsis

Numerical modelling of NASH gel has attracted increasing attention due to the popularity of geopolymer binders in recent years. Simulations can observe and predict the materials' behaviours at the molecular or atomic level, which can provide a deeper understanding of the materials and give insights into the material design at the macro-scale. In this chapter, the existing studies on MD simulation of geopolymers are reviewed. The modelling methods for geopolymers, structural properties, dynamics and mechanical behaviours of NASH gels, and the interaction mechanism in the composites are summarized. MD simulation has been recognized as a useful tool for investigating the properties of NASH gels at the nano-scale. Consequently, with reliable molecular models and an accurate force field, simulations of NASH gels can promote the develop of geopolymer materials.

2.2 Modelling of NASH Gels

The molecular structure of NASH gel comprises the amorphous aluminosilicate skeleton, water molecules, and free ions for charge balance. However, the current experimental characterization approaches can only provide an indirect

output of the atomic information based on spectroscopy, and there is a lack of studies on the nanostructure of NASH gel (Xu et al. 2021b). Recently, molecular dynamics simulation tools have been widely employed to investigate the structural characteristics and mechanical properties of such aluminosilicate gels.

2.2.1 Modification modelling method

The modification method is widely employed in MD simulations and is a relatively fast approach to construct models by changing the composition and types of atoms. It has also been adopted to generate NASH gel models for geopolymers based on structure similarity. For instance, Bagheri et al. (2018) assumed that the NASH gels present an approximate structure similar to CSH gels, which contain water in the form of interlayer or absorbed molecules. Thus, an alumino-silicate-hydrate (ASH) layered structure was employed in their study to investigate the water and ions transportation behaviours. In this method, a chemically similar zeolite structure is utilized to construct the layered structure with nanopores, followed by inserting water and ions to build the NASH model. However, this model has crystallinity in a few nanometres, which cannot accurately reflect the geopolymer's amorphous feature.

The NASH gel can also be created based on the existing sodium-alumino-silicate (NAS) glass models by inserting H_2O molecules. Different from zeolite, the NAS glass structure is an amorphous model. Starting from the configuration of silica glass, Sadat et al. (2016b) constructed the simulation cells, which contain almost 100% 4-coordinated Si atoms. The NASH gel models were created by randomly replacing partial Si with Al atoms. Simultaneously, Na ions were added to compensate for the negative charges. The molar percentages of SiO_2, Al_2O_3 and Na_2O can be varied to acquire systems with desired Si/Al ratios. A similar method was also adopted by Wang et al. (2020c). They partially changed the atom types to fit the structure to the composition of NASH gel based on the $Na_2Si_2O_5$ glass model. The geometry optimization processes were conducted to make the model reach the lowest energy state of the potential energy function and lead to a stable molecular structure for NASH gel. Compared to the models modified from zeolite structure, the models generated

from NAS glass are amorphous. However, the NAS skeleton is absolutely cross-linked and ultra-prefect as compared to the real geopolymer material.

2.2.2 Bottom-up modelling approach

Molecular models can be built from the basic elements. It is like building the simulation box with a large number of small blocks, which is also known as the bottom-up approach. Small building blocks (i.e. monomers) are combined to establish the amorphous structures.

For instance, the models can be constructed directly by randomly distributing atoms in the simulation boxes (Hou et al. 2020; Hou et al. 2018; Lyngdoh et al. 2019). The Si, Al, Na and O atoms in specific proportions are initially assigned at random positions to form the skeleton structure. Annealing and equilibrium processes are then conducted with MD simulation, with water molecules being introduced into the structure by employing the grand canonical Monte Carlo (GCMC) simulation. Another bottom-up method is to develop the model from small blocks of geopolymer oligomers. Bagheri et al. (2017) used 100 poly-sialate (i.e. $Al(OH)_3OSi(OH)_3$) molecules, 5% water molecules, and Na^+ ions to construct the NASH gel model. Sadat et al. (2016a; 2018a; 2018b) built the skeleton structure from three types of oligomers with Si/Al ratios of 1, 2 and 3, respectively. However, there are no hydrogen atoms in those oligomers and no reaction occurred between the oligomers. The water content in the system was finalized by adding a certain amount of H_2O molecules in the system.

Besides, Zhang et al. (2018b) used $Si(OH)_4$ and $NaAl(OH)_4$ molecules to develop NASH gel structure by simulating the reaction between these molecules. During the simulation, water molecules were formed when exterior hydroxyl radicals reacted, and the molecules polymerized in a typical reaction. It is more like to mimic the geopolymerisation reaction. In most of these works, the atomic structure of NASH gel is constructed using the traditional melt-quenching approach to obtain the amorphous structure. Besides, the water content and the Si/Al ratio are believed to have a substantial effect on the mechanical and thermophysical properties of geopolymer binders.

2.2.3 Modelling based on experimental results

Walkley et al. (2018) proposed a NASH gel molecular structure based on a geopolymer model obtained from the experimental characterization. They identified the geopolymer materials with 3Q-MAS solid state NMR spectroscopy. They stated that the NASH gel molecular structure predominantly comprised of Q^4(4Al), Q^4(3Al), Q^4(2Al) and Q^4(1Al) Si units in which Na ions is 6-coordinated, containing 3 or 4 bridge O and the remained are occupied by water molecules. A significant Al^{3+} is located in tetrahedral coordination, whereas the extra-framework Al species was also observed in the structure, coordinated by the bridge oxygens. All the bond angles and the molecular structure were provided, as shown in **Figure 2.1**.

Chitsaz and Tarighat (2020) employed this molecular model to conduct MD simulations. According to the optimum Si/Al ratio of 2, they slightly modified the molecular model and then computed the modulus of elasticity. Compared with the existing experimental results, they claimed that the calculated modulus is in good agreement with the test data, which can prove the feasibility of the proposed modified NASH gel model. However, this model uses only one molecule configuration to represent the NASH gel; the Si/Al ratio and water content are fixed by the composition. Thus, it cannot comprehensively show the diversity of the NASH gel structures and lack of flexibility when utilized as the model to investigate geopolymer materials.

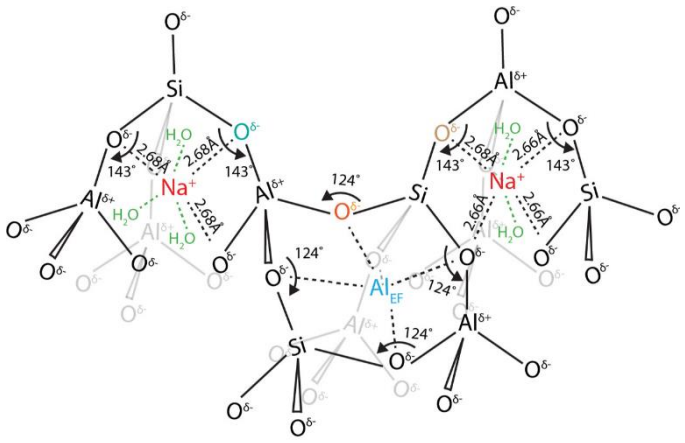

Figure 2.1 Schematic representation of the NASH gel showing charge-balancing Na, and charge-balancing Al (Walkley et al. 2018)

2.3 Recent Advances of MD Simulation of NASH Gel

Based on the various types of molecular models of NASH gel, researchers have explored and discussed many properties of such material. The valuable performance derived by MD simulation mainly includes microscopic analysis of the molecular structure, dynamics properties of the atoms and pairs, and mechanical performance of the nano-scaled simulation cells, etc.

2.3.1 Microscopic analysis of NASH gel

The microscopic analysis in MD simulations can provide basic information on the atomic structure of NASH gel at the nanoscale. The structure characterization can be reflected by the coordinates and interactions between atoms and pairs in the system. Understanding the atomic and molecular structures through MD simulation is fundamentally critical to the performance-oriented material design of geopolymer.

1) Radial distribution function

Radial distribution function (RDF) is extensively utilized to describe interatomic interactions. It can reflect the bond lengths distribution between various pairs. Xu et al. (2021b) summarized the simulation and RDF curves of geopolymer from various studies, as shown in **Figure 2.2**. The bond lengths can be obtained from the peaks' positions in the curves. The H-O, Si-O, Al-O, Na-O and O-O pairs can all be found in those curves. Sadat et al. (2016b) compared the normalized X-ray RDF simulation result to the experimental data to validate their molecular model. The matched peak positions revealed the reliability of the molecular structures. Moreover, the changes in bond lengths in RDF curves can also reveal structural variation and reflect the stability of NASH gels. Hou et al. (2018) conducted the RDF calculation of NASH gel at elevated temperatures from 300 K to 1500 K, and found the Si–O and Al–O bonds have been stretched and broken by high temperatures. Thus, the connectivity of the aluminosilicate network is gradually transformed into a branch and chain structure. On the other hand, RDF results can also reflect some other properties of the structure. Lolli et al. (2018) compared the RDF of NASH between

crystalline, defected crystalline and amorphous models. It is found that skeleton ring size is distinguished in various models and lead to the different capture ability of Na ions in the structures.

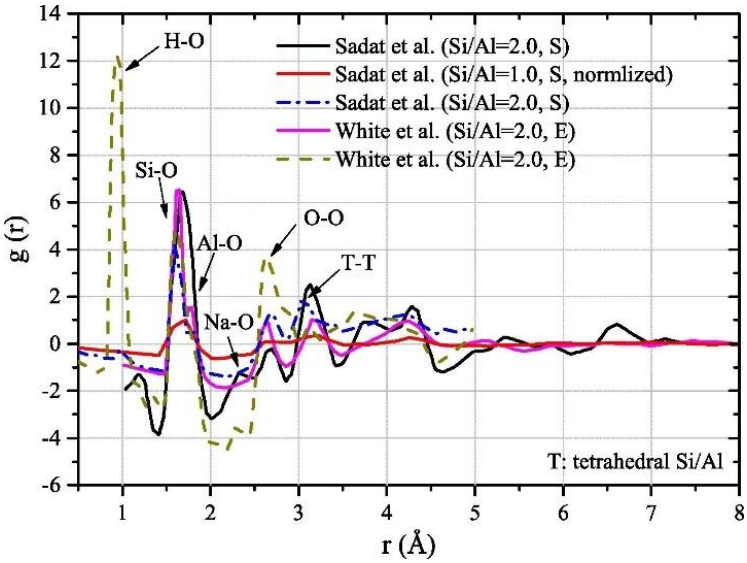

Figure 2.2 RDF curves of current MD simulations of geopolymers and experimental results (S: MD simulation, E: Experimental study) (Xu et al. 2021b)

2) Bond angle distribution

Apart from the bond length distribution, bond angles can also be observed by the MD simulation to illustrate the structural properties. In NASH gels, three bodies' angles distributions of O-Si-O, Si-O-Si, O-Al-O, and Si-O-Al are the main research objectives. They represent the structural information in the tetrahedrons (i.e. SiO_4 and AlO_4) or the connection between the tetrahedrons. Wang et al. (2020c) first compared their calculated bond angles to the experimental results and validated their models, and then compared the bond angles between NASH gel models with different SiO_2/Al_2O_3 ratios. It is found that the connection angle between the tetrahedrons becomes inhomogeneous when the SiO_2/Al_2O_3 ratio increases, but the angle in tetrahedrons still keeps unchanged. It can result in a decline in the stability of the entire structure. On the other hand, Lyngdoh et al. (2019) found that the angle distribution of Si-O-Si would be broadened when interlayered water was introduced into the system. It was explained as the Si-O-Si bond fully attached to water would be disordered.

3) Coordination number

The coordination number of an atom can reflect its chemical environment. The different bonded atoms and various coordination numbers show the distinguished types of the central atom in the system. The coordination number can be obtained based on the conception of RDF. Xiang et al. (2013) analysed the Q^n distribution (n bridging oxygen per network forming tetrahedron) in NASH models with a wide range of Al/Na ratios (i.e. from 1.5 to 0.6). They stated that Al atoms are mainly in 4-fold coordinated when Al/Na<1, while small amounts of 5-fold coordinated Al are present when Al/Na>1. Besides, 6-fold coordinated Al was also observed in the system, which is negligible. Moreover, Zhang et al. (2018b) compared the NASH gel simulation at 1,800 K and compared the Si_4(nAl) site distribution with experimental results. The results showed that when Si/Al ratio increased from 2 to 3, the percentage of Si_4(1Al) sites was highly increased, while that of Si_4(2Al), Si_4(3Al) and Si_4(4Al) dropped.

2.3.2 Dynamic study of NASH gel

In MD simulation, dynamics properties describe the change of molecular information during the simulation, generally in the period of the equilibrium stage. It means that even when the system gets to a stable status, atoms still move and some properties can be changed. The most important dynamics is the diffusion property, which is represented by the mean square displacement (MSD). It is utilized to describe the mobility of different atoms in the system.

1) Na ions

Hou et al. (2018) computed the Na ions diffusion values in NASH gel, and found that the ions first perform a ballistic motion and then are restricted by the skeleton "cage" for a long time, which prevents the ions from leaching out. Sadat et al. (2016a) also derived similar results and observed that the breakage of Al-O bonds under tension could influence the ions' mobility. With the decrease of Al tetrahedrons stability, Na ions in the system started to migrate faster through the network. Zhao et al. (2021) conducted the MSD of Na ions of

NAS glass at various temperatures from 300 to 4,000 K, and found that higher temperature significantly improves the diffusion rate, while the relationship between MSD and time is strongly nonlinear at relatively low temperatures.

2) Water molecules

Sadat et al. (2016a) computed the diffusion behaviours of water molecules, and found that the MSD of water in NASH gels is much lower than that of Na ions. It was explained as those water molecules were trapped within the nanovoids of the geopolymer structures. In the study of Zhang et al. (2018c), water at the surface and in the structure of NASH gel are both modelled. Results showed that the hydroxyl groups on the surface restricted the diffusion rate of interface water; and the water molecules confined inside the NASH gel just oscillate in the fixed position and hardly move.

3) Other ions

Some studies focused on external types of ions in the NASH gel to investigate their mobility and diffusion behaviours. Zhang et al. (2018c) modelled the sodium and magnesium sulphate solution layer on the surface of NASH gel, and found that compared to the Na ions, Mg ions penetrate more deeply and a larger number are bound to the NASH substrate stably. The SO_4 ions cannot penetrate the NASH gel, but are attracted by the surface-adsorbed cations. On the other hand, Hou et al. (2020) compared the diffusion rate of Na, K, Cs ions to investigate the nano-scale mechanism of ions immobilization. Results showed that the order of their mobility in NASH gel is $K^+ > Cs^+ > Na^+$. It could be due to the large ionic radius of Cs^+ limits its movement.

2.3.3 Mechanical properties of NASH gel

The mechanical properties of NASH gels are always derived from the uniaxial tensile simulation in MD simulation. Xu et al. (2021b) detailly described the behaviours of the simulation box under tensile loading. It is claimed that the Si-O-Al and Si-O-Si bonds are stretched and mainly bear the load until the yield stage, at which the bonds begin to break. The propagated cracks caused the drop of bearing stress and fracture at the final stage. Sadat et al. (2016b) examined

the mechanical properties of NASH gels with various Si/Al ratios, and concluded that there is an optimal Si/Al ratio (~2-3) that results in enhanced mechanical properties. Sadat et al. (2016a) also employed the MD simulation of NASH gels as a function of water content, and stated that increasing the water content decreased the stiffness and strength of the binder phase with a given Si/Al ratio. Hou et al. (2018) first observed the hydrolysis process that accompanied by the breakage of the aluminosilicate skeleton, which could further degrade the mechanical properties. It is also calculated that more Al-O bonds were broken than the Si-O bonds. Moreover, the strength and stiffness of NASH gel were greatly weakened by the elevated temperature, yet the ductility was significantly improved.

Nanoindentation is another widely used mechanical method that can also be employed in MD simulation. Sadat et al. (2018a) examined the mechanical properties of geopolymer binders with various Si/Al ratios under spherical nanoindentation. When changing the indenter sizes and loading rate, it was observed that the smaller indenter size and higher loading rate could increase the structural hardness. Besides, a higher Si/Al ratio leads to an increase in hardness and Young's modulus. It was due to the corresponding more Si-O bonds that can demonstrate higher intrinsic bond-strength than Al-O bonds.

Lyngdoh et al. (2020b) built the defected NASH gel models with pre-existing flaws in the simulation box, and computed the fracture toughness by employing uniaxial loading on the structures. They found that the simulation results are in line with experimental data. It was concluded that the crack propagation is facilitated by the evolution of Si–O and Al-O pairs, as well as the dissociation of confined water in the structure.

2.4 MD Simulation of Composites

In MD simulation, the interaction between the binder and other materials also attracts significant attention in addition to the properties of the binder materials. As stated in Chapter 1, cementitious composites can be mainly classified as organic and inorganic materials, or reactive and non-reactive additives.

However, the MD simulation of the interaction between NASH gel and other additives is relatively rare. There are limited studies focusing on NASH composites. Thus, in this chapter, MD simulation of CSH composites is also reviewed as the reference.

2.4.1 CSH composites

Polymer-cement is the most common composite in MD simulation studies, and understanding complex nano-composites would enable the effectively select, design and manufacture of polymers compatible with cementitious materials (Bahraq et al. 2022). Hou et al. (2019) utilized the CSHFF force field to investigate the interfacial structure, dynamics, energies and mechanical properties of CSH with different polymers, including polyethene glycol (PEG), polyvinyl alcohol (PVA), and polyacrylic acid (PAA). H-bonds were found at the interface to heal the defective silicate chains and prevent crack propagation. Zhou et al. (2017b) explained the different types of interactions at the polymer-cement interfaces in various composites by calculating the polarity of the function groups and the diffusivity tendency with ClayFF and CVFF force fields. Zhou et al. (2017a) simulated the CSH composites with the ReaxFF force field, and identified the strong bonding between PEG and CSH. The authors also explained that the breaking of C-O bonds in PEG by Ca ions from CSH phase can enhance the interfacial properties.

The interaction between CSH and polymer fibres has also been studied by MD simulation to optimize the properties of fibre reinforced cementitious composites. Zhou et al. (2019b) studied the structure-property relationship of PVA/CSH composites, and reported the existence of weak H-bonds between OH groups in PVA and non-bridging oxygen sites in CSH. Lu et al. (2021a) simulated the oxidation of the polyethene (PE) surface and the interaction with CSH. It was found that the tensile and strain capacities of the composites are significantly improved by 52%-128% after grafting 5%-10% of hydroxyl groups on the PE surface. The new formed chemical bonds can enhance the stability of the composites.

Graphene oxide (GO) is another popular functional material that has been used for the nano-modification of cementitious materials. Wang et al. (2020a) investigated the interfacial characteristics between GO and CSH by MD simulation. It was found that function groups of carboxyl and hydroxyl on the GO can contribute to enhancing the interfacial bonding, which ascribes to the stability of the chemical bond connection and surface roughness mechanical interlocking. Moreover, the interfacial water layer in the system could weaken the adhesion between GO and CSH phases.

2.4.2 NASH composites

Kai et al. (2020) built the CNT/NASH composites by placing one CNT at the centre of the NASH gel simulation box. With the ReaxFF force field, the C-O-Si bonds are constructed between CNT and the matrix. Apart from the energy and dynamics simulation at the interface, a pull-out simulation of CNT from the NASH gel part was simulated by applying a constant velocity of 0.001 Å/fs to the CNT. The results revealed that the interfacial bonding could provide a restriction to atoms in NASH gel and limit their diffusion, which enhances the matrix's stability. Moreover, increasing the interfacial bonding connection between CNT and NASH by 10% can improve the interfacial shear strength by 15 times, the Young's modulus by 60%, and the tensile strength by 80%. It has demonstrated that the connection between CNT and NASH can significantly impact mechanical properties.

Recently, Sekkal and Zaoui (2022) compared the NASH composites with pristine and functionalized CNTs, whose concentrations varied from 0 to 8.31 wt% and from 0 to 10 wt%, respectively. The uniaxial tensile simulation was also employed to investigate the mechanical properties of the CNT-NASH composites. It is found that the functionalized CNT in NASH gel could create covalent bonds through the C-OH interaction, which makes the structure denser and improves the mobility of CNTs into the matrix. In addition, the use of pristine CNT at an optimum dosage of 1.08 wt% can increase the elastic and indentation modulus by 74% and 94%, respectively. Moreover, the addition of 10% oxide CNT can enhance the elastic modulus and bulk density of NASH composites by 165% and 22.5%, respectively.

On the other hand, Zhang et al. (2021) investigated the adhesion mechanism of PVA fibre with alkali-activated slag/FA matrix by MD simulation. The Ca/(Si+Al) and Al/Si ratios were changed as the parameters in the simulation models. The calculated adsorption enthalpy revealed that the adhesion between PVA and alkali-activated slag/FA could be enhanced primarily by increasing the Ca/(Si+Al) ratio of the matrix. Additionally, the preference for Ca ions located around PVA molecules was observed both by simulation and experimental characterization. The authors concluded that the interaction is mainly contributed by electrostatic in the composite with a higher Ca ions content, while the adhesion is mainly from the hydrogen bond in the composite with lower Ca ions. The findings on the adhesion between PVA fibre and alkali-activated matrix can be a reference for studying the organic-inorganic interaction in NASH composites.

2.5 Summary

This chapter reviews the existing studies on MD simulation of NASH gels in geopolymer. The following conclusions can be drawn based on the above analysis and discussion.

(1) The NASH model can be built based on the modified ASH layered structure, bottom-up built amorphous gel, and experimentally characterized molecular configuration. The layered structure is crystalline at the nanoscale and is inconsistent with the amorphous nature of NASH gel. Although the experimentally characterized molecular structure is obtained from the real geopolymer material to some extent, it is only one representative section of the amorphous gel. Therefore, the bottom-up construction method is the commonly used approach to model the NASH gel, although the types of building elements are still obtained from some hypotheses. Thus, a more reliable and accurate molecular model for NASH gel is needed.
(2) MD simulations can provide detailed insights into the molecular structure information, including the pair distribution function, bond angle

distribution, and coordination numbers. Besides, dynamic properties of MSD can be computed to reveal the materials' stability. The variation of atom types, temperature, internal water, and additives has an impact on the mobility of the desired particles. Moreover, the mechanical properties of NASH gel can be derived from the uniaxial tensile simulation, including tensile strength, elastic modulus, and fracture toughness. It is a powerful and practical approach to investigate the effects of composition parameters (e.g. Si/Al ratios and water content) on the mechanical properties of NASH gels.

(3) The interaction mechanism between NASH gel and other materials attracts increasing attention in the MD simulation. At the atomic level, MD can provide a deep understanding of the complex structure and enable the effectively select and design of the compatible additives in composites. However, limited studies focus on the NASH composites only with CNT and PVA fibre. The covenant bonds and H-bonds were observed at the interface to provide connections between different materials, which can significantly impact the mechanical behaviours of the composites. More studies for various NASH gel composites are needed to optimize their properties as well as to reveal the interaction mechanisms.

Chapter 3

Methodology

3.1 Synopsis

The first step in a simulation is to set up a model system that can be abstracted from real systems with the knowledge available from experiments and previous theories. The central part is selecting a suitable simulation methodology and an accurate force field that best describes the systems of interest. This chapter outlines the simulation methodology and analysis techniques underpinning the work of the thesis. The chapter starts by introducing the concept of MD simulation, which comprises the basics of molecular mechanics, thermodynamic ensembles and simulation strategies. Then the specific force fields used to describe the potential functions of our materials are discussed, including reactive and non-reactive force fields. Afterwards, the general melt-annealing-equilibrium procedure used to generate amorphous structures is explained. Finally, trajectories and microscopic properties analysis techniques, including radial distribution function (RDF), mean square displacement (MSD) and uniaxial tensile simulation, are described. Other specific methods and techniques are discussed in the computation details subsection of each results chapter.

3.2 Molecular Dynamics Simulation

MD is a numerical computational approach that describes the physical motion of atoms in the system over a period of time. The motion is acquired based on classical mechanics at finite temperature and the interaction and energy between atoms are defined from the specific potential forms. The evolution of a single atom dynamic simulation can be used to explore thermodynamic properties of the total system, according to the statistical mechanics, averaging the trajectories, positions, and velocities of all atoms. Thus, MD simulation can act as a bridge to connect the microscopic properties and macroscopic performances, i.e. it can provide the hypothesis of the molecular interaction and predict the bulk properties.

Molecular mechanics uses traditional classical mechanics to model molecular systems. It is used to describe the inter- and intra-molecular motions with the classical equations according to Newton's second law. A function for a simple atomic system with N atoms can be written as:

$$\boldsymbol{F}_i = m_i \ddot{\boldsymbol{r}}_i = m_i \frac{\mathrm{d}^2 \boldsymbol{r}_i}{\mathrm{d}t^2} \tag{3-1}$$

where $\boldsymbol{F}_i$ is the force acting on atom i, m_i is the mass of atom i, $\boldsymbol{r}_i$ is the position of atom i and t is the time. Here, i = (1, 2, …, N) represents all the atoms in the system. To propagate the dynamics, the force acting on each atom needs to be calculated. The force on atom i is usually derived from the potential energy as:

$$\boldsymbol{F}_i = -\frac{\partial U}{\partial \boldsymbol{r}_i} \tag{3-2}$$

where U or to be exact $U(r^N)$ is the potential energy of the system that consists of N atoms. Ideally, the potential energy should be computed from first principle quantum chemical calculations. However, this is prohibitively expensive; therefore, the specific potential forms (force fields) are often employed to approximate the potential energy surface in MD simulation.

3.2.1 Ensembles

An MD simulation generates the phase space trajectory as a function of time. A thermodynamic ensemble can be defined as the phase space trajectory of the points satisfying the conditions of a particular thermodynamic state. There are generally three types of ensembles applied in MD:

Micro-canonical ensemble (NVE): is an isothermal system with a constant number of molecules (N), volume (V) and total energy (E). There is no molecular and energy exchange with the surroundings, but the temperature and pressure change with the conversion between the potential and kinetic energy of the particles in the system.

Canonical ensemble (NVT): In the system, the number of molecules (N), volume (V) and temperature (T) are all constant, and the system is surrounded by a fictitious infinite heat reservoir at temperature T. The walls surrounding the system are impermeable to molecules but have perfect thermal conductivity to ensure thermal equilibrium at any time. Thus, the total energy of the canonical ensemble system is an inconstant value.

Isothermal-isobaric ensemble (NPT): In this ensemble, the number of particles (N) is fixed. The pressure (P) is kept constant by exchanging compression work with the surroundings (i.e. the volume (V) is adjusted to keep the pressure constant). The system is also surrounded by a fictitious infinite heat reservoir at temperature (T) to keep the temperature constant. The NPT ensemble can mimic experimental conditions carried out at the macroscopic scale. Thus, this ensemble is the most employed in computational chemistry, especially during the equilibrium stage.

3.2.2 Simulation procedure

To start an MD simulation, an initial configuration of the system, at t=0, should be decided. The initial configuration of the system must be selected very carefully, particularly for the amorphous structures. It can influence the quality and equilibration time of the simulation. Choosing a configuration close to the state targeting in the simulation is suggested. The structure information is

usually obtained from experimental characterization, such as NMR and XRD results.

Next, the initial velocity is assigned to each atom. According to the classical mechanical law of motion, the forces of each atom in the system are integrated in time to propagate the trajectories. The most common integrator is the Verlet algorithm (Verlet 1967), which conserves the total energy of the system. During the integration, a time step shorter than the faster movements in the molecular system should be used to avoid instability. For various potential forms, the different frequencies of time steps may be used.

A thermostat and barostat are applied to the system to reproduce desired thermodynamic ensembles. In our work, the Nose-Hoover thermostat and barostat are employed to maintain the temperature and pressure of the system. The thermostatting and barostatting are achieved by adding dynamic variables to the system. For thermostatting, the variables are added to the particle velocities, and for barostatting, the variables are added to domain dimensions. Thus, the time-averaged temperature and stress tensor of the particles will match the desired values. The equations of motion used are from the work by Shinoda et al. (2004), and the time integration schemes refer to the time-reversible measure-preserving Verlet and RESPA integrators derived by Tuckerman et al. (2006).

During the heating process, a new velocity is assigned to the system to obtain a slightly higher temperature than the original one. This is repeated until the desired temperature is reached. Once this is achieved, the simulation continues until the thermodynamic properties become stable with respect to time (i.e. the system has equilibrated). Afterwards, the production stage is carried out to calculate the thermophysical and dynamical properties of the system.

3.3 Force Fields

The force fields (also known as potential forms) for describing the inter- and intra-molecular interactions are usually selected based on the material features

and types. Generally, it can be divided into two categories: non-reactive and reactive force fields. Despite the inability to simulate bond formation and breakage, non-reactive force fields can achieve molecular movements, structural properties and potential energy surfaces. The currently utilized non-reactive force fields for geopolymer can be further divided into general force fields, e.g. universal force field, COMPASS and Buckingham potential, and specific force field, e.g. ClayFF. For reactive force field, ReaxFF is the most popular one that is commonly employed for inorganic materials. In this study, ClayFF and ReaxFF force fields are the primary potential forms employed in this thesis. In general, a force field should incorporate three parts: atomic types, potential functions, and force field parameters. The exact parameters of the functions are fitted to either the *ab initio* quantum chemical calculations or experimental results. The following subsections briefly review the potential functions for ClayFF and ReaxFF force fields.

3.3.1 ClayFF force field

The ClayFF force field was developed mainly to simulate hydrated and multicomponent mineral systems and their interfaces with aqueous solutions (Cygan et al. 2004). It is based on the ionic-covalent interaction description of the hydrated metal-oxide structures. The ClayFF force field treats most of the interatomic interactions, except for that in water molecules, as non-bonded, which allows its compatibility in a variety of phases and adequately accounts for energy and momentum transfer between the fluid and solid phase. Thus, it can minimize the number of interaction parameters and allow the modelling of relatively large and is suitable for highly disordered systems. The ClayFF force field has been successfully used to model the oxide and hydroxide materials, interactions of aqueous species with oxide and hydroxide surfaces, and the behaviour of water and ionic species in the layered-structures phase (Botan et al. 2013; Cygan et al. 2021). The previous study of structural analysis, ions immobilization and surface adsorption of the alumino-silicate structures has confirmed that ClayFF force field is suitable for the NASH gel system simulation (Hou et al. 2020; Zhang et al. 2018c). It should be noted that, currently, ClayFF is the only specific force field that used for NASH gel

simulation, even though it is not initially parameterised for the geopolymer materials.

The total energy in molecular simulations is evaluated by adding the interaction energies of each atom pair in the system. Generally, the total energy is contributed from the electrostatic interactions (Coulombic energy), the van der Waals term (also referred to as the short-range interactions), and the bonded interactions (including bond stretching and angle bending):

$$E_{\text{total}} = E_{\text{coul}} + E_{\text{vdW}} + E_{\text{bond}} + E_{\text{angle}} \tag{3-3}$$

The coulombic energy is represented by the following form:

$$E_{coul} = \sum_{i \neq j} \frac{q_i q_j}{4\pi\varepsilon_0 r_{ij}} \tag{3-4}$$

where r_{ij} is the distance between atom i and j, q_i and q_j are partial charges centred on those atoms, ε_0 is the dielectric permittivity of vacuum (8.85419×10^{-12} F/m). The van der Waals energy term is often represented by the conventional Lennard-Jones (12-6) function:

$$E_{vdW} = \sum_{i \neq j} 4\varepsilon_{ij} \left[\left(\frac{\sigma_{ij}}{r_{ij}} \right)^{12} + \left(\frac{\sigma_{ij}}{r_{ij}} \right)^{6} \right] \tag{3-5}$$

where σ_{ij} and ε_{ij} are the van der Waals radius and well-depth parameters of the Lennard-Jones interaction potential, respectively. The combination of different ions interaction is obtained by the arithmetic mixing rule and geometric mean rule for the van der Waals radius and well-depth, respectively:

$$\sigma = \frac{1}{2}(\sigma_{ii} + \sigma_{jj}) \tag{3-6}$$

$$\varepsilon = \sqrt{\varepsilon_{ii}\varepsilon_{jj}} \tag{3-7}$$

To describe water and hydroxyl behaviour, the flexible simple point charge (SPC) based water model is used for ClayFF (Teleman et al. 1987). The covalent bonds between O–H can be represented by a functional form known as the simple harmonic term:

$$E_{bond} = K_b(r_{ij} - r_0)^2 \tag{3-8}$$

where K_b is the stretching force constant, r_0 refers to the equilibrium bond length. To improve the vibrational behaviour of the hydroxyl groups, the angle bend (three-body) term is included to describe the interaction. The X-O-H angel (X refers to H atom or other metallic atoms) energy is usually defined by the harmonic relationship:

$$E_{angle} = K_a(\theta_{ijk} - \theta_0)^2 \tag{3-9}$$

where K_a is a force constant, θ_{ijk} refers to the bond angle for the X-O-H, and θ_0 represents the equilibrium bond angle.

Details of all the parameters of the ClayFF force field for this study are listed in Appendix I.

3.3.2 Reactive force field

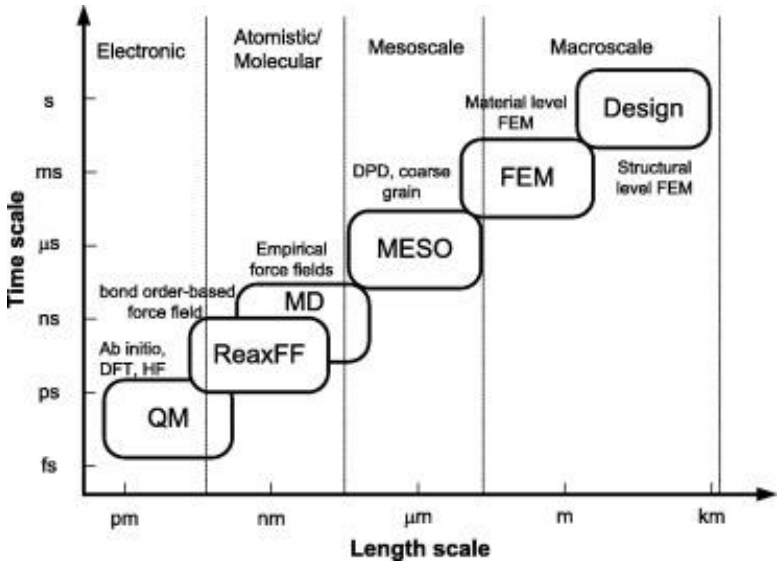

Figure 3.1 Application of ReaxFF in computational chemistry (Xu et al. 2021b)

ReaxFF is the most popular reactive force field currently used in inorganic nonmetal materials. Based on the bond-order and coordination number of all atoms, simultaneously adjusting the charges of various species dynamically, ReaxFF can simulate the bond forming and breakage during the simulation. The application scenario is illustrated in **Figure 3.1**, which indicates that ReaxFF can play a role in bridging the gap between quantum chemical (QC) and empirical force field (EFF). QC methods are generally applicable to all chemical systems, regardless of connectivity, but the computational intensity makes it

inappropriate for large systems, e.g. with more than 100 atoms. Non-reactive force field, on the other hand, is much more efficient that can simulate systems with millions of particles. However, due to its relative simplicity in describing the interaction between particles through potential functions, it cannot describe the reactive systems, even though it has been very successful in describing the physical characteristics. Therefore, ReaxFF has been developed on the foundation of EFF (Van Duin et al. 2001). Based on the EFF method, the bond order/bond energy relation has been calculated from interatomic distances and updated at every simulation step to allow the change of pairs' connectivity. It means there is no fixed connectivity assignment for the chemical bonds, instead by the bond order (BO). Thus, at bond breakage, the energies and forces associated will go to zero upon dissociation. Moreover, the non-bonded short-range interactions in the system are circumvented by the shielding term in the vdW and Coulombic interaction.

ReaxFF aims to provide a transferable potential applied to a wide range of chemical environments. The general guidelines and restrictions include: 1) No discontinuities in energy or forces, even during reactions; 2) Each element is described by just one force field atom type, e.g. the metal oxide oxygen is described by the same parameters as the oxygen in organic molecules; 3) No pre-definition of reactive sites is necessary, i.e. given the right temperature and chemical environment reactions will happen automatically. ReaxFF has been widely utilized in cementitious materials in recent years. Previous studies on water dissociation in CSH gels (Fan and Yang 2018; Zhou et al. 2017a), guest ions ultra-confined in CSH (Zhang et al. 2018a), and silica-water interfaces (Fan et al. 2017) showed that ReaxFF could accurately describe the structure, reactivity and mechanical properties of such inorganic gel system.

Similar to that of non-reactive force fields, ReaxFF also divides the total energy into several partial components as given below:

$$E_{total} = E_{bond} + E_{lp} + E_{over} + E_{under} + E_{val} + E_{pen} + E_{tor} + E_{conj} + E_{vdW} + E_{coul} \quad (3\text{-}10)$$

where E_{bond} is the bond energy; E_{lp} represents the lone pair energy; E_{over} is the penalty energies preventing the atom over-coordination and E_{under} accounts for

the π-electron between under-coordinated atoms; E_{val} and E_{tor} are the energies correlated with three-body valence angle strain and four-body torsional angle strain, respectively; E_{pen} is an additional energy penalty for an atom with two double bonds; E_{conj} describes the conjugated effect; E_{vdW} and E_{coul}, are van der Waals and Coulomb contributions calculated between all the atom pairs regardless of connectivity, and includes a shielding parameter to avoid excessive repulsion at short distances. The equations for the above parts are list as bellow:

Based on the BO, the bond energy is calculated directly from the interatomic distances, $r_{ij.}$ The BO of σ bond, π bond and ππ bond are described by the following functions:

$$\begin{aligned} BO'_{ij} &= BO'^{\sigma}_{ij} + BO'^{\pi}_{ij} + BO'^{\pi\pi}_{ij} \\ &= exp\left[p_{bo,1}\left(\frac{r_{ij}}{r_0^{\sigma}}\right)^{p_{bo,2}}\right] + exp\left[p_{bo,3}\left(\frac{r_{ij}}{r_0^{\pi}}\right)^{p_{bo,4}}\right] \\ &\quad + exp\left[p_{bo,5}\left(\frac{r_{ij}}{r_0^{\pi\pi}}\right)^{p_{bo,6}}\right] \end{aligned} \tag{3-11}$$

$$\begin{aligned} E_{bond} = &-D_e^{\sigma} BO_{ij}^{\sigma} exp\left[p_{be,1}\left(1-\left(BO_{ij}^{\sigma}\right)^{p_{be,2}}\right)\right] - D_e^{\pi} BO_{ij}^{\pi} \\ &- D_e^{\pi\pi} BO_{ij}^{\pi\pi} \end{aligned} \tag{3-12}$$

where p_{bo} terms and D_e are empirical parameters.

Afterward, the Δ_i' can be calculated from the BO, which is the degree of deviation of the sum of the uncorrected bond orders around an atomic centre from its valency, as following:

$$\Delta_i' = \sum_{j=1}^{nbond} BO'_{ij} - Val_i \tag{3-13}$$

where Val_i is the valency of atom i (e.g. Val_i =4 for carbon and Val_i =1 for hydrogen atom).

Lone pairs on heteroatoms significantly affect the response of these atoms to over- and under-coordination. The presence of these lone electron pairs influences the valence angles around atoms. In addition, by delocalizing, they

can contribute to the stability of conjugated systems. The following equation describes the deviation of the number of lone pairs around an atom from the number of lone pairs at normal coordination.

$$E_{lp} = \frac{p_{lp} \cdot \Delta_{lp,1}}{1 + exp(-75\Delta_{lp,1})} \tag{3-14}$$

For an over-coordinated atom ($\Delta_i > 0$), which means the calculated BO exceeds the maximum reasonable BO, Equation (3-15) imposes an energy penalty on the system. The form of the below equation ensures that E_{over} will quickly vanish to zero for under-coordinated systems ($\Delta_i < 0$).

$$E_{over} = p_{over} \cdot \Delta_i \cdot \frac{1}{1 + exp(\Delta_i \cdot \lambda_6)} \tag{3-15}$$

For an under-coordinated atom ($\Delta_i < 0$), we want to take into account the energy contribution to the resonance of the π-electron between attached under-coordinated atomic centres. This is described in the equation:

$$E_{under} = -p_{under} \cdot \frac{1 - exp(\Delta_i \cdot \lambda_7)}{1 + exp(-\Delta_j \cdot \lambda_8)} \cdot f_6(BO_{ij,\pi} \cdot \Delta_j) \tag{3-16}$$

For bond terms, it is significant that the energy contribution from valence angle terms goes to zero as the bond orders in the valence angle go to zero. Equation (3-17) is employed to calculate the valence angle energy contribution.

$$\begin{aligned} E_{val} = {} & f_7(BO_{ij}) \cdot f_7(BO_{jk}) \cdot f_8(\Delta_j) \\ & \cdot \left\{ k_a - k_a exp\left[-k_b (\theta_o - \theta_{ijk})^2 \right] \right\} \end{aligned} \tag{3-17}$$

To reproduce the stability of systems with two double bonds sharing an atom in a valency angle, like allene, an additional energy penalty, as described in the equation, is imposed.

$$\begin{aligned} E_{pen} = {} & \lambda_{19} \cdot f_9 \cdot (\Delta_j) \cdot exp\left[-\lambda_{20} \cdot (BO_{ij} - 2)^2 \right] \\ & \cdot exp\left[-\lambda_{20} \cdot (BO_{jk} - 2)^2 \right] \end{aligned} \tag{3-18}$$

For angle terms, it is need to ensure that dependence of the energy of torsion angle ω_{ijkl} accounts properly for BO close to 0 and for BO greater than 1.

$$E_{tors} = f_{10}(BO_{ij}, BO_{jk}, BO_{kl}) \sin\Theta_{ijk} \cdot \sin\Theta_{jkl} \left[\frac{1}{2}V_2 \cdot exp\left\{p_l \left(BO_{jk} - 3 + f_{11}(\Delta_j \cdot \Delta_k)\right)^2\right\} \cdot (1 - \cos 2\omega_{ijkl}) + \frac{1}{2}V_3 \cdot (1 + \cos 3\omega_{ijkl})\right] \quad (3\text{-}19)$$

The equation describes the contribution of conjugation effects to the molecular energy.

$$E_{conj} = f_{12}(BO_{ij}, BO_{jk}, BO_{kl}) \cdot \lambda_{26} \cdot \left[1 + \left(\cos^2 \omega_{ijkl} - 1\right) \cdot \sin\theta_{ijk} \cdot \sin\theta_{jkl}\right] \quad (3\text{-}20)$$

To account for the van der Waals interactions, a distance-corrected Morse-potential is used, as described in Equation (3-21). By including a shielded interaction, excessively high repulsions between bonded atoms (1-2 interactions) and atoms sharing a valence angle (1-3 interactions) are avoided.

$$E_{vdWaals} = D_{ij} \left\{exp\left[\alpha_{ij} \cdot \left(1 - \frac{f_{13}(r_{ij})}{r_{vdw}}\right)\right] - 2 \cdot exp\left[\frac{1}{2}\alpha_{ij} \cdot \left(1 - \frac{f_{13}(r_{ij})}{r_{vdw}}\right)\right]\right\} \quad (3\text{-}21)$$

As with the van der Waals interactions, Coulomb interactions are taken into account between all atom pairs. To adjust for orbital overlap between atoms at close distances a shielded Coulomb potential is used.

$$E_{coulomb} = C \cdot \frac{q_i \cdot q_j}{\left[r_{ij}^3 + \left(\frac{1}{r_{ij}}\right)^3\right]^{1/3}} \quad (3\text{-}22)$$

Atomic charges are calculated using the Electron Equilibration Method (EEM). Further details of the functions is explained in the publication from van Duin et al. (2001).

Details of all the parameters of the ReaxFF force field used in this study can be found in Appendix I.

3.4 Generating Amorphous Structures

The amorphous structures, including amorphous NASH gels and amorphous silica materials, are all obtained from a melt-annealing-equilibrium procedure using the reactive force field. The initial structures of these materials are the configurations acquired from a combination of randomly located monomers (i.e. for amorphous NASH gel) or the repeated crystalline unit cells (i.e. for amorphous silica material).

The first step in the melt-annealing-equilibrium procedure is to heat the system to the desired temperature (in the NVT ensemble) higher than the melting point (several thousands of degrees K). During the melting process, the memory effect is removed and bonds are dissociated. The desired high temperature is kept for a few pico-seconds until the system reaches a stable stage. After that, the system is slowly cooled down to ambient temperature in the NVT ensemble. The cooling rate should be small enough for the probability distribution of the current state to be near thermodynamic equilibrium at all times. Besides, the specific cooling rate varies for different materials, which is around several K/ps. During the cooling process, new bonds are formed between atoms in the system and a new amorphous structure is developed. Subsequently, when the room temperature is reached, the system is subjected to an equilibrium run in the NPT ensemble (at 300 K and 0 Pa).

3.5 Trajectories and Properties Analysis

The structural and properties analysis is based on the positions and distances between those atomic pairs in the trajectories obtained in the production running process in MD simulation. It indicates that all the properties dynamically fluctuate at the equilibrium status. The RDF, MSD and uniaxial tensile simulation are commonly used to characterize the molecular structure, dynamics, and mechanical behaviours of the materials.

3.5.1 Radial distribution function

For characterizing the atomic structure, radial distribution function (RDF) is extensively utilized to describe interatomic interactions. It describes how the density of surrounding atoms varies as a function of the distance from the central atom. The physical meaning can be shown in **Figure 3.2**. In MD simulation, the RDF is calculated by counting the number of atoms between the given ranges of separation, which can be defined by the following equation:

$$g(r) = \frac{dN}{\rho 4\pi r^2 dr} \tag{3-23}$$

where *dN* refers to the average number of atoms within a given shell thickness of *dr*, ρ refers to the bulk density of the system and *g(r)* is the RDF. The unit of thickness (i.e. the variable *r* in the equation) in this study is angstrom (i.e. Å). Therefore, RDF shows the distance distribution of atom pairs, which indicates the bond lengths and give significant structural information and illustrate the spatial correlation of atoms. Moreover, the computed RDF can be compared with the experimentally determined X-ray pair distribution function to validate the molecular model, computational procedure and the appropriateness of parameters used in the simulation.

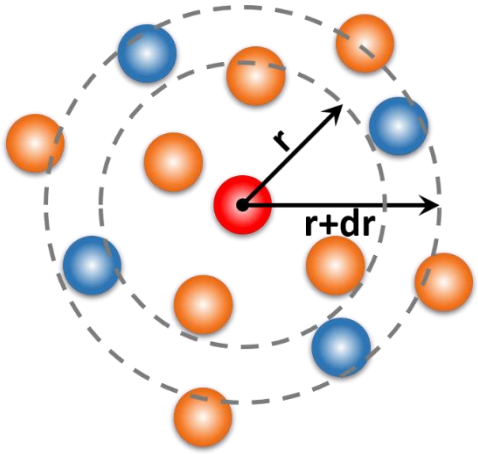

Figure 3.2 Schematic diagram of radial distribution function

3.5.2 Mean square displacement

The mean square displacement (MSD) characterizes the translational motion behaviours of various atoms in the MD simulation systems. It calculates the deviation of the position of a particle with respect to a reference initial position

over time during the simulation, which is the most common measure of the spatial extent of random position. It is computed from the following equation:

$$MSD(t) = \langle |r_i(t) - r_i(0)|^2 \rangle \quad (3\text{-}24)$$

where $r_i(t)$ represents the position of atom i at time t, and $r_i(0)$ refers to the original position. The time (i.e. the variable t in the equation) in this study is in the scale of femtosecond (i.e. fs). Most of the time, MSD takes into account the 3D-dimensional coordinates, which calculates the atom's mobility in the 3D spatial model in MD simulation. It reveals the atoms' diffusion during simulation time. A larger MSD value at time t indicates the atoms diffuse more rapidly and are displaced far away from the initial position. The diffusion coefficients (D) can be derived from the slope of the MSD curves, and be calculated from the following equation:

$$D = \frac{1}{2n} \lim_{t \to \infty} \frac{\langle |r_i(t) - r_i(0)|^2 \rangle}{t} \quad (3\text{-}25)$$

where n is the number of motion dimensions, e.g. n is 3 in the 3D spatial MD simulation. Consequently, D value is positive correlated to the MSD curve. The comparison of D values can reveal the mobility and diffusion rate between different types of atoms or the same type of atom in various systems. Thus, the structural stability and ions leaching issue can be reflected by the MSD calculation. To acquire the dynamic MSD curves, the displacement distance of the atoms should be recorded during a certain time period at the equilibrium stage of the simulation system.

3.5.3 Uniaxial tensile simulation

Uniaxial tensile simulation can be employed to investigate the mechanical properties and fracture behaviours of the materials on the nano-scale in the MD simulations. From the uniaxial tensile simulation, the stress-strain curve can be obtained from the calculation of displacement and the internal stress tensors. Thus, the failure mechanism can be explored. Besides, the fracture mode can be displayed by the trajectories of the atom in MD simulation. The stress tensor components are calculated by the following equation:

$$S_{ab} = -\left[mv_a v_b + \frac{1}{2}\sum_{n=1}^{N_p}(r_{1a}F_{1b} + r_{2a}F_{2b}) + \frac{1}{2}\sum_{n=1}^{N_b}(r_{1a}F_{1b} + r_{2a}F_{2b}) + \frac{1}{3}\sum_{n=1}^{N_a}(r_{1a}F_{1b} + r_{2a}F_{2b} + r_{3a}F_{3b}) + \frac{1}{4}\sum_{n=1}^{N_d}(r_{1a}F_{1b} + r_{2a}F_{2b} + r_{3a}F_{3b} + r_{4a}F_{4b}) + \frac{1}{4}\sum_{n=1}^{N_i}(r_{1a}F_{1b} + r_{2a}F_{2b} + r_{3a}F_{3b} + r_{4a}F_{4b})\right] \quad (3\text{-}26)$$

where the first term is a kinetic energy contribution for atom *i*; the second term is a pairwise energy contribution where *n* loops over the N_p neighbours of atom *i*, r_1 and r_2 are the positions of the two atoms in the pairwise interaction, and F_1 and F_2 are the forces on the two atoms resulting from the pairwise interaction. The third term is a bond contribution of similar form for the N_b bonds, for which atom *i* belong to. There are similar terms for the *N*a angle, N_d dihedral, and N_i improper interactions atom *i* is part of.

To obtain the results of the uniaxial tensile simulation, the super-cells or amorphous structures in scale with box edge lengths of at least several tens of nanometres are always used. It should be noted that using a large number of atoms can provide a stable statistic simulation result. But it also depends on the computational resources, as the larger molecular system consumes much more simulation time. The structure is subjected to a uniaxial tensile loading through gradual elongation with a constant strain rate. The employed strain rate is usually the constant engineering strain, which means the increment of box length in elapsed time is constant.

There are several means in MD simulation that can conduct the uniaxial tensile simulation. The first method is changing the dimension of the simulation box at a constant rate. The periodic box is stretched along the tensile direction. In the simulation process, NPT ensemble is defined for the system. The pressure in non-stretched directions is kept at zero to allow the normal direction to relax without any restriction. The pressure along the stretched directions is calculated as the stress. Thus, this method for tensile simulation can eliminate the constraint, consider the Poisson's ratio during deformation, and is suitable for the single-phase simulation system. Another method is providing a velocity to the boundary atoms in the box, whose movement can influence nearby atoms, to stretch the simulation cell. The total internal stress tensor along the stretched

direction is calculated as the stress result. The whole process is achieved by fixing the upper and bottom layers of the simulation box before stretching, the non-periodic and shrink boundary at the stretched direction are set, and NVT ensemble is employed during the simulation. This method is suitable for the fracture or pull-out simulation of the composite systems to investigate the interfacial properties, which can guarantee the unique interface in the simulation cell.

3.6 Concluding Remarks

In this chapter, the concept of MD simulation is first described by paraphrasing the functions. It involves the basic functions of molecular mechanics, ensembles and the simulation algorithm in this study. Afterwards, the force fields employed for the simulation of NASH gels are specified, e.g. the ReaxFF, ClayFF and OPLS force fields. Subsequently, the modelling construction procedures and analysis approaches for trajectories and properties are illustrated and discussed. In the following chapters, the above methods will be employed to build a reliable molecular model for NASH gel and further discuss the structural-properties relationships and investigate the interaction mechanisms of it with other organic or inorganic materials in the composites.

Chapter 4

Molecular Simulations of the Structure-Property Relationships of NASH Gels*

4.1 Synopsis

A good understanding of the relationship between the micro- and macroscopic properties of NASH gel is crucial for designing and developing geopolymer binders. This study develops molecular models for NASH gels based on aluminosilicate oligomers with different Si/Al ratios and configurations. Our models mimic the geopolymerisation process through a poly-condensation reaction between hydroxyls, generating water and forming the aluminosilicate network. The simulation results indicate that more than 50% of the hydroxyls in oligomers are reacted, reflecting the geopolymerisation degree. The oligomers with a higher Si/Al ratio and linear configuration exhibit a higher

* The work in this chapter was published in:

Guan, X., Jiang, L., Fan, D., Hernandez, A. G., Li, B.* & Do, H.* (2022). "Molecular simulations of the structure-property relationships of NASH gels." *Construction and Building Materials*, 329, 127166.

reaction degree, while those with cyclic configurations exhibit a higher complexity for network structure. Decreasing the Si/Al ratio narrows the bond angle distribution and reduces the skeleton stability of NASH gel structure. This also decreases the dynamic water mobility due to the higher restriction of hydrogen atoms. Chains' breakage and the associated hydrolysis reaction at their ends are observed with the consumption of almost 2.5% of the generated water molecules. Furthermore, the enhancement in tensile strength is mainly attributed to increased bridge oxygen numbers, especially for those in Si-O-Si bonds. The elastic modulus is mainly influenced by the amount of hydroxyl and network complexity. In addition, increasing the Si/Al ratio increases the number of Si-O-Si bonds and decreases the hydroxyls, enhancing the tensile strength and elastic modulus of NASH gels. NASH gels constructed with cyclic oligomers show around 20% higher tensile strength than those with linear oligomers. Thus, this study will provide valuable insights on the molecular structure understanding and design optimization of geopolymer materials.

4.2 Introduction

As stated in previous chapters, OPC is believed to be one of the most important manufactured materials globally. The production of OPC was estimated to be over four billion tonnes in 2015 and has been increasing ever since (Van Oss 2009). However, the cement industry is estimated to have contributed 5-7% of global anthropogenic CO_2 emissions (Turner and Collins 2013). Given the global effort to reduce CO_2 emission alongside the ever-increasing demand for cement, cutting down greenhouse gas emissions from cement manufacture presents a significant challenge. Therefore, the decarbonization of cement production has attracted much attention and is becoming a more prominent issue for the traditional OPC industry.

Amongst the emerging technologies, novel binders such as geopolymer have attracted much interest due to a much smaller environmental footprint than OPC. For this reason, geopolymer binders appeal to the construction industry, along with their excellent mechanical strength and thermal and acid resistance

(Pacheco-Torgal et al. 2012). The detailed reaction mechanism of geopolymerisation reaction has been introduced in Chapter 2. Thus, the macroscopic outcome of this reaction is analogous to the hydration of a traditional OPC paste.

Currently, the exploitation of geopolymer cement is still limited, mainly due to the lack of regulatory standards backed by long term testing and development (Duxson et al. 2006a). In addition, there are serious concerns about the inability to predict and control the durability of geopolymers (Lolli et al. 2018). Furthermore, due to the complicated and amorphous nature of geopolymer, the atomic structure information remains scarce despite extensive research in the last three decades (Lolli et al. 2018; Provis et al. 2005). Thus, this urges a better understanding of the linkage between microscopic structures and macroscopic properties (Provis et al. 2005). Significant works have been dedicated to understanding the local structure and formation of geopolymer gels utilizing various materials characterization techniques, including X-ray diffraction (XRD) and scanning electron microscopy (SEM) (Lyu et al. 2013; Williams et al. 2011). However, none of these techniques can quantitatively define the geopolymers' chemical or molecular structures. Fourier transform infrared spectroscopy (FTIR) has been used to identify the formation of primary chemical bonds, such as Si−O−T (T: Si or Al), Si−OH, and Al−OH, in geopolymer precursors, but the network and interconnectivity of these bonds remain a mystery (Rees et al. 2007a; Rees et al. 2007b). Other methods such as nuclear magnetic resonance (NMR) spectroscopy can be used to assess the coordination of Si and Al sites and investigate the change in chemical structures during geopolymerisation, but some of the sites are difficult to distinguish (Criado et al. 2008; Duxson et al. 2005). In addition, X-ray/neutron pair distribution function analysis has recently been used as a complementary tool to FTIR and NMR spectroscopies for examining the molecular structure of geopolymers (White et al. 2013a; White et al. 2013b; White et al. 2011). Despite all these efforts, a conclusive molecular structure of geopolymer gels remains elusive, primarily due to their amorphous nature.

Recently, MD simulations have been employed to gain a detailed, comprehensive insight into the local structural characteristics and the mechanical properties of such aluminosilicate gels. As introduced in previous chapters, the first modelling method is the modification from exist models, e.g. zeolite or NAS skeleton. But those structures cannot accurately display the amorphous NASH gel structures: some are crystalline at nano-scale, some are ultra-perfect at the skeleton structure. The other is the bottom-up approach which generate NASH gel from basic building elements. In most of these works, the atomic structure of NASH gels is constructed using the traditional melt-quenching approach to obtain the amorphous structure. Besides, the water content and the Si/Al ratio are believed to have a substantial effect on the mechanical and thermophysical properties of geopolymer binders. Knowing the combination of water distributions and Si/Al ratio is crucial for designing and controlling the macroscopic properties of geopolymer binders. However, the information regarding this is still scarce in the literature.

This study aims to develop molecular models to investigate the relationship between the micro-and macroscopic properties of NASH gel using MD simulations. The NASH gel models are created by quenching various oligomers with different Si/Al ratios and configurations to mimic the geopolymerisation process. The microscopic properties of the developed models, including bulk density, bond-angle distribution, radial distribution functions, molecular structure variations, and dynamic mean square displacement, are computed for comparison. Furthermore, uniaxial tensile deformation of the NASH gels is also simulated to obtain the mechanical properties and illustrate the structure-properties relationships.

4.3 Computational Details

4.3.1 Model construction

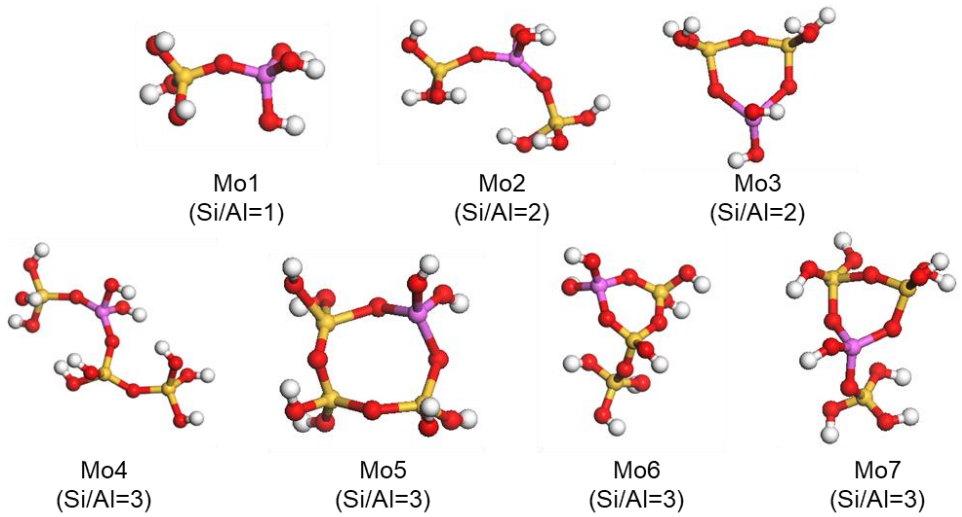

Figure 4.1 Seven different types of building blocks (oligomers) for NASH gel model: yellow is silicon, pink is aluminium, red is oxygen, purple is sodium, and white is hydrogen.

Geopolymerisation is the process of gelation and reorganization of many small molecules (oligomers), which in this case are aluminates and silicates dissolved from aluminosilicate sources (Duxson et al. 2006a). Furthermore, those molecules are dehydrated and polymerized to form the cross-linked three-dimensional network structure. Nuclear magnetic resonance (NMR) spectroscopy indicates the existence of the 4-coordinated configurations of Si and Al, with the evidence of Si and Al tetrahedron species (Davidovits 1994). Besides, Al-27 NMR results and Loewenstein's principle both suggest the absence of two linked Al tetrahedrons (Lolli et al. 2018). Thus, the linear aluminosilicate species with Si/Al from 1 to 3 (Mo1, Mo2 and Mo4 in **Figure 4.1**) were proposed. Swaddle et al. (Kinrade and Swaddle 1989; North and Swaddle 2000) also used NMR spectroscopy to prove the existence of soluble, isolated aluminosilicate molecules with various configurations in alkali solution with relatively high concentrations and pH value, which includes Mo3, Mo5 and Mo7 in **Figure 4.1**. Therefore, this study uses a bottom-up approach to mimic the geopolymerisation reaction from the various aluminosilicate oligomers. Seven oligomers are used (**Figure 4.1**), with different configurations and Si/Al ratios. Initial amorphous structures have been made from the single

type of above oligomers, and seven cubic systems are obtained with almost 40,000 atoms and an initial density of 2.0 g/cm^3. The sodium ions with the same number as aluminium atoms are added to compensate for the negative charge of Al tetrahedrons. Afterwards, the structures are subjected to the MD simulation. The modelling method is based on its amorphous nature and the existence of various types of oligomers in geopolymer. Different from existing methods, this modelling job starts from the hydrated oligomers instead of dry skeleton building blocks, which are then subjected to the reaction process, which is melt-annealing simulation with a reactive force field. The bonds in oligomers will be broken and a new amorphous structure can form. After reaction simulation, no more additional water molecules are added into or removed from the systems, which can better simulate the real geopolymerisation process. **Figure 4.2** shows the typical initial model constructed with 600 atoms and a Si/Al ratio of 2 as an example.

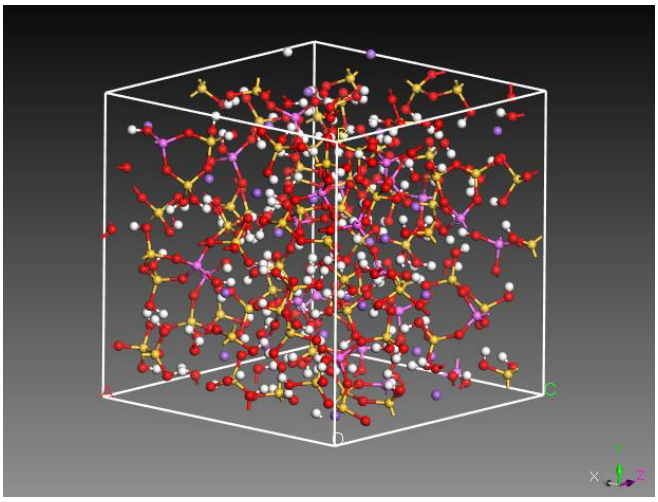

Figure 4.2 Molecular model made from oligomer Mo6 (Si/Al=2.0) with 600 atoms: yellow is silicon, pink is aluminium, red is oxygen, purple is sodium, and white is hydrogen.

4.3.2 Force fields

The force fields that have ever been used for NASH gels have been depicted in Chapter 3. Although several studies reported that some general force fields, such as COMPASS (Bagheri et al. 2018), universal, Dreiding (Bagheri et al. 2017) and the specific force field ClayFF (Cygan et al. 2004), are suitable for NASH simulation, they cannot provide insights for specific systems in which chemical reactions are involved. Thus, the bond breakage and the complex

polymerization procedure must be modelled using reactive force fields. Among others, ReaxFF is the most popular one that has been applied in cementitious materials systems. In this study, ReaxFF was employed to describe the interatomic interactions between Na, Al, Si, O and H atoms. Previous studies on water dissociation in CSH gels (Fan and Yang 2018; Zhou et al. 2017a), guest ions ultra-confined in CSH (Zhang et al. 2018a), and silica-water interfaces (Fan et al. 2017) showed that ReaxFF can accurately describe the structure, reactivity and mechanical properties of such inorganic gel system. The parameters for Si, O and H are referred to a previous study about C-S-H gel system (Hou 2014). The parameter for Na is referred to the ReaxFF developed for $NaSiO_x$/water system in which Na ions have the similar chemistry environment as that in alkali activator for geopolymer (Hahn et al. 2018). Moreover, the parameter for Al is referred to a MD study of zeolite system which has the comparable aluminosilicate chains as geopolymers (Bai et al. 2012). Those parameters describing the interaction between atoms enables the reactive MD simulation of NASH gel system, and have been fitted against various quantum mechanical calculations to prove their accuracy in the previously mentioned studies. The parameter details are listed in the Appendix I.

4.3.3 Simulation algorithm

4.3.3.1 Melt-annealing-equilibrium of NASH gel structures

All the models are first relaxed via energy minimization using a conjugated gradient algorithm as implemented in the large-scale atomic/molecular massively parallel simulator (LAMMPS) (Plimpton et al. 2007). The systems are then heated up to 300 K in the NVT ensemble for five ps using a timestep of 0.25 fs before an annealing procedure. At the start of the annealing process, the systems are raised to 3,300 K to remove any memory effects, followed by a cooling procedure with a cooling rate of 3 K/ps down to 300 K. Afterwards, the systems are equilibrated for 200 ps in the NPT ensemble at 300 K and 0 Pa. Finally, the systems are subjected to another NVT ensemble run at 300 K for

another 200 ps for production. The annealing process is crucial to creating amorphous NASH gels.

There are two main factors need to be determined in this melt-annealing-equilibrium procedure: the melting temperature and the cooling gradient during annealing. The selected melting temperature should be high enough to break the covalent bonds in the oligomers but cannot destroy the initial NASH gel structure. This is the criterion of temperature selection, which can remove the memory effects in oligomers to generate an amorphous structure. On the other hand, the intermediates of aluminosilicates generated during annealing procedure are the metastable structures. Thus, the small temperature gradient in the cooling process is necessary to achieve the relaxed structure at each timestep. However, the smaller temperature gradient causes the longer annealing period and more computational time. In this study, the cooling rate is selected to ensure both structural equilibrium and computational effectiveness.

4.3.3.2 Tensile deformation

A uniaxial tensile deformation simulation is performed to obtain the mechanical properties of the developed NASH gels using LAMMPS. The tensile deformation is conducted at 300 K, and the pressures along the x and y directions are set to 0. The uniaxial deformation is employed along the z-direction with a constant engineering strain rate of 0.001/ps, which means the increment of box length (ΔL) in elapsed time is constant. In this study, the varied strain from 0 to 1 means the simulation box in z-direction has been changed from its original length to twice of that. Since the NASH gel performs an amorphous isotropic structure, the uniaxial tension along the z-direction reveals the mechanical performance of this material. The engineering stress-strain curves are obtained for different systems by calculating the pressure tensor along the z-direction during the tensile deformation. Thus, the ultimate tensile strengths are acquired from the peak values of those curves and Young's modulus can be calculated from the slope of the curve in the elastic segment, which is at the point of 40% of the ultimate tensile strength.

4.4 Results and Discussion

4.4.1 Modelling of NASH gel

Seven types of NASH gel models have been prepared from different oligomers, respectively, with various Si/Al ratios and different molecular configurations. The basic information and RDF of these NASH gels is described in this section to characterize the reliability of the developed NASH gel models. **Table 4.1** lists the size of simulation cells and bulk densities of the NASH gels. Those NASH gel structures with different Si/Al ratios have cell sizes with cubic edge lengths of around 75 Å, and the equilibrium densities are around 2.0 g/cm^3. As compared with some experimental results, it is readily seen that the equilibrium modelling density is in the reasonable range.

Table 4.1 General properties of equilibrated NASH gels obtained from various oligomers

NASH model	Si/Al ratio	Oligomer configur-ation	Oligomer numbers	Number of atoms	Edge length of cubic cell (Å)	Simulation density (g/cm^3)	Experiment density (g/cm^3)
M1	1	linear	2,500	40,000	75.11	1.92	1.8-2.2 (Assi et al. 2018; Nematollahi et al. 2015; Wang et al. 2005)
M2	2	linear	1,820	40,040	73.97	2.05	
M3	2	cyclic	2,110	40,090	75.98	2.05	
M4	3	linear	1,430	40,040	74.86	1.99	
M5	3	cyclic	1,600	40,000	75.64	2.05	
M6	3	cyclic	1,600	40,000	75.11	2.03	
M7	3	cyclic	1,600	40,000	76.34	2.00	

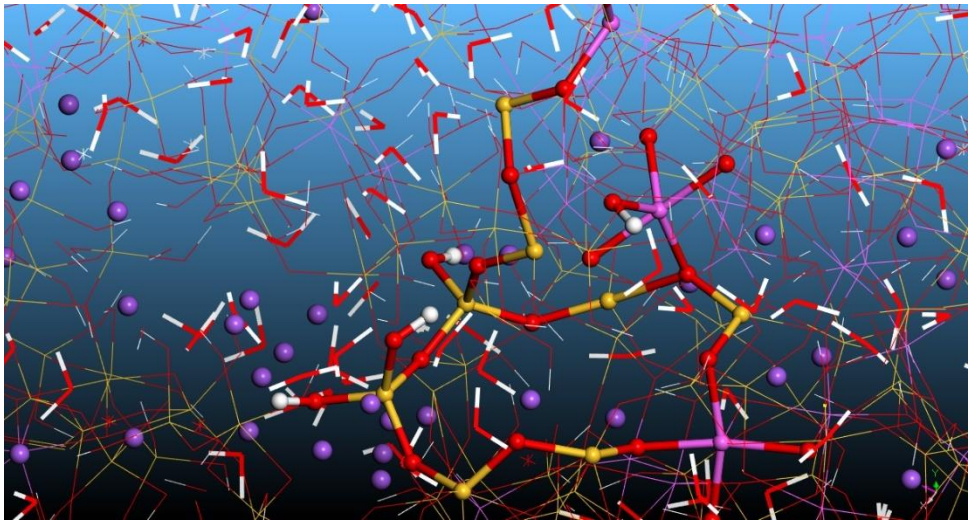

Figure 4.3 NASH gel (M4) structure after annealing and equilibrium stage: yellow is silicon, pink is aluminium, red is oxygen, purple is sodium, and white is hydrogen

Figure 4.3 displays the NASH gel structure (M4) after annealing. The water molecules and sodium ions are represented by sticks and balls, respectively. The Si-O-Al skeleton is represented by lines, with part of that highlighted with ball and stick to display the NASH gel skeleton more clearly. It shows that the Na ions distribute in the amorphous structure, some water molecules have been generated after annealing, and larger rings and longer linear chain of Si-O-Al skeleton can be found in the figure, which indicates the reaction between oligomers indeed happened. Moreover, most of the Si atoms are 4-coordinated with O atoms, while Al atoms with various coordination are found.

Figure 4.4 shows the RDF curves of various NASH gels. The RDF curves of seven NASH gels show similar peak positions, but the intensities of peaks present slight differences. The peaks of the RDF curve represent the bond length distribution of different pairs. The first peak representing the H-O bond in the bond length range of 0.9 to 1.1 Å contains H-O bonds in both water molecules and unreacted hydroxyl radicals in the equilibrated NASH gels. In general, the H-O pair distance in water molecules in NASH gels should be similar to that in free bulk water. Even though Zhang et al. (2018c) reported the very slightly longer bond length of water in geopolymer in free water due to the strong attraction from O atoms, the general bond length of H-O in free water is 0.98-1.01 Å (Soper and Benmore 2008), which is in agreement with the H-O peak range in this simulation. The other most apparent peak in RDF curves is the Si-

O bond in bond length from 1.5 to 1.8 Å. Linked with the Al-O bond, they form the basic skeleton structure of NASH gel. The Si-O bond is stable and mainly exists in the tetrahedron structure in NASH gel (Duxson et al. 2006a). Very close to the peak of the Si-O bond, the Al-O peak positioned in the bond length range from 1.7 Å to 2.1 Å. A lower Si/Al ratio brings a higher Al-O peak in the RDF curve. As a weaker bond in the NASH skeleton than Si-O, the types Al-O bond types and percentage in NASH gels can significantly affect their mechanical properties (Sadat et al. 2016b). Moreover, the Na-O peak, radius distribution ranges from almost 2.0 Å to 3.0 Å, is not very obvious. Lolli et al. (2018) found that Na ions are primarily located in NASH gel's oxygen circles; thus, the O atoms in the skeleton form ring-structures to capture sodium ions. Therefore, the ring size determines the O-Na bond length. Various structures and different sizes of O atoms rings make the broader distribution of the Na-O bond. Other peaks in RDF curves are contributed by pairs of O-O (r≈2.7 Å), Si-Si (r≈3.0 Å), Al-Al (r≈2.9 Å) and Si-Al (r≈3.7 Å). Indeed, there is no direct chemical bond between these pairs, the relatively short interatomic distance is contributed from the position of water molecules, space location of bridge O atoms or the structural layout of the aluminosilicate skeleton.

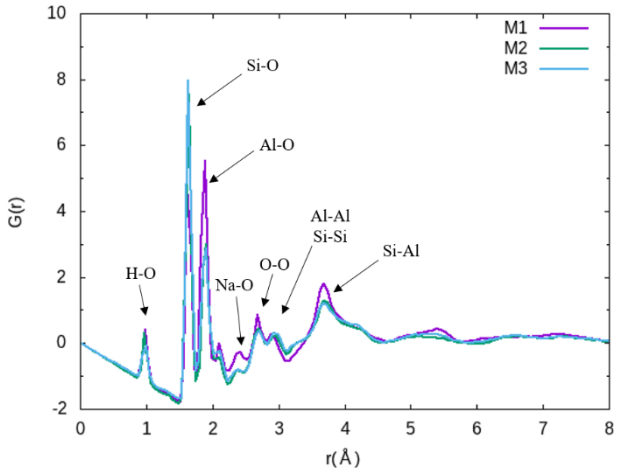

(a)

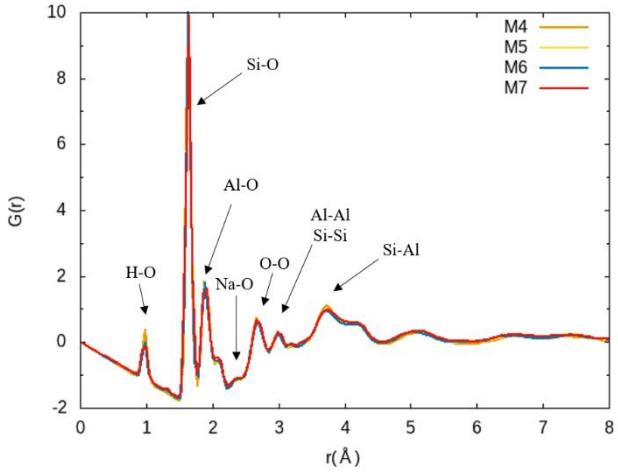

(b)

Figure 4.4 Comparison of X-ray radial distribution function (RDF) of NASH gels developed from various types of oligomers: (a) RDF curves of M1 to M3; (b) RDF curves of M4 to M7.

One of the representative simulated X-ray RDF curves of M4 NASH gel is compared with experimental results in **Figure 4.5** to examine the modelling method. The experimental RDF curves of geopolymer materials are obtained from the previous studies (White et al. 2013a; White et al. 2010). The peaks show high relevance with the simulation results. White et al. (2013a) reported the experimental X-ray PDFs of metakaolin based geopolymer during the geopolymerisation process. The peak at 1.5-2.0 Å correlates to the T-O bond, where T denotes tetrahedral Si and/or Al. The intensity shoulder at 1.9-2.0 Å indicates the metakaolin Al-O bond, which presents higher r values than Si-O. Similar trends are also observed for the simulated spectra. Moreover, **Figure 4.4** shows that the intensity of the Al-O peak declines with the increase of the Si/Al ratio. The effect of the Al content on the mechanical properties will be

discussed in the following sections. Similarly, the variation of Si-Al peaks intensity in different NASH gel structures is also caused by the Al content.

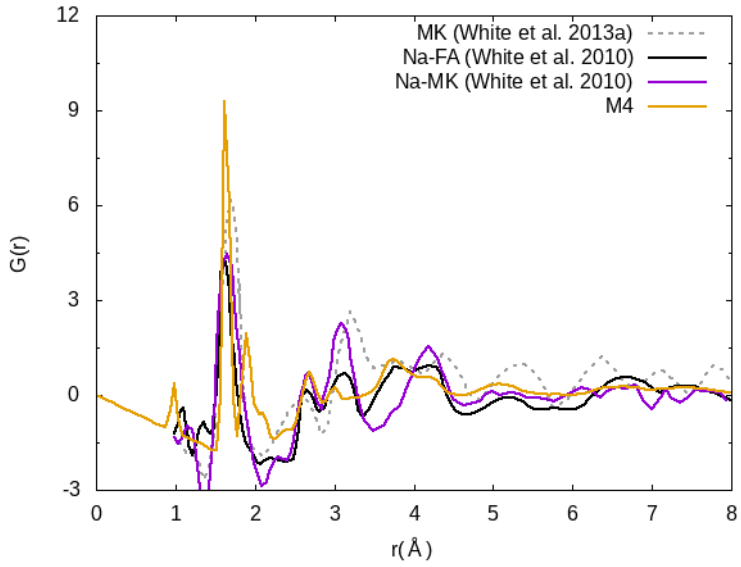

Figure 4.5 Comparison of X-ray RDF curves of M4 NASH gel to the geopolymer materials from experimental results (White et al. 2013a; White et al. 2010)

4.4.2 Microscopic properties

4.4.2.1 Geopolymerisation from the oligomer

The chemical environment of the oxygen atom has been analysed to investigate the reaction process of geopolymers. Bonds breakage and formation in the aluminosilicate network are considered by employing a reactive force field. Since most of the reactions exist on the oxygen atoms, the oxygen atom types have been analysed to describe the geopolymerisation.

4.4.2.1.1 Reaction on oxygen atoms

Figure 4.6 shows the number of oxygen atoms in various types in percentage during the geopolymerisation process of the M4 NASH gel. The oxygen atoms in the oligomer can be categorized into two groups: hydroxyl oxygen (O_h) and bridge oxygen (O_b) which link the T (i.e. Si or Al) atoms. The water molecules percentage in NASH gel is calculated from the number of oxygen atoms with the configuration of two hydrogen atoms within the radius cutoff of 1.2 Å, which means those oxygen atoms associated with two hydrogen atoms within the radius of 1.2 Å are considered as water molecules. Moreover, the number of

hydroxyl radicals is also calculated from the O-H pair cutoff of 1.2 Å, and the types are clarified from different atoms associated with the O_h atoms, with Si-O pair cutoff of 2 Å and Al-O pair cutoff of 2.5 Å. All the numbers are averaged from 100 equilibrium trajectories.

In M4 NASH gel, the number of Si-OH and Al-OH reduces obviously after geopolymerisation, while the percentage of O_b increases from 23.1% to 43.4%. Moreover, 20.0% of O atoms are subjected to form water molecules. It illustrates the poly-condensation reaction between hydroxyls on T atoms and generated new O_b and water molecules. Thus, the number of water molecules generated in NASH gel, to some extent, can represent the geopolymerisation degree. Besides, in **Figure 4.6(b)**, except for the unreacted Si-OH and Al-OH, the other hydroxyls are generated by the association of hydrogen radicals with O_b and forming T-(OH)-T structure. The hydrogen radicals can connect to O_b, and some hydroxyls can associate with Al in aluminosilicate chain or Na^+ ions. A similar mechanism has also been reported by Hou et al. (2018). It is found that only a tiny amount of these hydroxyls exists in M4 NASH gel, that on Si-O-Al bond is 3.0% and on Al-O-Al bond is 1.6%, but zero of that occurs on Si-O-Si bond. This is because O_b in Al-O-Si bond has a hydrophilic nature and is more likely to react with water, differing from the hydrophobic nature of O_b in Si-O-Si bond. Therefore, Si tetrahedrons are much more stable in the geopolymerisation reaction. Besides, fewer hydroxyls on the Al-O-Al bond are due to the originally seldom number of Al-O-Al bonds in the system. The reactivity comparison will be further discussed in later sections.

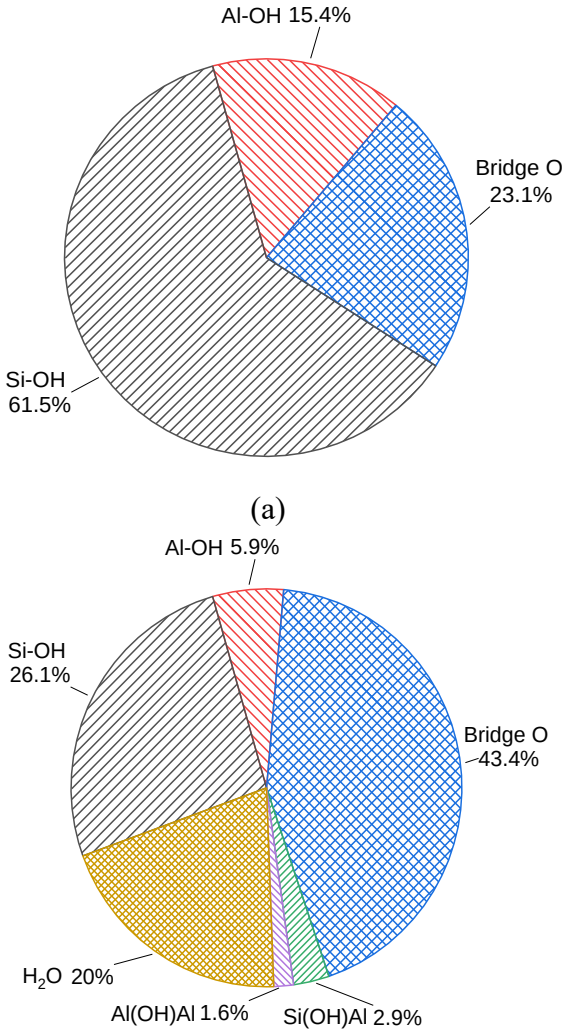

Figure 4.6 Percentages of types of hydroxyls, water molecule and bridge oxygen in oligomer and NASH gel (model with Si/Al=3.0, M4), represented by the percentages of various types of O atoms in total oxygen: (a) in Mo4 oligomer; (b) in M4 NASH gel

4.4.2.1.2 Geopolymerisation degree in various models

Oxygen atom types have also been analysed for various NASH gels to reveal the reaction during the simulation and compare the difference in geopolymerisation degree. **Figure 4.7** presents the amount of generated water oxygen (O_w) and total bridge oxygen (O_b) in seven NASH gels, indicating the geopolymerisation degree and network complexity. Water content is a significant parameter in geopolymer material that can impact the material properties. Some researchers (Sadat et al. 2016a) have changed water content in NASH gels in MD simulation and found that higher water content or more water pores will negatively affect mechanical strength. However, as mentioned in the previous section, no further water content modification was considered in this

study. All water molecules were automatically generated from the geopolymerisation reaction. Moreover, the percentage of hydroxyl radicals consumed during the reaction process has also been calculated to represent the reaction degree more directly.

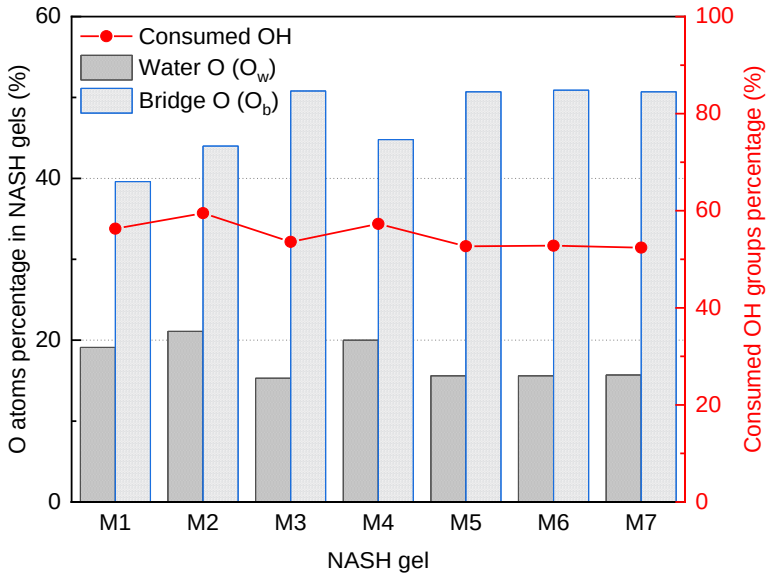

Figure 4.7 Percentage of oxygen atoms of water oxygen (O_w) and bridge oxygen (O_b) in NASH gels and the consumed percentage of hydroxyl radical during geopolymerisation of M1 to M7

Figure 4.7 compares the O_w and O_b percentages in NASH gels. Firstly, those with various Si/Al ratios (e.g. M1, M2 and M4) are compared. There are more original hydroxyls groups in the oligomer Mo1 than those in Mo2 and Mo4, which indicates more chances for oxygen atoms collision and can bring a higher reaction degree. However, the O_w percentage in M1, M2 and M4 are 19.1%, 21.1% and 20.0%, respectively, meaning that M1 has a relatively lower reaction degree. Due to the low Si/Al ratio, too many Al atoms in the system negatively affect the geopolymerisation reaction. Besides, more O_b at a higher Si/Al ratio indicates the more complex structure in NASH gels. Secondly, NASH gels generated from linear oligomers have more O_w than those with cyclic ones when comparing M2 with M3 and M4 with M5 to M7. At the same Si/Al ratio, linear oligomer structures have more original OH radicals than cyclic ones due to molecular stoichiometry. Thus, more O_w are generated. Although cyclic structures show less geopolymerisation degree, more O_b and higher complexity network structure is found than those linear ones. Thirdly, M5, M6 and M7 have achieved the same water content and complexity after MD simulation,

indicating that geopolymerisation degrees show no difference in various cyclic oligomers at the same Si/Al ratio. Finally, data of consumption percentage of hydroxyl radicals directly represents the reaction degree. It is readily seen that all the percentages for M1 to M7 exceed 50% when a higher Si/Al ratio and linear configuration can bring a slightly higher geopolymerisation degree.

4.4.2.2 Bond angle in NASH gel

4.4.2.2.1 Bond angle change from the oligomers

Bond angle variation is another significant feature that reflects the reaction by simulation. In this study, the bond angle distributions of O-Si-O, O-Al-O, Si-O-Si, Al-O-Al, and Si-O-Al are obtained using R.I.N.G.S code (Le Roux and Jund 2010). The results of M4 NASH gel are described in **Figure 4.8**.

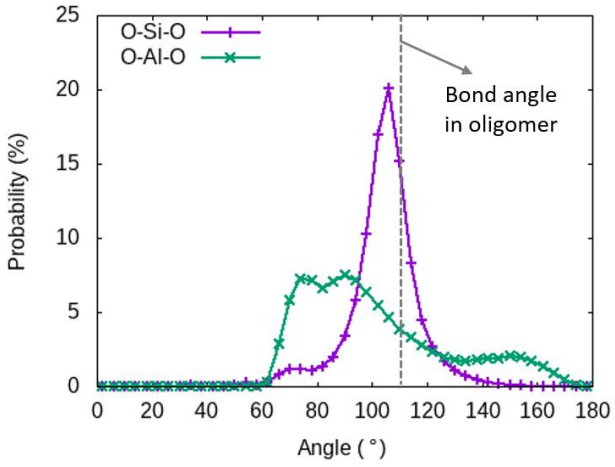

(a)

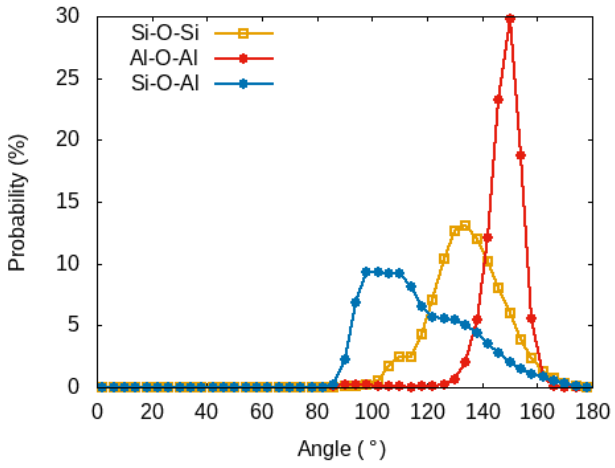

(b)

Figure 4.8 O-T-O and T-O-T bond angle distribution in M4 NASH gel: (a) O-Si-O and O-Al-O bonds; (b) Si-O-Si, Al-O-Al and Si-O-Al bonds

The O-Si-O and O-Al-O bonds exist in the Si and Al tetrahedrons in the oligomers, with original angles both calculated as 109.5º. As shown in **Figure 4.8(a)**, in M4 NASH gel, the peak value of the O-Si-O bond angle distribution curve can be observed at 107º, which is very close to the original angle and matches well with the experimental result in silica (109.7º) (Henderson et al. 2009). O-Si-O bonds do not change much during the reaction, and most of the Si atoms are still located in stable 4-fold coordination. Differently, the distribution of O-Al-O angle is much broader, mainly due to the existence of a variety of coordinated configurations of Al in NASH gel. Singh et al. (2005) have reported that 5-coordinate and 6-coordinate Al were observed in geopolymer by MAS-NMR. Besides, Walkley et al. (2018) observed a new type of Al atom in NASH gel by experiment, which is extra-framework Al and shared the electrons with bridge oxygen atoms. In this study, several types of bond angle on Al atoms are also observed (i.e. 75º, 90º and 150º). Hou et al. (2018) reported similar results after simulated water absorption in a dry N-A-S skeleton. The hydroxyl radical inserted into Al tetrahedrons leads the other oxygen atoms to move and change the bond angles.

Figure 4.8(b) shows the bond angle distribution of the T-O-T bond, which represents the angle between the tetrahedrons. The Si-O-Si angles are distributed from 100º to 180º, and the peak value locates at 136º. Xu et al. (2021b) compared the calculation of Si-O-Si bond angle in geopolymer simulation with different force fields and found that distribution is closely related to the force fields chosen. Lyngdoh et al. (2019) found that the peak would be broadened when water molecules were distributed in NASH system. The Si-O-Al bond angle distributes a smaller angle than Si-O-Si, with two prominent peaks at 105º and 130º. The more diversely coordinated Al atoms contribute to the broader distribution. Besides, a few Al-O-Al bonds exist in the M4 NASH gel, which has a negligible number in the system and a concentrated angles distribution at around 150º.

4.4.2.2.2 Bond angle distribution in various NASH gels

Figure 4.9 shows the bond angle distributions of NASH gels of M1, M2 and M4. As shown in **Figure 4.9(a)**, for O-Si-O bond, the peak values of M1, M2

and M4 overlap at 107º. However, for the lower Si/Al ratio, the probability at a smaller angle (i.e. 70º-90º) is relatively higher. At a lower Si/Al ratio, some O-Si-O bond angles have been compressed, which reduces the stability of the system. In the M1 system, more hydroxyl radicals and water molecules stretch the aluminosilicate network and weaken the structure. For the O-Al-O bond angle, the distributions do not change much with the Si/Al ratio. All curves in **Figure 4.9(b)** show three peaks at around 75º, 90º and 150º. The Si/Al ratio changes the percentage of aluminate blocks in NASH gels but has no significant impact on its coordinates and chemical structure.

In addition, **Figure 4.9(c)** shows the peak of the Si-O-Si bonds angle has moved to a higher degree side, changing from 130º to 135º, with a higher Si/Al ratio. The experimental results of the Si-O-Si angle in silica measured by nuclear magnetic resonance (Mauri et al. 2000) also gave values around 142º. Higher Si/Al ratio in M4 indicates fewer aluminate blocks element in the system, which may bring a more stable structure; thus, the Si-O-Si angle distribution is closer to the crystal value. However, **Figure 4.9(d)** represents a pronounced difference of Si-O-Al bond angle at various Si/Al ratios. For structure M1, the peak at around 100º is much higher than the others. This indicates that aluminate and silicate blocks are located closely at a low Si/Al ratio, affecting mechanical properties. Therefore, the bond angle analysis has indicated that NASH gels with a higher Si/Al ratio have a more stable structure and better mechanical properties. Compared to the Si/Al ratio effect, oligomer configuration (i.e. linear or cyclic) has a negligible influence on the bond angle distribution of NASH gels. The comparison of the distribution curves of structure M4, M5, M6 and M7 are displayed in Appendix II.a.

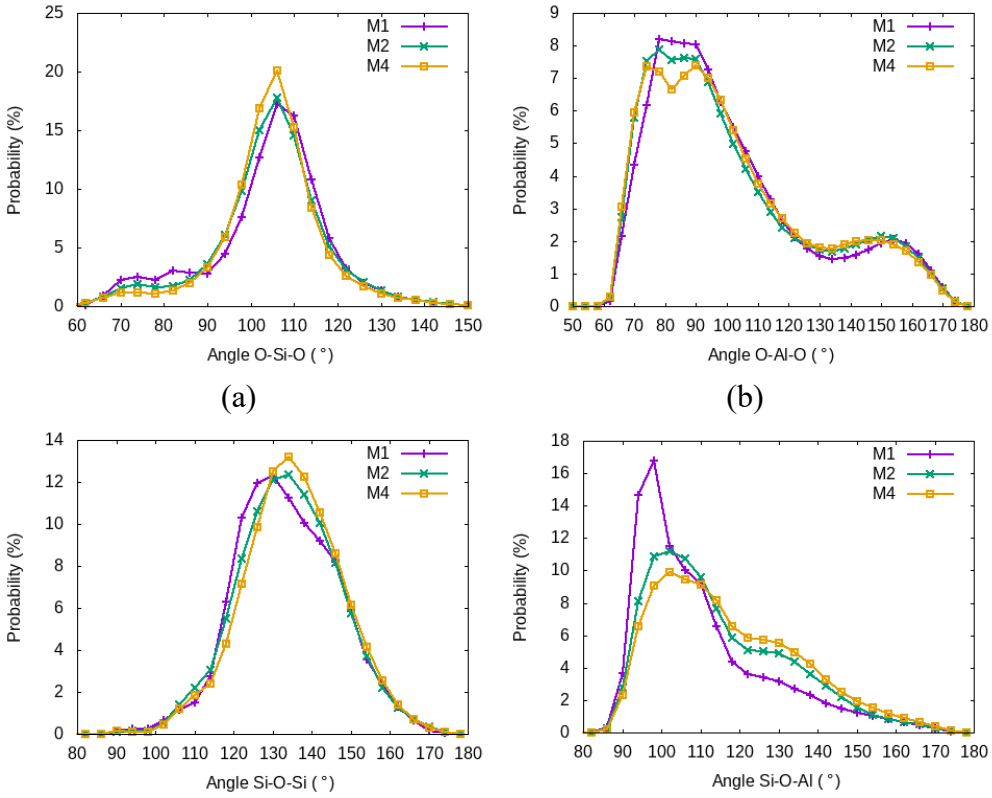

Figure 4.9 Bond angle distributions of O-T-O and T-O-T bonds in NASH gels: M1, M2 and M4 (Si/Al from 1 to 3)

4.4.2.3 Dynamic properties

The mobility of atoms in NASH gels is estimated based on their mean square displacement. The displacements of the atoms are recorded at 10 fs intervals and averaged over 200 ps to acquire the MSD.

Figure 4.10(a) illustrates the MSD curves of different atoms in the M4 NASH gel. Si and Al atoms in NASH gels perform as the structural skeleton. Thus, their MSD locate at an extremely low level of around 0.1 $Å^2$, which reveals that the atoms are restricted in the network of T-O-T bonds. Moreover, the mobility of Na ions is much higher, with a value of around 1.0 $Å^2$. The ions are distributed in the pores and vacancy of the network structure, which is more likely to immigrate. It is also in accordance with the experimental observation of the alkali efflorescence phenomenon in geopolymer (Kani et al. 2012). The diffusion of O is higher than that of Si and Al. This is because partial O atoms perform as bridge oxygen in NASH gels and are restricted in the skeleton, but other O atoms exist in reactive hydroxyl radicals and water molecules.

Therefore, the converged MSD value of O atom is higher than that of Si and Al. Subsequently, hydrogen atoms exist either in water molecules or hydroxyl radicals. Its MSD value shows the highest level.

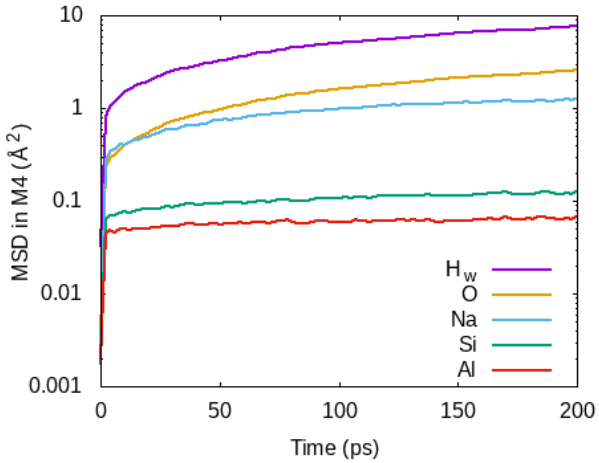

(a)

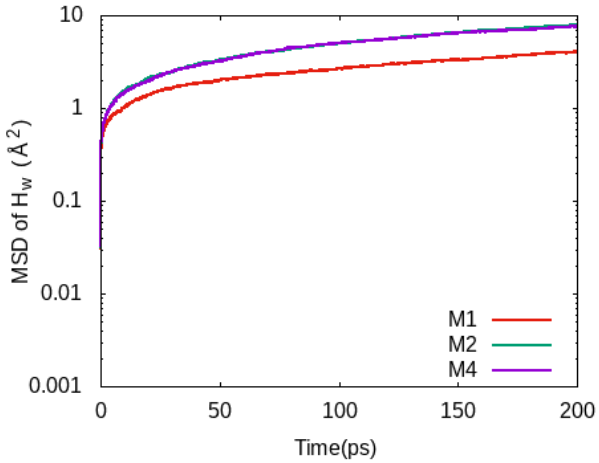

(b)

Figure 4.10 Mean square displacement: (a) curves of H_w, O, Na, Si and Al versus time for M4 NASH gel; (b) curves of H_w for M1(Si/Al=1), M2(Si/Al=2) and M4(Si/Al=3) NASH gel.

Since a significant amount of H atoms exist in hydroxyls and water molecules, the diffusion of H atoms can represent the mobility of total water (i.e. including water molecules and hydroxyls) in NASH gels, and the comparison of various structures is displayed in **Figure 4.10(b)**. Water mobility increases significantly with the Si/Al ratio, mainly governed by microscopic structures. The following two reasons can explain this. Firstly, slightly more water molecules are generated at a higher Si/Al ratio, as shown in **Figure 4.7**. As the mobility of the water molecule is higher than that of the hydroxyl radical, NASH gels with more

water exhibit a higher MSD of H atoms. Secondly, the number of aluminium atoms is reduced by Si/Al ratio. As illustrated in previous sections, aluminium tetrahedrons in NASH gel are more likely to attract the water molecules, and O_b connected to Al are more likely to attract the H^+, which can both restrict the movement of hydrogen atoms. Therefore, lower Al atoms content also contributes to the higher water diffusion rate.

4.4.3 Mechanical performances

4.4.3.1 Tensile behaviour of NASH gels

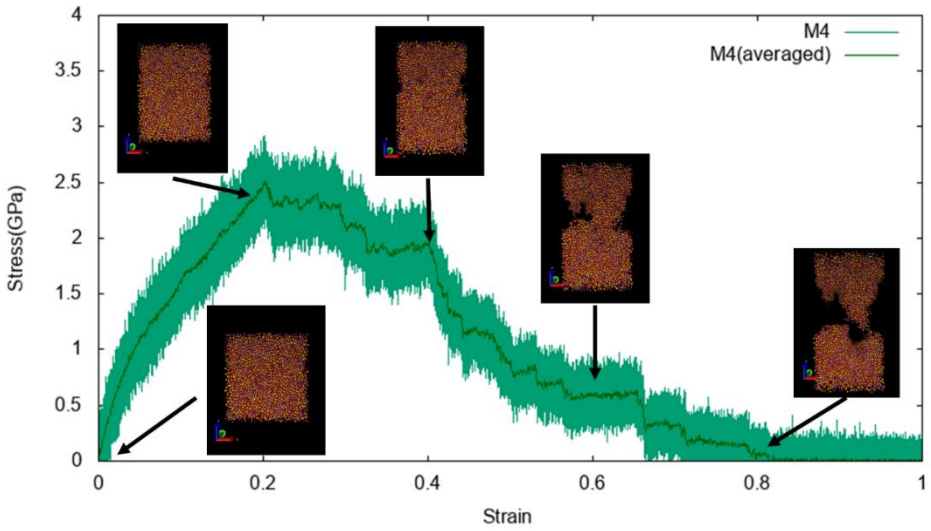

Figure 4.11 Stress-strain curve of uniaxial tensile simulation with snapshots at various stages during tensile deformation of M4 NASH gel

Figure 4.11 shows the typical tensile stress-strain relationship of the M4 NASH gel. The strain ranging from 0 to 1 indicates the simulation cell was stretched to twice its original length along the z-direction. The data were averaged over 200 samples, and a simple curve was plotted to represent the stress-strain relationship for comparison. Young's modulus and tensile strength of NASH gel can be calculated from the slope of the elastic segment and peak value on the stress-strain curve, respectively. There is an apparent elastic stage in the tensile stress-strain curve of M4 NASH gel until the stress reaches 1.2 GPa at a tensile strain of 0.1. When the stress slightly declines to 2.3 GPa, the yield stage at strain from around 0.2 to 0.3 is observed. Then, the stress gradually drops in the failure stage, with a shoulder peak at strain from 0.3 to 0.4. Finally, the stress steps into a dramatically declining period from 2 GPa at a strain of 0.4;

meanwhile, more cracks grow and coalesce rapidly through the structure until the strain increases to 0.8, resulting in the entire fracture at last. The snapshots in **Figure 4.11** display the configurations variation and cracks growth of M4 NASH gel during the tensile deformation process.

When deformation is applied to the NASH gel, except for the stretching of aluminosilicate network structure and cracks growth, it is found that some water molecules in the system simultaneously dissociate, and many hydroxyls are re-formed at the end of aluminosilicate chains. Structural rearrangement also appears when some T-O bonds break, and a new configuration is obtained induced by tensile stress. The calculated oxygen atom percentages in various types can reveal both the hydrolysis reaction and reconstruction of the aluminosilicate structure. The data was acquired from averaging 100 configurations at 20 steps in tensile deformation (**Figure 4.12**). All the percentages represent the ratios of the specific type of oxygen atoms to total oxygen in the system, making it possible for the quantitative analysis of O type transformation.

The hydrolysis reaction is indicated in **Figure 4.12(a)** and **(b)**. The process can be mainly separated into three steps. Firstly, in the elastic stage, the percentage of water molecules maintains at around 20.0% without chemical dissociation, and no more hydroxyls are generated. It is the aluminosilicate clusters and rings structure that bears the tensile deformation. Subsequently, the percentage of water oxygen atoms starts to decline slightly, indicating the entry of the yield stage, followed by a more obvious drop to almost 19.6% when the strain ranges from 0.2 to 0.4. Simultaneously, the percentage of hydroxyls on silicon and aluminium hydroxyls increases from 26.1% and 5.9% to 26.4% and 6.2%, respectively. It reveals that in this failure stage, a large number of water molecules dissociate, and new hydroxyls are formed at the edge of cracks or pores in terms of a hydrolysis reaction. Afterwards, the hydrolysis reaction slows down but continues until the system's total fracture. In total, the percentage of O_w has decreased from around 20% to 19.5%, while that of Si-OH and Al-OH has increased by 0.4%. It means that almost 2.5% of the water

molecules have been dissociated and transformed into hydroxyls during the tensile process.

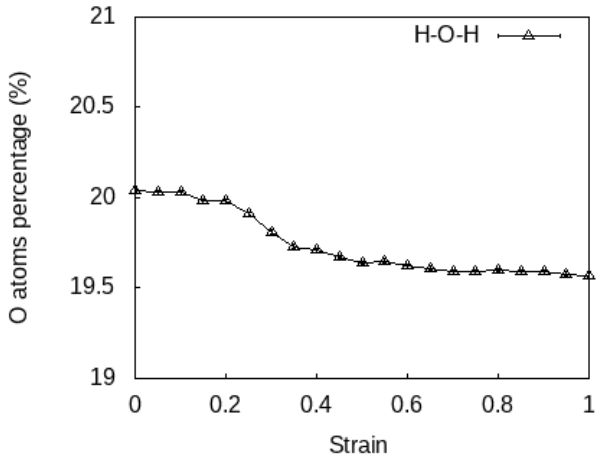

(a)

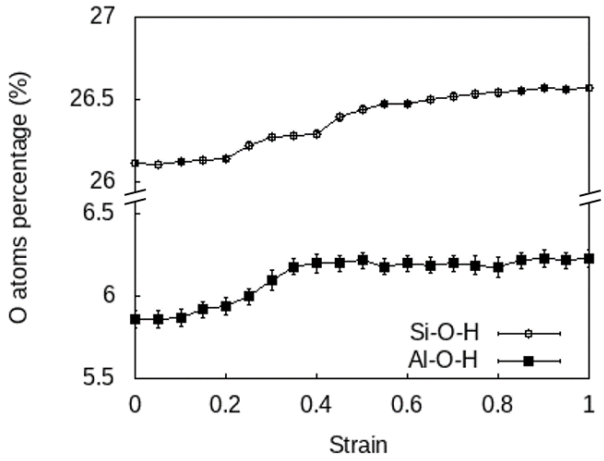

(b)

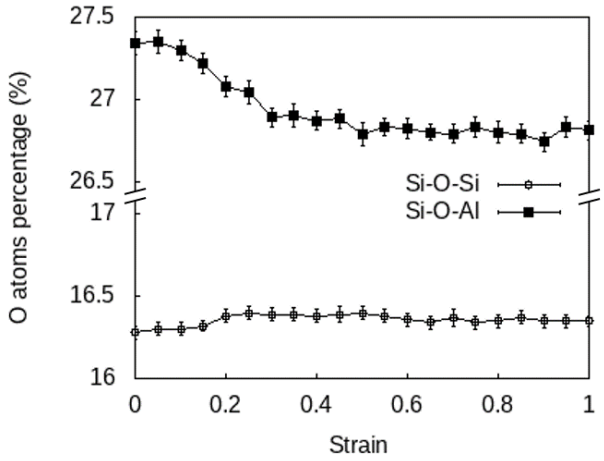

(c)

Figure 4.12 Variation of water, hydroxyl and bridge oxygen atom percentages in the tensile deformation process

On the other hand, **Figure 4.12(c)** reveals the structural rearrangement of the aluminosilicate network. As the variation of water molecule percentage, the number of Si-O-Al bonds is constant at the beginning but declines in the yield stages. The drop occurs at strain around 0.1, which means some Si-O-Al bonds start to break at the end of the elastic stage. The data drops from 27.3% to 26.9%. In the failure stage, more cracks and pores appear in the NASH gel structure, but Si-O-Al bonds keep relatively stable. Moreover, the variation of O_b in Si-O-Si is negligible, which explains that the Si-O bond is much stronger. Thus, tensile strain mainly starts from the breakage of Al-O instead of the Si-O bond.

Furthermore, the full stiffness tensors of seven NASH gel structures can be computed. As an example, the data for model M4 is displayed in **Table 4.2**. Unlike the layered C-S-H molecular model for OPC material, this geopolymer model shows the approximately isotropic property. It indicates the amorphous nature of this model, which is in line with the experimental studies. The stiffness tensors for all the other models from M1 to M7 are referred to Appendix II.c.

Table 4.2. Computed full stiffness tensors (C_{ij}) of NASH gel M4

Stiffness tensors (GPa)							
C_{11}	47.02	C_{44}	14.84	C_{24}	0.28	C_{45}	0.92
C_{22}	43.69	C_{55}	12.92	C_{25}	-0.43	C_{46}	0.38
C_{33}	47.65	C_{66}	13.38	C_{26}	0.68	C_{56}	0.50
C_{12}	19.35	C_{14}	0.50	C_{34}	-0.19		
C_{13}	20.46	C_{15}	0.67	C_{35}	0.18		
C_{23}	17.30	C_{16}	-0.02	C_{36}	0.36		

4.4.3.2 Effects of Si/Al ratio and oligomer configurations

Table 4.3 Simulation results of tensile strength and Young's modulus of NASH gels

NASH gel	**Si/Al ratio**	**Tensile strength (GPa)**	**Young's modulus (GPa)**
M1	1	1.57 ± 0.33	19.74 ± 1.05
M2	2	2.11 ± 0.43	24.95 ± 1.56
M3	2	2.82 ± 0.41	25.94 ± 1.79
M4	3	2.51 ± 0.40	23.21 ± 1.66
M5	3	3.11 ± 0.37	22.38 ± 1.35
M6	3	2.99 ± 0.39	23.78 ± 1.42
M7	3	3.14 ± 0.34	24.18 ± 1.67

The calculated tensile strengths and elastic moduli of the NASH gels are summarized in **Table 4.3**. Tensile strength varies with the NASH gels, and elastic moduli range from around 20 to 25 GPa. The results are also comparable to the observed mechanical properties of geopolymer matrix. Several studies have investigated the micromechanical properties of various types of geopolymer materials by nanoindentation technology (Beleña and Zhu 2009; Luo et al. 2020; Lyngdoh et al. 2020a; Němeček et al. 2011) and found that the modulus and hardness of NASH gel depend on the raw material types, reaction degree, curing methods, etc. Moreover, various phases in the geopolymer matrix show a significant difference in micromechanical properties by nanoindentation. Das et al. (2015) prepared fly ash-based geopolymer and reported the elastic modulus of around 17 GPa in the NASH phase, 30 GPa in partially activated FA phase, 45 GPa in FA with cavity phases and 70 GPa in the unreacted FA phase. The modulus in the pure NASH phase is in line with the simulation results in the current study.

In addition, it is found that some mechanical properties of NASH gel from the simulations in the literature are higher than those in this study (Hou et al. 2018; Sadat et al. 2016a; Sadat et al. 2016b), which might be due to the different modelling methods. Most of those simulation models are built from dry skeleton structures, and water was inserted after N-A-S structure construction. However, in this study, models are generated by the reaction of oligomers reaction degree, which is more realistic. Besides, the water content in the structure and the geopolymerisation degree is more like the real geopolymer matrix. Thus, results in the current simulation are closer to the experimental data.

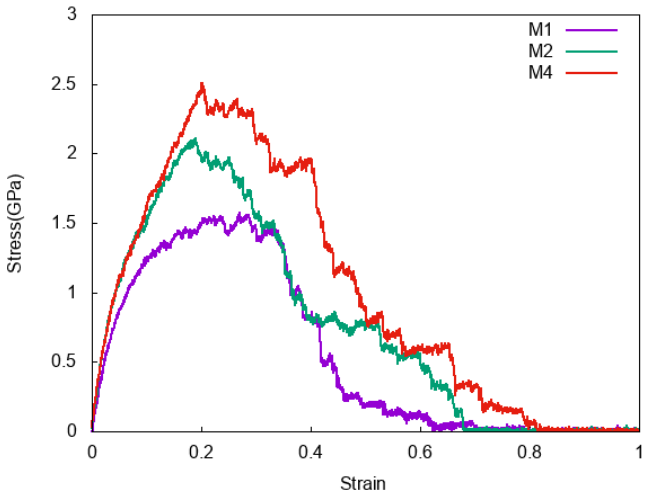

(a)

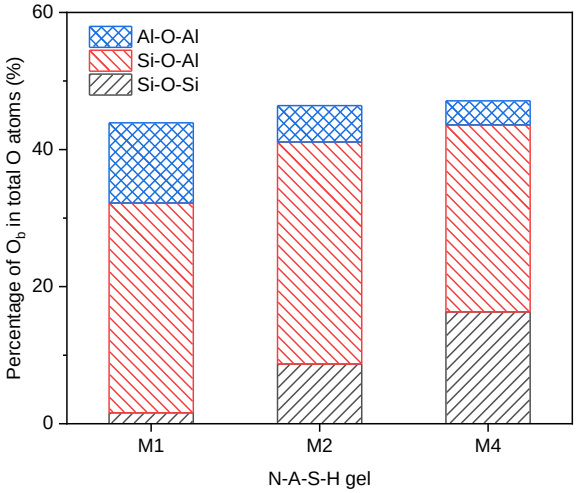

(b)

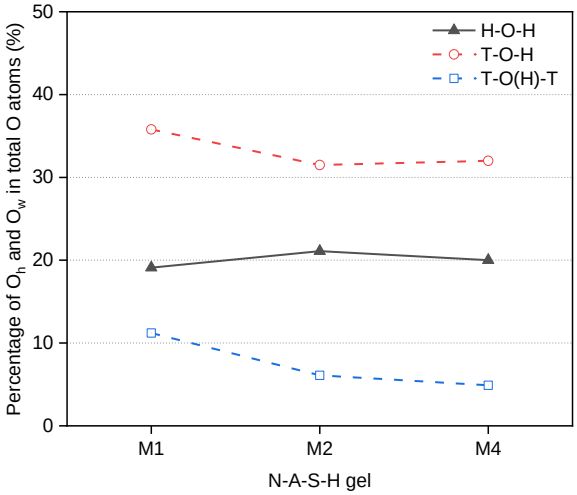

(c)

Figure 4.13 Tensile deformation and comparison of NASH gels: (a) uniaxial stress-strain simulation curves of NASH gels developed from linear oligomers with different Si/Al ratio: M1 (Si/Al=1), M2 (Si/Al=2) and M4 (Si/Al=3); (b) percentages of various bridge oxygen (O_b) types in total oxygen atoms in NASH gels; (c) percentages of hydroxyl oxygen (O_h) and water oxygen (O_w)

in total oxygen atoms in NASH gels

Figure 4.13(a) shows the uniaxial tensile stress-strain curves of NASH gels developed from linear oligomers with different Si/Al ratios. The tensile strength increases with the Si/Al ratio. The tensile strengths of the three NASH gels are attained at a strain around 0.2. Differently, Young's moduli of M2 and M4 are close to each other, which are higher than that of M1. Moreover, the M1 structure has a more prolonged yielding stage than M2 and M4. It is observed that the Si/Al ratio in NASH gel has significantly influenced the mechanical properties, which agrees well with findings reported in the previous studies (Hou et al. 2018; Sadat et al. 2016b).

Figure 4.13(b) illustrates the percentage of various types of O_b in total oxygen atoms in the NASH gels. As depicted in the histogram, O_b is divided into three groups: O_b that connects Al-Al, Si-Al or Si-Si atoms. When the Si/Al ratio increase from 1 to 3, the percentage of Si-O-Si bonds increases dramatically from 1.6% to 16.3%. On the contrary, numbers of Al-O-Al bonds decline versus Si/Al ratio from 11.7% to 3.5%. The Al-O-Al structure is unstable and relatively low-probably to be formed during the geopolymerisation process (Sadat et al. 2016a). Moreover, the Si-O-Al bond keeps a relatively constant percentage of around 30%. At the Si/Al ratio of 3, Si-O-Al bond still presents as the dominant part of O_b. Sadat et al. (2016b) investigated N-A-S glass in tension using MD simulations and discovered bond-breakage was solely observed for the Al-O bonds when the strain increased. Too many Al-O-Al bonds cause instability on the NASH gel structure. In this study, **Figure 4.12** also supports the evidence of the higher stability of Si-O than Al-O bonds. Thus, it is found that more Si-O-Si bonds in NASH gels contribute to the higher tensile strength, while more Al-O-Al bonds tend to weaken the mechanical property.

The M1 NASH gel performs the lower Young's modulus of 19.7 GPa than M2 and M4 showing similar values. Duxson et al. (2005) proved by experiment that the increase of Young's modulus of geopolymer is mainly related to the better homogeneity of the microstructure and not due to the simple improvement in strength. Therefore, the water content, polymerization degree, chain length, and voids distribution significantly influence Young's modulus. **Figure 4.13(c)**

describes the O_w and O_h percentage versus the Si/Al ratio. There are many more O_h in M1 than that in M2 and M4. The percentage of hydroxyls on T of M1 is 36%, while that of M2 and M4 are around 31%. The percentage of hydroxyls on O_b of M1 is 11%, while that of M2 and 4 are around 5%. Since the hydroxyls group mainly exist at the end of aluminosilicate chains, more hydroxyls mean poor complexity of network structure. This is believed as the main driving force for the variation of Young's modulus in terms of atomic structure. In summary, O_b types can significantly influence the tensile strength of NASH gel, but elastic modulus may be impacted by the number of hydroxyls and the structural network complexity.

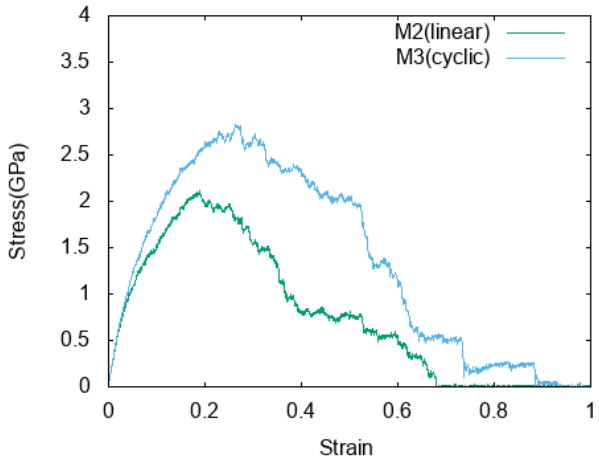

(a)

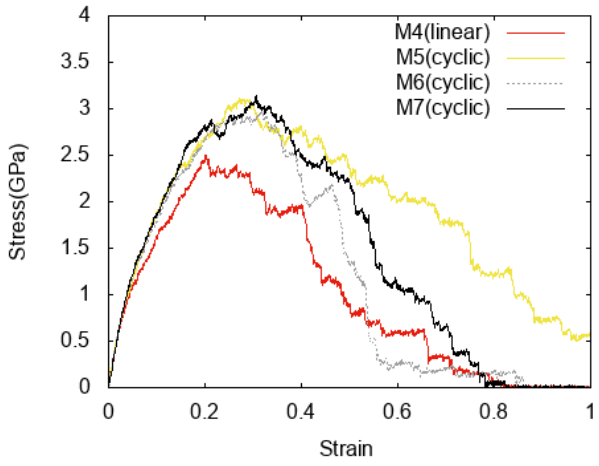

(b)

Figure 4.14 Uniaxial stress-strain curves of NASH gels that generated from linear or cyclic oligomers: (a) Si/Al=2; (b) Si/Al=3

Figure 4.14 compares NASH gels generated from linear or cyclic oligomers. Those structures with the same Si/Al ratio are shown in each figure. Compared

to the linear structure, cyclic ones present much higher tensile strength and slightly higher modulus. As listed in **Table 4.3**, at Si/Al ratio of 2, the tensile strength of cyclic structure (M3) is around 35% higher than that of linear one (M2), and that increment for Si/Al ratio of 3 is around 20-25%. The cyclic oligomer leads to an apparent positive effect on the mechanical properties of NASH gels. As discussed in previous sections (**Figure 4.7**), NASH gels from cyclic oligomers have more O_b percentages and higher complexity in finalized network structure than those from linear oligomers. This leads to a higher tensile strength of NASH gels. This conclusion is also acceptable to explain the tensile strength of linear and cyclic structures. Besides, the number of both hydroxyls and water molecules of cyclic ones is less than that of linear ones. This explains that cyclic structures show better mechanical properties than linear structures. On the other hand, those NASH gels from different cyclic oligomers (M5, M6 and M7) show almost the same tensile strength and elastic behaviours, indicating that the different configurations in cyclic oligomers may have a negligible impact on mechanical properties. The main difference is found in the failure stage, as displayed in **Figure 4.14(b)**, while the stress of M6 drops sharply but that of M5 declines much smoother, and it does not gain entire fracture even at the strain of 1. This is related to the chains, rings, and voids distribution in the microscopic structures and will be investigated in future work.

4.5 Concluding Remarks

The NASH gel's microscopic structures, reaction process, and mechanical properties are studied using reactive MD simulation developed based on a practical bottom-up modelling method. Based on the structure-properties relationships of NASH gels, the following conclusions can be made.

(1) NASH gel models developed from oligomers with various Si/Al ratios and configurations based on a realistic bottom-up modelling method can mimic the geopolymerisation reaction. The poly-condensation reaction between hydroxyls on Si and Al atoms, which develops the aluminosilicate network and generates water molecules, is successfully simulated and described.

(2) Geopolymerisation degree is estimated based on the number of water molecules and bridge oxygen atoms. More than 50% of the hydroxyls in oligomers are consumed to generate water and new bridge oxygen. NASH gels with a higher Si/Al ratio and linear configuration show a higher reaction degree, while those with cyclic oligomers exhibit a higher complexity network structure.

(3) The Si/Al ratio in NASH gels can influence their structures in skeleton bond angle distribution and water mobility. Decreasing the Si/Al ratio, which indicates more Al elements in NASH gels, can reduce the bond angle of aluminosilicate chains and further decrease the structure's stability. The increase of Al atoms also increases the attraction to hydroxyls and hydrogen, restricting the dynamic water diffusion.

(4) The aluminosilicate chains breakage and hydrolysis reaction are observed during the tensile deformation of NASH gels at the yield stage. It is found that 2.5% of the generated water molecules are dissociated, reflecting the number of breakage chains. Moreover, breakages of aluminosilicate chains mainly occur on the Al-O bonds instead of Si-O bonds.

(5) The Si/Al ratio and configuration of oligomers significantly impact the mechanical properties of NASH gels. Increasing the Si/Al ratio enhances both tensile strength and elastic modulus of NASH gels. The NASH gels with cyclic oligomers exhibit more than 20% higher tensile strength than those with linear oligomers. The enhancement in tensile strength is mainly attributed to increased bridge oxygen, especially Si-O-Si bond numbers. The increase of elastic modulus is mainly attributed to the reduction in hydroxyl radicals and enhanced network complexity of NASH gels.

In summary, the geopolymerisation process of NASH has been simulated, and the structure-properties relationship has been described comparatively between different aluminosilicate oligomers. It provides valuable insights on the understanding and design optimization of geopolymer materials. Moreover, based on the developed model, mechanical and dynamic properties can be further investigated to correlate, illustrate and predict the macro properties of geopolymer material.

Chapter 5

Molecular Dynamic Study of Interaction between Amorphous Silica and NASH Gels[†]

5.1 Synopsis

Nano-modification has been an effective approach to improve the mechanical properties and durability of geopolymer materials. This study investigates the interaction between amorphous nano-silica and sodium-alumino-silicate-hydrate (NASH) gel at the atomic level. A realistic composite model is constructed to characterise the geopolymerisation reaction on the amorphous nano-silica substrate. The atomic structure, dynamic properties, and mechanical performances of NASH gels with Si/Al ratios from 1.5 to 3.0 are compared to investigate the role of amorphous silica in geopolymer. The reaction between

[†] The work in this chapter is submitted to journal

Guan, X., Xu, M., Li, B.[*] & Do, H.[*] (2022). "Molecular dynamic study of interaction between amorphous silica and sodium-alumino-silicate-hydrate gels." *The Journal of Physical Chemistry C*, Under review.

the two phases is observed in the interfacial transition zone (ITZ) with a thickness of around 10 Å. With the incorporation of amorphous silica, the reaction degree and complexity of the generated aluminosilicate skeleton structure in NASH gel have been improved by approximately 10% and 6%, respectively. Consequently, NASH gel modified by silica exhibits a denser structure and lower ions' diffusion rate than the neat NASH gel, particularly at a low Si/Al ratio. Moreover, the simulation results indicate that the tensile strength of the ITZ is higher than that of NASH with or without amorphous silica, while the tensile strength of the silica-modified NASH gel is 10~40% higher than that of the neat NASH gel. The NASH gel modified by silica can achieve the optimum uniaxial tensile strength of around 4.1 GPa at Si/Al ratios of 2.5 and 3.0. Thus, this study has proved the reactivity of nano-silica in geopolymer and profiled its positive effects on NASH gel at the atomic level.

5.2 Introduction

In recent decades, nanoparticles have been incorporated into geopolymer materials to improve their performance (Jindal and Sharma 2020). Due to the unique physical and chemical features derived from their ultrafine particle size, it can produce the construction material with improved mechanical properties and durability (Lazaro et al. 2016). Ahmed et al. (2022) reviewed geopolymers modified with various types of nanoparticles, and concluded that nano-silica is the most widely used nanomaterial in geopolymer composites. Nano-silica used in construction materials dominantly consists of amorphous silicon dioxide, which is in spherical particles with a primary diameter of lower than 150 nm and is obtained from vaporizing silica between 1,500 and 2,000 ^{o}C in an electric arc furnace by reducing quartz (Quercia and Brouwers 2010). It is found that nano-silica in geopolymer matrix not only physically fills up fine pores and voids in the microstructure, but also chemically reacts with the precursors (Li et al. 2021).

Existing studies have demonstrated that the use of nano-silica can enhance the mechanical strength and durability of geopolymer (Lo et al. 2017; Zidi et al.

2021). Mustakim et al. (2021) investigated the effect of nano-silica dosage on the properties of geopolymer concrete, and found that adding 1.5% nano-silica increases the compressive strength by 11%. This is caused by the densified matrix and the enhanced geopolymerisation after the incorporation of nano-silica. However, an excessive amount of nano-silica slightly decreases the compressive strength of geopolymer due to their agglomeration effect. Similar observations have been reported by other studies (Khater 2016; Kotop et al. 2021; Nuaklong et al. 2020). Rabiaa et al. (2020) reported that the flexural strength of geopolymer concrete can be increased by 23% after incorporating 4% of nano-silica. Adak et al. (2017) found that the elastic modulus of geopolymer concrete is increased by 21% after adding 6% of nano-silica. For the durability of geopolymer materials with nano-silica, Nuaklong et al. (2018) reported that adding 1% of nano-silica decreases the water absorption capacity of high calcium fly ash geopolymer concrete by 55.3%. Deb et al. (2016) studied the effect of adding nano-silica on the mass loss and compressive strength of geopolymer mortar after a sulfuric acid attack for 90 days, and found that both the mass loss and strength loss are reduced significantly by the addition of 2% nano-silica. In general, the nano-silica can modify geopolymer through densifying microstructure (Ibrahim et al. 2018), creating extra crystalline phases (Ismail et al. 2014), producing nucleation site and thicker geopolymer gel (Revathi et al. 2018), decreasing structural pore size (Lo et al. 2017), and enhancing the polymerisation degree (Sun et al. 2020) in geopolymer composites. It can be found that most existing studies investigate the mechanism of nano-silica modification by characterising the microstructure of geopolymer products. However, few studies have been devoted to investigating the influence of nano-silica on the geopolymerisation reaction at a molecular or atomic level. The change of atomic structure, the chemical composition of NASH gel, and the reaction kinetic at the geopolymer-silica interface remain unclear.

Moreover, the MD simulation can be used to study the atomic interaction at the interface of composite materials. Bahraq et al. (2022) summarized that the interfacial mechanism, structure details, energy and mechanical/dynamic properties can be obtained by MD simulations. Sadat et al. (2018b) investigated the atomic structural properties (e.g. bond length and angle variation) at the

interface between NASH and CSH gels, and calculated the fracture toughness, tensile strength and tensile modulus of the composites. Kai and Dai (2021) performed MD simulations of the geopolymer binder-aggregate interface with a reactive force field. They chemically analysed the interfacial bond between geopolymer and crystalline SiO_2, structurally identified the interfacial transition zone (ITZ) and mechanically computed the interfacial strengths. Thus, MD simulation is an effective computational tool for characterising the interfacial mechanism of cementitious composite materials. However, the atomic interaction between NASH gel and amorphous nano-silica, and the geopolymerisation reaction at the interface remain unclear.

In this work, reactive MD simulation is employed to investigate the geopolymerisation reaction on the surface of the amorphous nano-silica substrate. The geopolymerisation reaction is simulated based on a bottom-up approach at an atomic level, which is the poly-condensation reaction between various protonated aluminosilicate oligomers. Based on the composite model, the atomic structure, dynamic properties and mechanical performances of the geopolymer-silica interface can be characterised, followed by the investigation on the interaction between two phases. The role of amorphous silica in geopolymerisation reaction is analysed by comparing the original neat NASH gel with the NASH gel modified by silica.

5.3 Computational Details

5.3.1 Model construction

5.3.1.1 Modelling of the amorphous silica

Considering the main chemical composition of nano-silica is amorphous silica, the orthorhombic amorphous SiO_2 cell with an edge dimension of a few nanometres is often selected to build a representative molecular model for nano-silica. The amorphous structure is obtained from the melt-annealing-equilibrium process from the crystalline structures, which is a general method for generating amorphous materials in experiment or simulation work (Issa et

al. 2020; Li et al. 2017; Vo et al. 2020). The initial crystalline silica model is obtained from the unit cell of α-crystalbalite structure, as shown in **Figure 5.1** . A simulation cell with a size of 19.9 Å × 19.9 Å × 20.8 Å is first built. The orthorhombic crystal cell is then subjected to the melt-annealing-equilibrium procedure to acquire the amorphous silica model.

5.3.1.2 Geopolymerisation reaction and NASH gels

A similar melt-annealing-equilibrium (lower melting temperature than that for amorphous silica) approach is employed to construct the amorphous geopolymer NASH gel model. Firstly, several hundreds of oligomers with various original Si/Al ratios (i.e. 1, 2 and 3) and different configurations (i.e. linear or cyclic), together with the same number of Na ions (for charge balancing of the AlO_4 tetrahedrons) are randomly placed into the cubic simulation box to make an initial model with an initial density of 2.0 g/cm^3. To make the NASH gel models with various final Si/Al ratios (i.e. 1.5, 2.0, 2.5, 3.0), different compositions of the oligomers are used to generate the four initial models, each with around 20,000 total atoms, as listed in **Table 5.1** . The compositions are determined based on the targeting final Si/Al ratios and with the rules that oligomers with the same Si/Al ratio (i.e. Mo2 and Mo3, or Mo4, Mo5, Mo6 and Mo7) occupied the same percentage in each model. Secondly, those initial structures are subjected to the melt-annealing-equilibrium process to acquire the equilibrated amorphous NASH gel structures, during which the geopolymerisation reaction happens, and the 3-D cross-linked network structure can be established.

5.3.1.3 Composites and the interface

The composite models are constructed based on the above-generated models to investigate the interface between nano-silica and geopolymer gel. A vacuum layer is made on the upper XY plane surface of the amorphous silica cell. The corresponding types and numbers of oligomers are randomly placed into the vacuum layer, but kept a distance of 3 Å from the surface of the silica substrate. Afterwards, the composite systems are subjected to the same melt-annealing-equilibrium simulation as that for geopolymerisation reaction, during which the

poly-condensation reaction happens on the amorphous silica substrate. As a result, four composite systems are prepared with four typical original Si/Al ratios in NASH gels, named NASH-s. The total atom number in the composites is set as around 23,000 and the detailed compositions are listed in **Table 5.1**. The interface between NASH gels and amorphous silica can be observed and the properties of silica-modified NASH gels can be compared with the neat NASH gels.

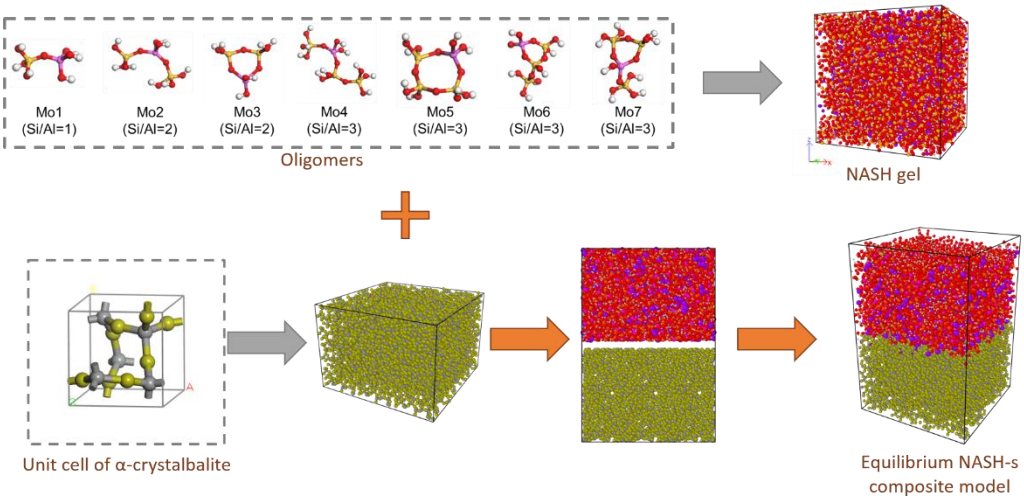

Figure 5.1 Diagram of the modelling procedure of the NASH gel and NASH-silica composite: yellow is silicon in NASH, pink is aluminium, red is oxygen in NASH, purple is sodium, white is hydrogen, grey is silicon in SiO_2, and gold is oxygen in SiO_2

Table 5.1 The number of oligomers used for the initial model of the NASH gels and composites

NASH model	Numbers of the oligomers							Si/ Al ratio	Na ions	NASH atoms	Silica atoms
	Mo 1	Mo 2	Mo 3	Mo 4	Mo 5	Mo 6	Mo 7				
C15	648	162	162	27	27	27	27	1.5	1,080	19,791	0
C15-s	432	108	108	18	18	18	18		720	13,194	10,368
C20	192	288	288	48	48	48	48	2.0	960	19,824	0
C20-s	124	186	186	31	31	31	31		620	12,803	10,368
C25	86	129	129	129	129	129	129	2.5	860	19,952	0
C25-s	56	84	84	84	84	84	84		560	12,992	10,368
C30	0	0	0	195	195	195	195	3.0	780	20,085	0
C30-s	0	0	0	125	125	125	125		500	12,875	10,368

5.3.2 Force field

The force field used for MD simulation in this study is the reactive force field (ReaxFF), developed by Van Duin et al. (2001). It is used to express both the inter- and intra-molecular interactions based on bond order and coordination number of all atoms, simultaneously adjusting the charges of various species dynamically. Thus, this force field can automatically calculate the bond dissociation and formation, and simulate chemical reactions. Some studies have successfully employed this force field to simulate the CSH and NASH gels (Fan and Yang 2018; Hou et al. 2018), amorphous silica (van Duin et al. 2003; Yeon and van Duin 2016), and the interface between different compositions (Fan et al. 2017; Kai et al. 2020). The parameters for various species of atoms in this study can be referred to the Appendix I.

5.3.3 Simulation procedure

5.3.3.1 Melt-annealing-equilibrium

The simulation is carried out using the large-scale atomic/molecular massively parallel simulator (LAMMPS) (Plimpton et al. 2007) package with a time step of 0.25 fs. Firstly, the cubic α-crystallite model, which is boundary periodic and with 576 atoms, is energy-minimized based on the conjugated gradient algorithm with an energy tolerance criterion of 10^{-4}, followed by an equilibrium running under the canonical (NVT) ensemble with a temperature of 300 K (room temperature) for 5 ps. Afterwards, the simulation cell is heated up to 7,000 K for 5 ps to melt the crystal phase and remove any memory effects before the slowly cooling step with a temperature reducing rate of 10 K/ps until 300 K. Subsequently, the structure is equilibrated under the isothermal-isobaric (NPT) ensemble with a temperature at 300 K and a pressure of 0 Pa for 200 ps to obtain the equilibrated density. Finally, the simulation cell is duplicated by 3 × 3 × 2 to obtain an orthorhombic supercell with the dimensions of 58.86 Å × 58.86 Å × 40.98 Å and 10,368 atoms in total, before being subjected to NVT ensemble at 300 K for another 200 ps. The method to generate the amorphous silica structure can be referred to Yuan and Huang (2012). On the other hand, the neat amorphous NASH gel structures with various Si/Al ratios are also obtained from

a similar melt-annealing-equilibrium procedure. However, the melting temperature is 2,100 K and the cooling rate of the system is 3 K/ps.

To simulate the geopolymerisation reaction on the amorphous silica substrate, the initial oligomers are placed above the obtained amorphous silica model along the z-direction. Afterwards, the boundary at the z-direction is set as non-periodic and shrink-wrapped condition. Therefore, there is only one interface between the NASH gel and amorphous silica in the model in the middle of the simulation box. Subsequently, the composite systems are subjected to the same melt-annealing-equilibrium procedure as that for the neat NASH gel structures to simulate the comparable compositions of oligomers at the same reaction condition.

5.3.3.2 Structure characterization

The structural analysis of the NASH gel molecular models is based on the trajectories obtained from the MD simulation. The bond lengths between different pairs can be represented by the radial distribution function (RDF). Moreover, it can also be compared with the X-ray total scattering experimental result of materials for model validation. The result of RDF is averaged from 100 trajectories in NVT simulation duration of 20 ps.

During MD simulation, the bulk density of the simulation boxes can be calculated from the total weight and volume of the simulation cell. It can be compared to the experimentally measured density results. Moreover, the density distribution of the simulation cell and intensity of each atom type can also be computed for the equilibrated models. In this study, density distribution is profiled along the z-direction of the composite systems, which is perpendicular to the interface. The atom intensity is calculated by separating the simulation box into slabs with a thickness of 2 Å along the XY plane. The data are obtained by averaging 200 trajectories during the simulation under NVT ensemble of 5 ps.

Reaction degree is another parameter that reveals the structural properties and the effect of amorphous silica on geopolymerisation reaction. Under the reactive

MD simulation, the equilibrium NASH gel models are acquired from the poly-condensation reaction, in which the oligomers are polymerised and water molecules released. Thus, the geopolymerisation reaction degrees in various systems are reflected by the number of consumed OH groups. On the other hand, the number of bridge oxygen atoms in the system reveals the amount of connected tetrahedrons and the complexity of the 3-D cross-linked network structure.

5.3.3.3 Dynamic properties

The mean square displacement (MSD) calculates the diffusion of various atoms in the systems in MD simulation. To acquire the dynamic MSD curves, the displacement distance of the atoms is recorded at 25 fs intervals and averaged over 100 ps during the NVT production stage. The diffusion coefficients are obtained from the slope of the MSD curves. The comparison of D values indicates the mobility difference between different types of atoms or the same type of atom in various systems.

5.3.3.4 Uniaxial tensile simulation

The mechanical properties of the NASH gels or the NASH-silica composite systems are computed from the uniaxial tensile simulations of the models along the z-direction (perpendicular to the interface). As the models are equilibrated with a non-periodic boundary along the z-direction, the densities of the edge layers of the XY plane are relatively lower, as shown in **Figure 5.2**. Therefore, the uniform tensile simulation achieved by adjusting the z-coordinates of all atoms (i.e. the simulation method applied in Chapter 4) cannot be employed. In this study, the thin upper and bottom layers of the simulation box are fixed and the uniaxial tensile loading is applied to the upper layer along the z-direction under the NVT ensemble at 300 K, to employ a constant engineering strain rate of 0.01/ps to the unfixed part. It indicates that the length of the simulation box in the z-direction changes linearly with time. During the tensile loading, the internal stress of all the atoms along the z-direction is calculated and summed to acquire the stress-strain curves of various systems. The thicknesses of the fixed layers are 5 Å for the pure NASH gels and amorphous silica but are 10 Å

for the NASH gels in the composite systems, as shown in **Figure 5.2**. The density of the top of the composite system is found to be relatively low due to the non-periodic boundary at the z-direction. To guarantee effective fixing, a thicker fixed layer is employed in this study.

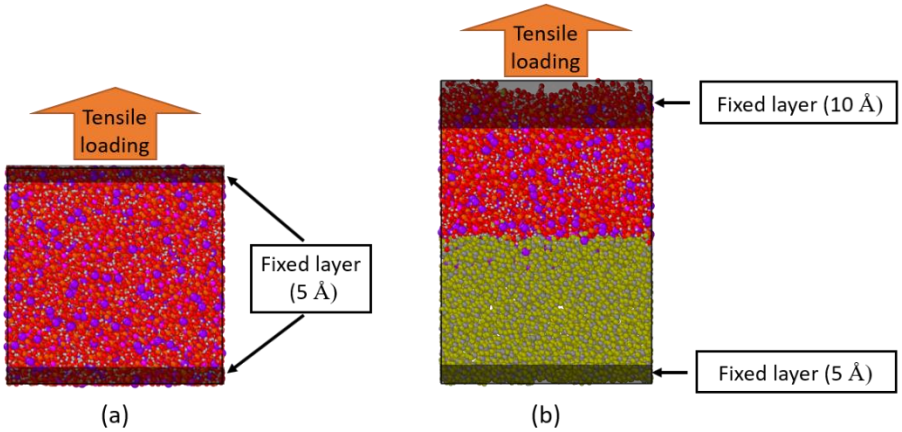

Figure 5.2 Tensile loading diagram of the equilibrated structure of: (a) C25 NASH gel and (b) C25-silica composite: yellow is silicon in NASH, pink is aluminium, red is oxygen in NASH, purple is sodium, white is hydrogen, grey is silicon in SiO_2, and gold is oxygen in SiO_2

5.4 Results and Discussion

5.4.1 Microscopic characteristic

5.4.1.1 Density distribution in the composites

To study the effect of amorphous silica on the geopolymerisation reaction, four composite systems with different original Si/Al ratios (i.e. 1.5, 2.0, 2.5 and 3.0) have been built accordingly. A snapshot of the annealed and equilibrated structure of model C25-s is shown in **Figure 5.3** as a typical example. It can be found that the region below 45 Å in the z-direction is the amorphous silica substrate and the above layer is the NASH gel modified by silica. The average bulk density of the silica phase is around 2.4 g/cm^3, which agrees with the solid density of nano-silica used in cementitious materials (Adak et al. 2017; Shahrajabian and Behfarnia 2018). On the other hand, the average density of the NASH gel is around 2.0 g/cm^3, which is also close to the experimental

results from the literature (Nematollahi et al. 2015; Wang et al. 2005). Overall, both models for amorphous silica and NASH gel are reasonable based on the materials' densities. It is observed that there is a zone at the interface that contains atoms both from silica and NASH phases, which is defined as the interfacial transition zone (ITZ) of this composite. It indicates that after the reaction and equilibrium process, the atoms in one of the phases can interact, diffuse, and even react with the atoms from the other phase. Besides, the Na ion's intensity curve shows a significant peak in the ITZ, indicating a high probability of Na ions in the ITZ. This subsequently affects the density of ITZ and the diffusion of Na ions.

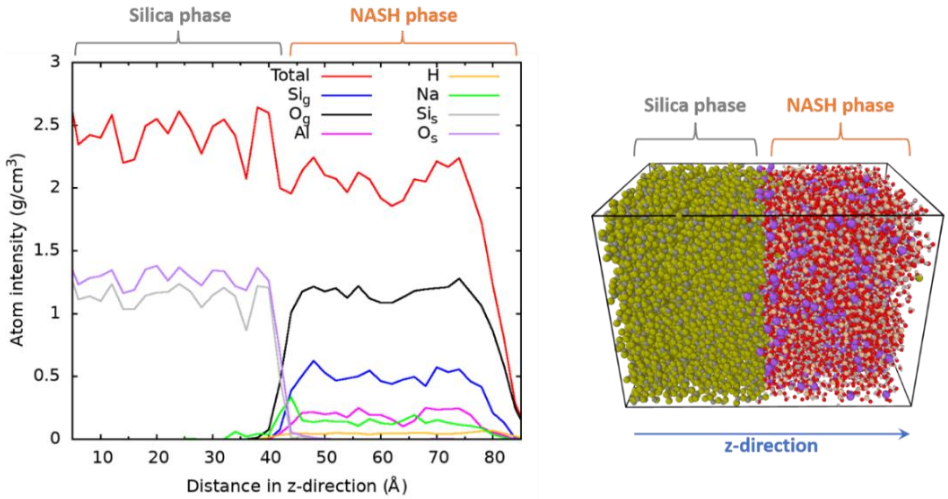

Figure 5.3 Density distribution of C25-silica composite system along z-direction: Si_g and O_g are silicon and oxygen atoms originally from the NASH oligomers, Si_s and O_s are silicon and oxygen atoms originally from the amorphous silica

Moreover, the atom intensity curves of the four composite systems are compared in **Figure 5.4(b)**. Similar density values and ITZ regions can be found in all the systems. As displayed in **Figure 5.4(a)**, the ITZ is marked in blue colour and the NASH-s phase is shown in orange colour. The ITZs are the regions between the z-direction positions where the intensity of Si_s and Si_g atoms starts to decline. As seen in **Figure 5.4(b)**, the ITZs in the four systems are all in the range of 38-48 Å. Thus, the properties of ITZ in this study are computed based on this region. In the upper region, the density of the composites (i.e. above 75 Å) is not evenly distributed due to the non-periodic and shrink-wrapped boundary and is much lower than that of the region from 48 to 75 Å. Consequently, the upper region is not considered as the normal

NASH gel, and the properties of NASH modified by silica (i.e. NASH-s) in this study are computed based on the region from 48 to 75 Å.

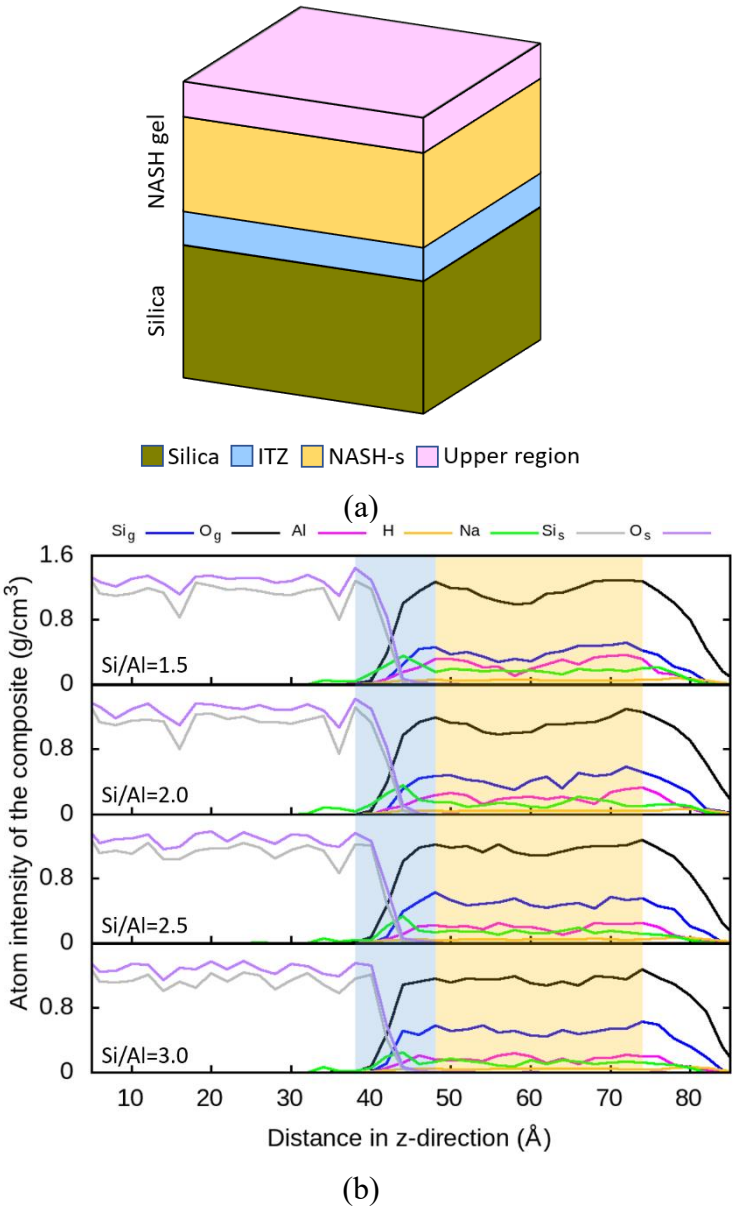

Figure 5.4 (a) Definition of different layers in the composite system: amorphous silica substrate, interfacial transition zone (ITZ), NASH-s regions; (b) atom intensity distributions along the z-direction in the composite systems with various original Si/Al ratios of 1.5, 2.0, 2.5 and 3.0

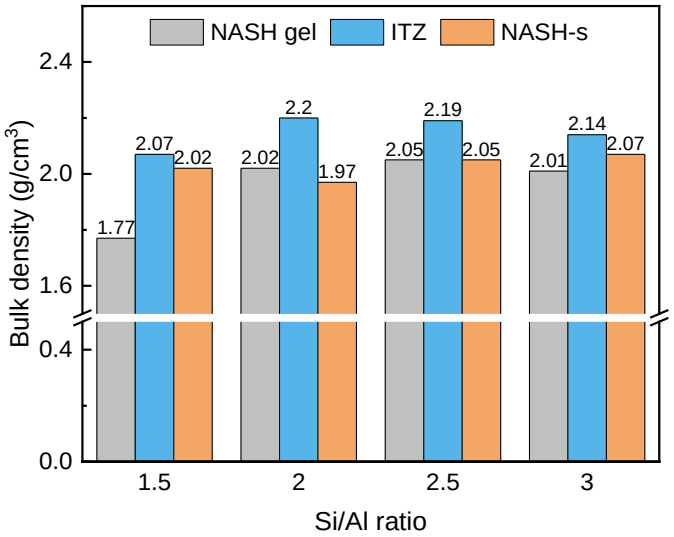

Figure 5.5 The bulk density of the neat NASH gel, the ITZ and NASH-s gel in the composite systems with various original Si/Al ratios of 1.5, 2.0, 2.5 and 3.0

The average bulk densities of the regions are calculated and compared for the neat NASH gels with various Si/Al ratios, as shown in **Figure 5.5**. The density of the neat NASH gels increases with the Si/Al ratio. The neat NASH gel with a Si/Al ratio of 1.5 shows the lowest density of 1.77 g/cm^3, while the other three models have densities around 2.0 g/cm^3. The neat NASH gel with a Si/Al ratio of 2.5 exhibits the highest density of 2.05 g/cm^3. On the other hand, the densities of ITZs in the four composites are much higher than those of neat NASH gels. They range from 2.07 g/cm^3 to 2.29 g/cm^3 as the Si/Al ratio increases from 1.5 to 3.0. This is caused by the higher density of amorphous silica material compared to NASH gels. A similar density increase at the interface is also found by experiment in the literature. Hosan et al. (2021) observed fewer pores and higher density at the ITZs on slag and fly ash particles with the incorporation of nano-silica by SEM. Moreover, the bulk densities of NASH gels modified by silica are around 2.0 g/cm^3. At a Si/Al ratio of 1.5, the density of NASH-s (e.g. 2.02 g/cm^3) is 14% higher than that of the neat NASH gel. However, the densities of NASH-s vary marginally as the Si/Al increases. The results indicate that using amorphous silica can bring a denser structure to the NASH gels generated on its surface, especially for those with lower original densities. This result agrees with the experimental finding that nano-silica can provide a denser and more homogenous microstructure for the geopolymer matrix (Ibrahim et al. 2018).

5.4.1.2 RDF of the NASH gels

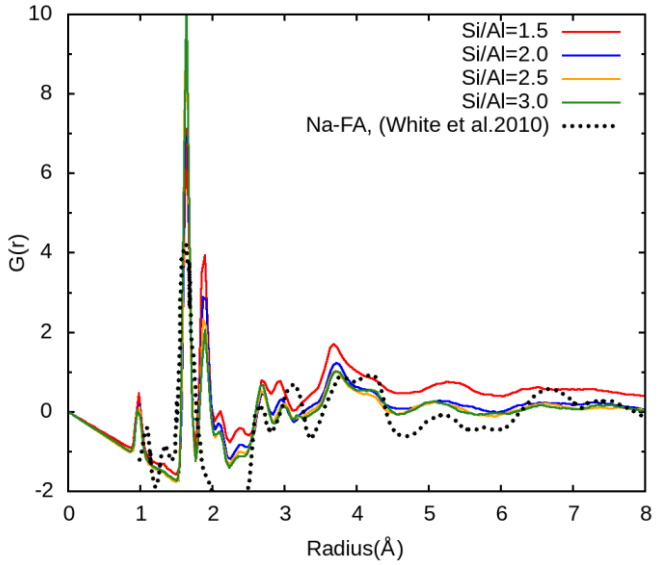

Figure 5.6 Comparison of X-ray radial distribution function curves of NASH gels with Si/Al ratio from 1.5 to 3.0 to the curve of geopolymer materials from experimental results (White et al. 2010)

The RDF curves of the four neat NASH gel models are plotted in **Figure 5.6** and are compared with the experimental result to validate the simulation model. It can be found that there are no significant differences in the peaks' positions of various pairs in the structures of the four models, indicating that they have the same bond types. The first peak at around 1 Å represents the H-O bond in water and hydroxyl radicals. The two highest peaks at 1.6 and 1.9 Å correspond to the Si-O and Al-O bonds, respectively, forming the aluminosilicate skeleton in NASH gels. The intensities of the Si-O and Al-O bonds vary slightly in four models, which is correlated to the various Si/Al ratios. A higher Si/Al ratio means more Si and less Al atoms in the system, and thus the higher Si-O and lower Al-O bond peaks are found in the RDF curves. Moreover, the small peak at around 2.5 Å in the curves represents the Na-O bond. The other peaks in the curves are correlated with O-O, Si-Si and Si-Al pairs, whose interatomic distances are not calculated from direct chemical bonds but the spatial structures of the skeleton. White et al. (2010) reported the experimental X-ray PDF results of Na-based FA geopolymer during the geopolymerisation reaction. The H-O bond at around 1 Å and T-O bond (T is Si or Al) at 1.5-2.0 Å are found in the experimental results, which is in a good agreement with the simulation results

in this study. Furthermore, Lolli et al. (2018) reported that Na ions in the NASH structure mainly located in oxygen circles. Walkley et al. (2018) studied the synthetic NASH gel by solid state NMR spectroscopic and observed the Na ions coordinated by bridge oxygen and water oxygen with bond length of around 2.66 Å. Their findings are in line with the simulated results in this study. Overall, the developed model in this study can simulate the NASH gels.

5.4.1.3 Comparison of RDF

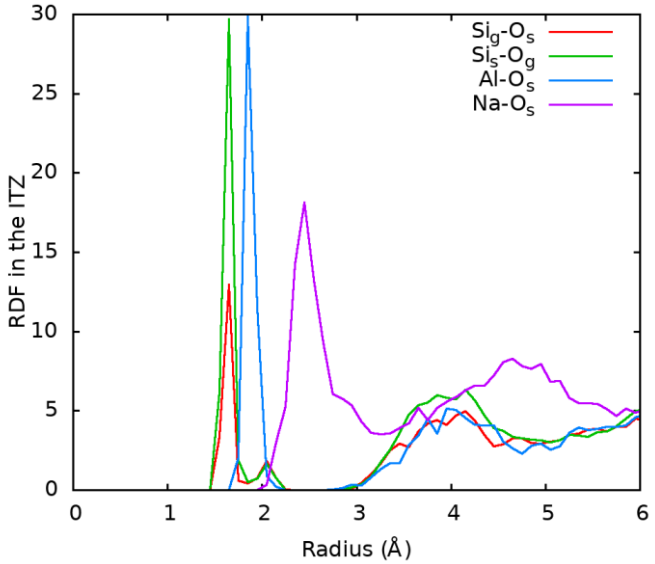

Figure 5.7 The radio distribution function (RDF) of various pairs between atoms from amorphous silica and NASH oligomers in the ITZ of C25-s composite systems: Si_g and O_g are silicon and oxygen atoms originally from the NASH oligomers, Si_s and O_s are silicon and oxygen atoms originally from the amorphous silica, Al and Na are Al and Na atoms from NASH gel

The RDF in ITZ can reflect the atomic interaction between silica phase and NASH-s phase at the interface. The RDF curves of several pairs in ITZ of the C25-s composite system are displayed in **Figure 5.7**. The Si and O atoms in the system have been separated into two types, i.e. Si_g and O_g atoms originally belonging to the aluminosilicate oligomers, and Si_s and O_s atoms originally belonging to the amorphous silica. Overall, the apparent peaks of curves in the figure reveal that these pairs have strong interactions and can form covalent or ionic bonds in ITZ. There is a sharp peak for pairs of Si_g-O_s and Si_s-O_g at a radius of around 1.6 Å, which represents the covalent bond in Si tetrahedrons. This indicates that O and Si atoms in amorphous silica can both react with aluminosilicate oligomers, forming the NASH gel structure. The peaks of Si_g-

O_s and Si_s-O_g curves are at the same radius' position, meaning that the Si-O bonds in two phases present the same property. Furthermore, the occurrence of peaks of Al-O_s and Na-O_s pairs reflects there is a strong interaction between O atoms from silica phase and Al or Na ions from NASH gel. The positions of peaks at around 1.9 Å and 2.5 Å in the NASH-s are also comparable to those in neat NASH gels. It means that O_s plays the same role as O_g in the aluminosilicate structure. Consequently, it is observed that the amorphous silica can react with the NASH gel at an atomic level, and the structure of reaction product is similar to that of the neat NASH gel.

Figure 5.8 compares the RDF curves of Si-O, Al-O and Na-O pairs in various phases with an original Si/Al ratio of 2.5, including the neat NASH gel, amorphous silica substrate, ITZ, and NASH-s. As seen in **Figure 5.8(a)**, the main peaks of the Si-O bond in various phases locate at the same position around 1.65 Å. It means the Si-O bonds have the same length in both silica and NASH gel phases. It has been reported that the Si-O bond is very stable and exists in the four-coordinated oxide tetrahedron structure in NASH gel (Duxson et al. 2006a), which is the same as that in amorphous silica structures (Issa et al. 2020; Mantisi et al. 2012). Thus, the bond type of Si-O in these materials keeps unchanged in geopolymerisation. (Issa et al. 2020; Mantisi et al. 2012). Thus, the bond type of Si-O in these materials keeps unchanged in geopolymerisation. **Figure 5.8(b)** shows the RDF curves of Al-O bond in various phases. The absent of Al-O curve in silica is due to no Al atoms exist in the silica phase. Like the Si-O bond, all Al-O peaks locate at the same position of 1.85 Å. It means the silica substrate also has a negligible impact on the Al-O bond length in geopolymerisation

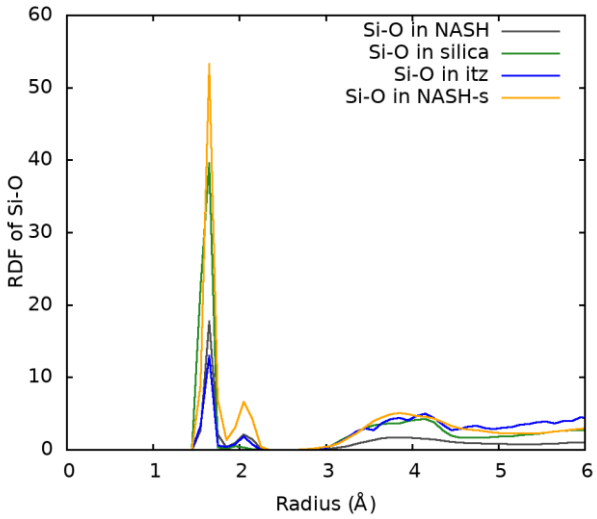

(a)

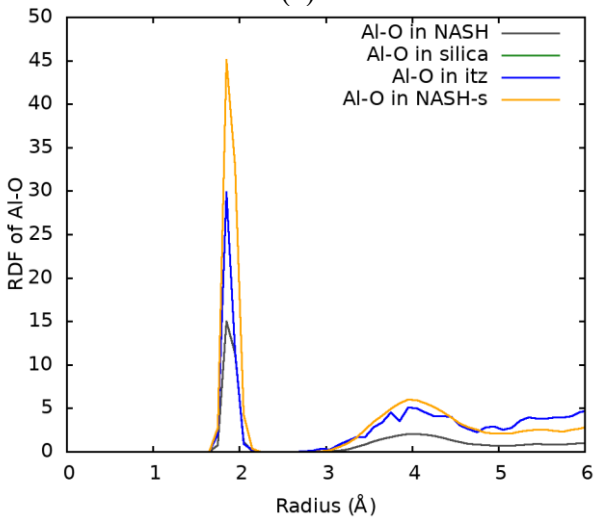

(b)

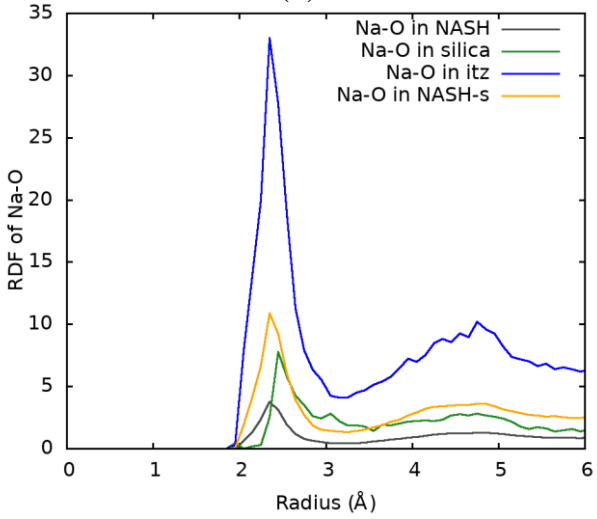

(c)

Figure 5.8 The comparison of radio distribution function (RDF) of various pairs in the neat NASH, amorphous silica phase, ITZ and NASH-s phase in the C25-s composite system: (a) RDF comparison of Si-O pairs; (b) RDF comparison of Al-O pairs; (c) RDF comparison of Na-O pairs

Figure 5.8(c) compares the RDF of Na-O pairs in various phases. The main peak of Na-O pairs in all phases locates at around 2-3 Å, but a slight difference of the peaks' positions in the four curves is found in various phases. Specifically, the peaks of RDF curves in the neat NASH, the NASH-s and ITZ start at 2 Å and reach the highest values at 2.37 Å, while that of silica phase starts at 2.25 Å and reaches the highest value at 2.46 Å. The shift of the peak to the larger radius means a weaker interaction between Na and O atoms in the silica phase. The Na-O pair's RDF curve in NASH and ITZ phase represents the interaction of Na ions with both bridge oxygen and water oxygen atoms. Walkley et al. (2018) identified the geopolymer materials with 3Q-MAS solid state NMR spectroscopy and proposed the NASH gel molecular structure, in which Na ions are 6-coordinated (i.e. containing 3 or 4-coordinated by bridge O and the remaining are occupied by water molecules). The more water molecules occupation leads to the shorter Na-O bond length. Besides, Lyngdoh et al. (2019) simulated the water adsorbed NASH gel and observed a minor peak at 2.0 Å, which is brought by water molecules, except for the main Na-O peak at 2.3 Å. This indicates that the bond length between Na and water O is shorter than that between Na and bridge O. Therefore, the peak of Na-O bond shifts to a larger radius as there is no water molecule in the silica phase, indicating a weakened interaction between Na and O in the silica phase.

5.4.2 Reaction degree and diffusion rate

5.4.2.1 Geopolymerisation reaction degree

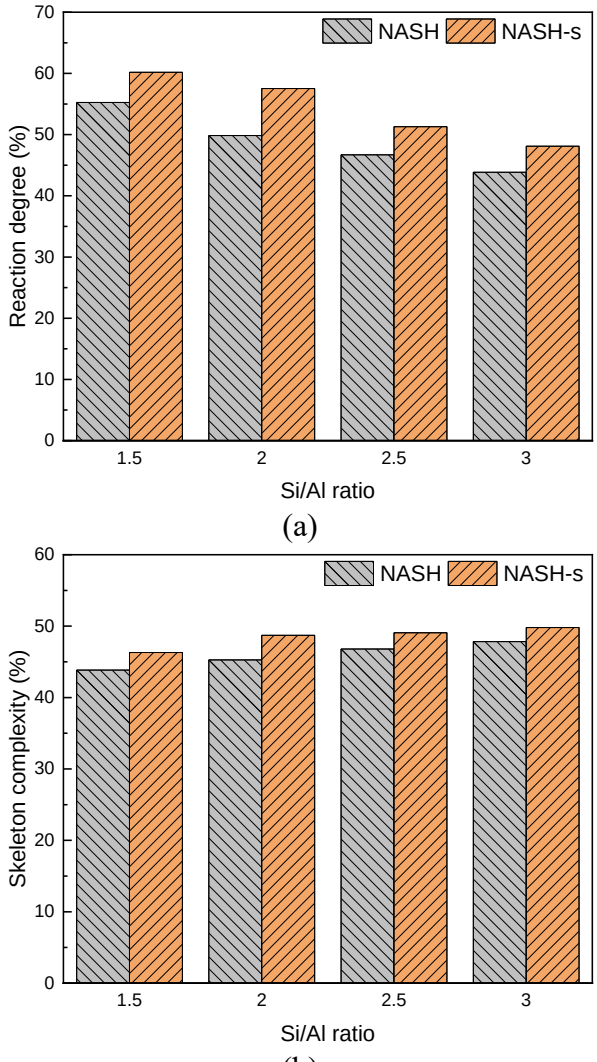

Figure 5.9 Comparison of reaction degree and skeleton complexity of NASH (i.e. pure NASH gel) and NASH-s (i.e. NASH gel generated on silica substrate) with various Si/Al ratios of 1.5, 2.0, 2.5 and 3.0: (a) reaction degree; (b) skeleton complexity

To analyse the effect of amorphous silica on the geopolymerisation, the reaction degree and NASH skeleton complexity are compared between the neat NASH and the silica-modified NASH gels with various original Si/Al ratios. Since the nature of geopolymerisation is the poly-condensation reaction between hydroxyl radicals in the oligomers, the reaction degree is calculated from the ratio of consumed OH radicals' number in the equilibrium structure to the total original OH radicals' number in the oligomers. The skeleton complexity is

represented by the percentage of bridge oxygen atoms (i.e. the O atoms which connect Si and Al tetrahedrons in the structure) to the total oxygen atoms. As shown in **Figure 5.9(a)**, the reaction degree of the neat NASH gels decreases from 55.3% to 44.8% as the Si/Al ratio increases from 1.5 to 3.0. This is due to the larger numbers of OH radicals in the original oligomers at a lower Si/Al ratio, which can increase the probability of atoms collision. In contrast, the skeleton complexity of NASH gel increases with the Si/Al ratio, as displayed in **Figure 5.9(b)**. It is contributed from the more original bridge O atoms in the oligomers at a higher Si/Al ratio. Despite a lower reaction degree, a larger amount of bridge O atoms can be found in the neat NASH gels at a higher Si/Al ratio. It indicates that more Si and Al tetrahedrons are connected to form a more complex 3-D network structure.

The reaction degree and skeleton complexity of NASH can be enhanced by incorporating amorphous silica substrate. In the silica-modified NASH gel with various Si/Al ratios, the reaction degree is improved from the range of 44~55% to the range of 48~60%; the bridge oxygen percentage is increased from the range of 43~48% to the range of 46~50%. It means the reaction degree and skeleton complexity of NASH gels have been improved by around 10% and 6%, respectively. As a result, in the geopolymerisation on an amorphous silica substrate, more OH radicals can react to form a more complex aluminosilicate 3D-crosslinked network structure. It would contribute to improving both the mechanical performance and durability of NASH gels.

Many experimental studies also stated the induced higher geopolymerisation degree by incorporating nano-silica, as the fewer and smaller sizes of unreacted particles of fly ash or slag were found from microscopic characterization (Deb et al. 2015; Phoo-ngernkham et al. 2013). Besides, better thermal stability of geopolymerisation products was observed by TGA, which reveals the thicker NASH gel product attained in silica-modified geopolymer (Revathi et al. 2018). This is attributed to the more sources of Si elements (Mustakim et al. 2021) and more nucleation sites (Revathi et al. 2018) brought by nano-silica. Therefore, this modelling study has explained a similar mechanism at an atomic level and quantitatively calculated the enhancement of reaction degree.

5.4.2.2 Diffusion properties in various regions

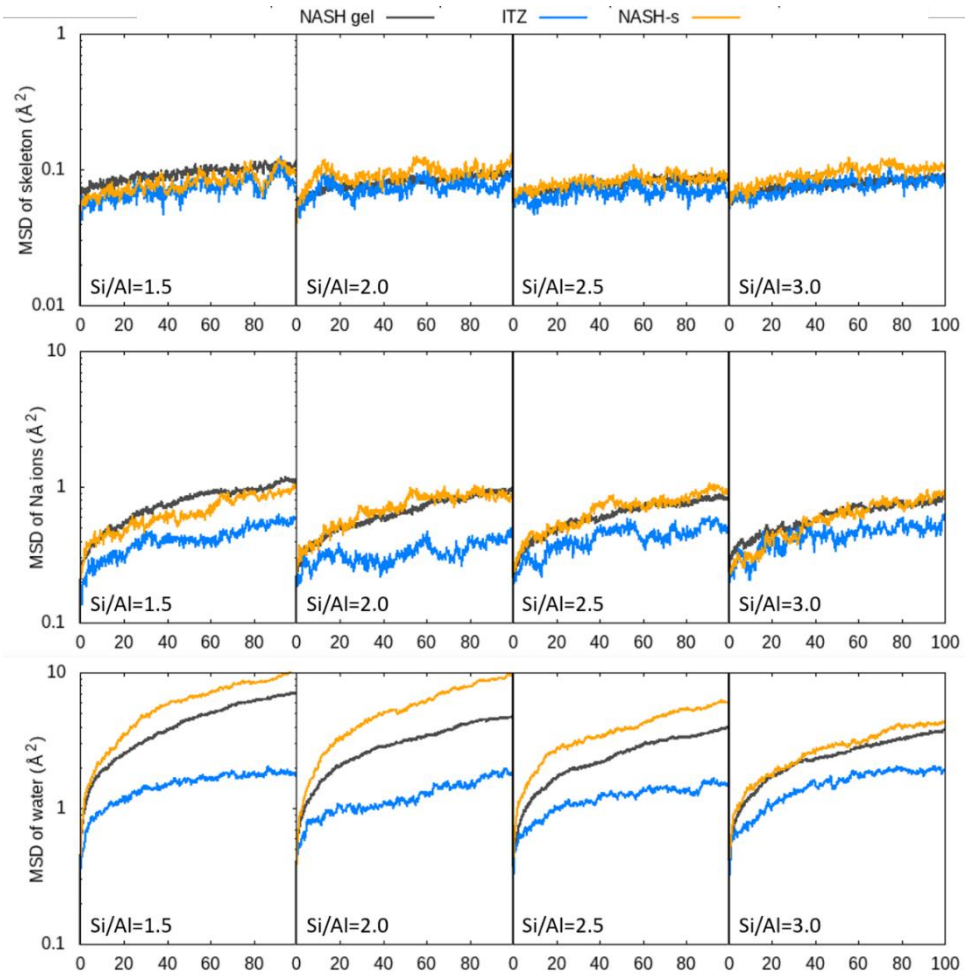

Figure 5.10 The mean square displacement (MSD) of skeleton, Na ions and water molecules in the neat NASH gels, ITZ and NASH-s phase in the composite systems with various original Si/Al ratios of 1.5, 2.0, 2.5 and 3.0

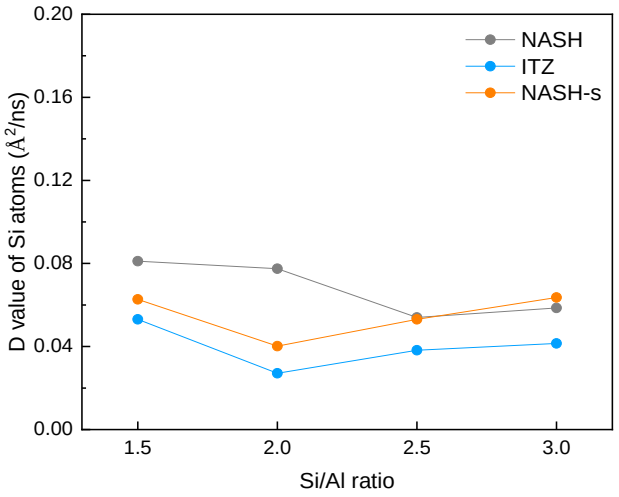

(a)

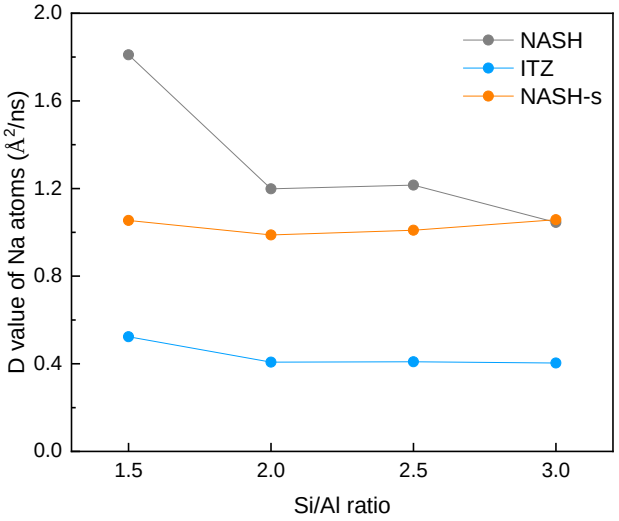

(b)

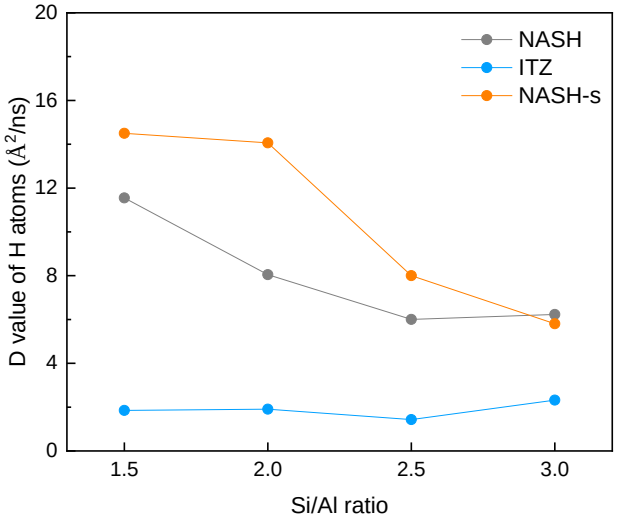

(c)

Figure 5.11 The diffusion coefficients (D values) of skeleton, Na ions and water molecules in the neat NASH gels, ITZ and NASH-s phase in the composite systems with various original Si/Al ratios of 1.5, 2.0, 2.5 and 3.0: (a) D values of Si atoms; (b) D values of Na atoms; (c) D values of H atoms

The mobility of various atoms in the NASH structures is compared to reflect the structure stability and ions' immobilization or leaching behaviour of material (Hou et al. 2020). **Figure 5.10** plots the MSD curves for different phases with various Si/Al ratios, and **Figure 5.11** compares the calculated diffusion coefficients (i.e. D values). The mobility of the aluminosilicate skeleton in NASH gel is represented by Si atoms, while that of the water molecule is calculated from H atoms in the system. Besides, Na ions are used to display the ions' diffusion rate.

As seen in the MSD curves, the D value of H atoms is higher than that of Na ions, and that of Si atoms is at an extremely low level in all Si/Al ratios. Specifically, the calculated D values of Si atoms are all smaller than 0.1 $Å^2$/ns. This means that the Si atoms are tightly restricted by the aluminosilicate chains, indicating the stability of the aluminosilicate structures. Differently, the D value of Na ions ranges from 0.4 to 1.8 $Å^2$/ns, which shows a higher mobility of Na in the structures than that of H atoms. The Na ions are always restricted in the pores and vacancy of the cage structures in NASH gel, but have a much higher mobility than the skeleton atoms (Hou et al. 2020). Besides, the D values of H atoms are higher than the other two atoms, reflecting water has a relatively high mobility in NASH structure. Moreover, the diffusion rates of the atoms almost decline with the increase of Si/Al ratio. For instance, the D values of Na ions in the neat NASH gels drop continually from 1.81 to 1.05 $Å^2$/ns as the Si/Al ratio increases. The D values of H atoms in neat NASH also decline continually from around 12 to 6 $Å^2$/ns as the Si/Al ratio increases. This indicates that NASH gel with a higher Si/Al ratio has a higher stability.

Furthermore, there is a slight difference in the MSDs in the neat NASH and NASH-s. The D values of Na ions in the NASH-s are smaller than those of the neat NASH, indicating that the stability of NASH gel is improved by the incorporation of amorphous silica. A similar phenomenon is also found in experimental study by Sun et al. (2020). They found that the efflorescence of geopolymer mortar can be inhibited by adding nano-silica as it can consume Na ions in the pore solution and densify the structure. Additionally, the difference in Na ions' D values between the neat NASH and NASH-s continuously

decreases as the Si/Al ratio increases. At a Si/Al ratio of 1.5, the D values of Na ions in the NASH-s phase (i.e. 1.05 $Å^2$/ns) is 58% of that in the neat NASH gel (e.g. 1.81 $Å^2$/ns). However, the D values of Na ions in the neat NASH and NASH-s are both around 1.18 $Å^2$/ns at a Si/Al ratio of 3.0. It reveals that the enhancement of stability of NASH gel by silica modification is weakened as the Si/Al ratio increases.

The D values of H atoms in the NASH-s phase are larger than those in the neat NASH gel, as seen in **Figure 5.11(c)**. This can contribute to the transportation of partial Na ions from the silica-modified NASH gel to the ITZ and silica phase, which reduces their restriction to water molecules. In the NASH gel, some water oxygen atoms are ionically bonded to the Na ions, as stated in section 5.4.1.2. Consequently, the reduction of Na ions in the NASH-s decreases the bonding effect, which enhances water molecules' mobility.

5.4.3 Tensile behaviour of the composites

5.4.3.1 Stress-strain curve of the neat NASH gel

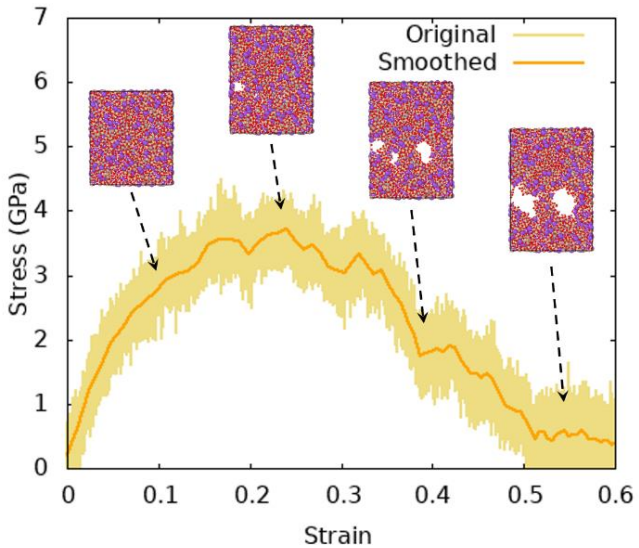

Figure 5.12 Tensile stress-strain behaviour of C25 NASH gel model with snapshots at various strains of 0.1, 0.25, 0.4 and 0.55

Figure 5.12 shows the typical uniaxial tensile stress-strain curve of the neat NASH gel with a Si/Al ratio of 2.5. The curve is smoothed by approximating the data with a Bezier curve that connects the endpoint. The snapshots in the figure display the front view of the simulation boxes at tensile strains of 0.1,

0.25, 0.4 and 0.55. At a strain below 0.1, there is an elastic segment in the stress-strain curve. No obvious crack is found in the simulation box, and the stress is mainly borne by the covalent bond stretching in the structure. The elastic modulus can be calculated from the slope of the curve in this segment. Afterwards, the neat NASH gel enters the yield stage with the appearance of cracks. With further stretching of the simulation box, the highest stress is attained as the uniaxial tensile strength. The cracks continually propagate, and the stress drops quickly at the failure stage until the total fracture of the simulation box.

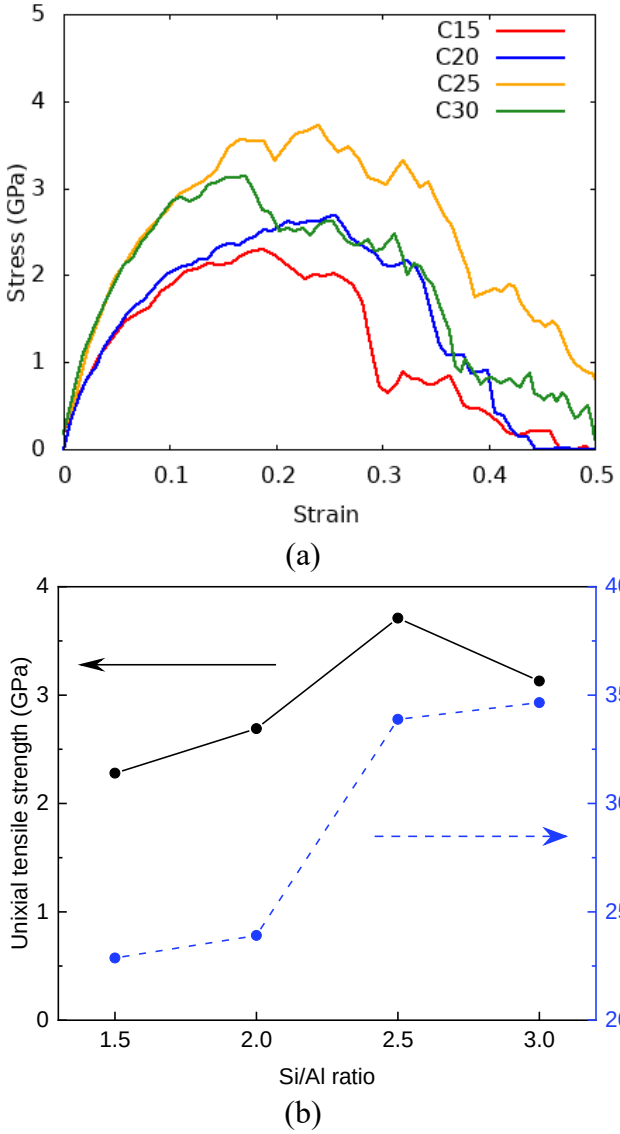

Figure 5.13 Uniaxial tensile behaviour of the neat NASH gels with various Si/Al ratios of 1.5, 2.0, 2.5 and 3.0: (a) stress-strain curves; (b) tensile strength and elastic modulus

Figure 5.13(a) compares the smoothed stress-strain curves of the neat NASH gels with various Si/Al ratios of 1.5, 2.0, 2.5 and 3.0. **Figure 5.13(b)** displays their calculated uniaxial tensile strengths and elastic moduli. It is readily seen that the mechanical properties of the NASH gels vary significantly with the Si/Al ratio. For instance, the tensile strength of NASH raises from 2.28 GPa at the Si/Al ratio of 1.5 to the highest value of 3.71 GPa at the Si/Al ratio of 2.5 (i.e. 63% enhancement). In addition, the elastic modulus of NASH gels continually increases from 22.9 GPa to 34.7 GPa as the Si/Al ratio increases. Particularly, there is a sharp increase as the Si/Al ratio increases from 2.0 to 2.5. Thus, the optimum Si/Al ratio in the neat NASH gels is identified as around 2.5, which is in a good agreement with simulation results by Sadat et al. (2016b). Moreover, the computed tensile strengths and moduli are in line with the other simulation and experimental results (Das et al. 2015; Hou et al. 2018; Lolli et al. 2018). Guan et al. (2022) reported that the tensile strength and elastic modulus are correlated to the bridge oxygen and OH radials numbers, respectively. Similarly, the enhancement in mechanical result of NASH is mainly attributed to the higher complexity of the aluminosilicate network at a higher Si/Al ratio.

5.4.3.2 Stress-strain curve of the composites

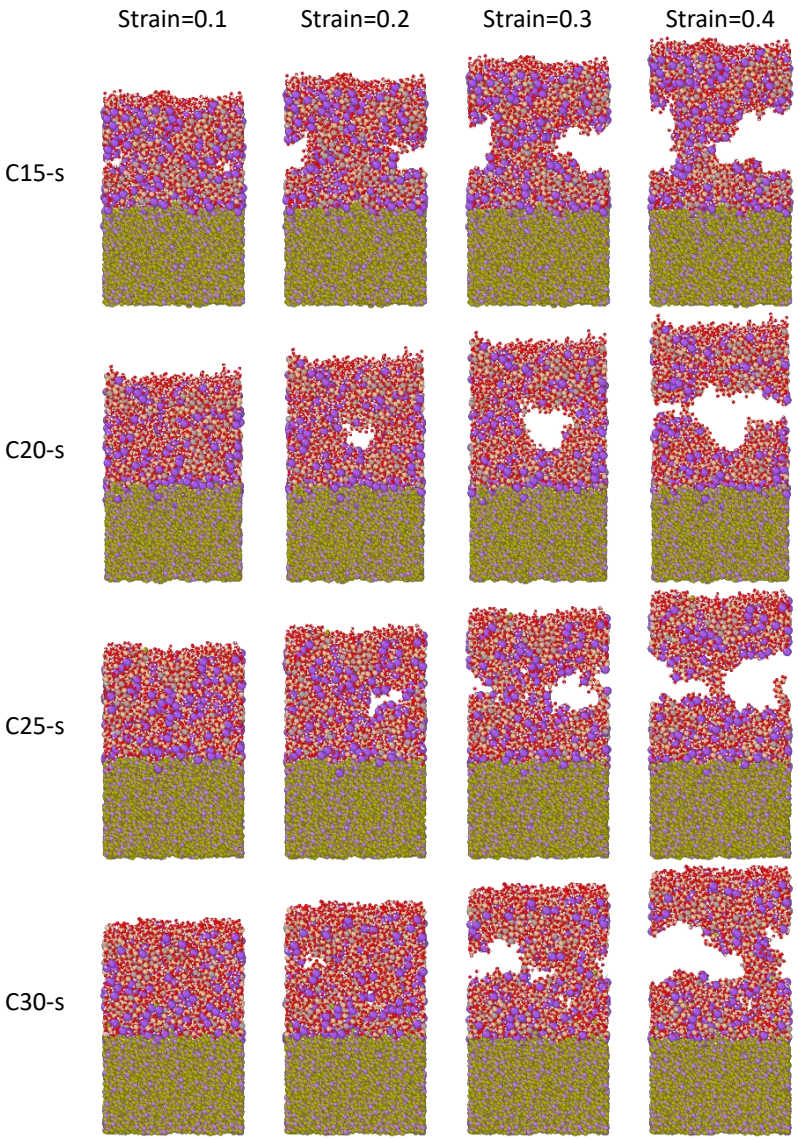

Figure 5.14 The front view of simulation boxes under uniaxial tensile loading of the NASH-silica composites with various Si/Al ratios of 1.5, 2.0, 2.5 and 3.0

Figure 5.14 displays the front view of the four composite models during the tensile simulations at the strains of 0.1, 0.2, 0.3 and 0.4. The snapshots show that the dimension of silica phase is marginally changed during the tensile loading, indicating that silica has a higher stiffness than other phases. The main cracks and fractures of the models all exist in the upper layers of the composites, indicating that the silica substrate has a stronger bond and higher strength than the NASH gel modified by silica. In addition, the ITZs also exhibit better mechanical properties than the silica-modified NASH gels. This result agrees with the density analysis of various phases in section 5.4.1.1.

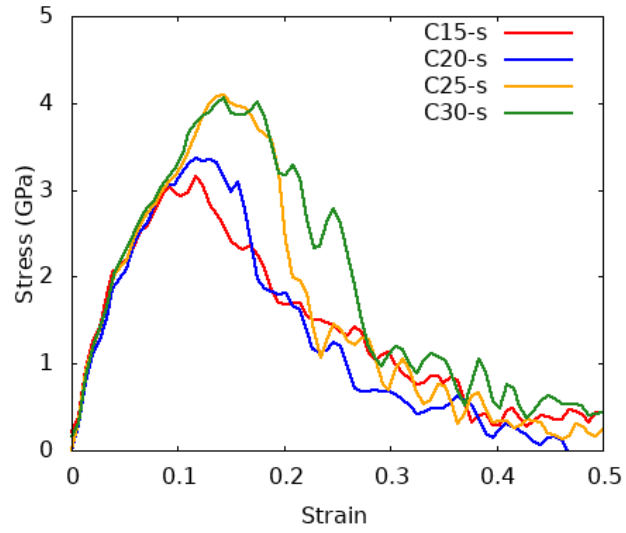

(a)

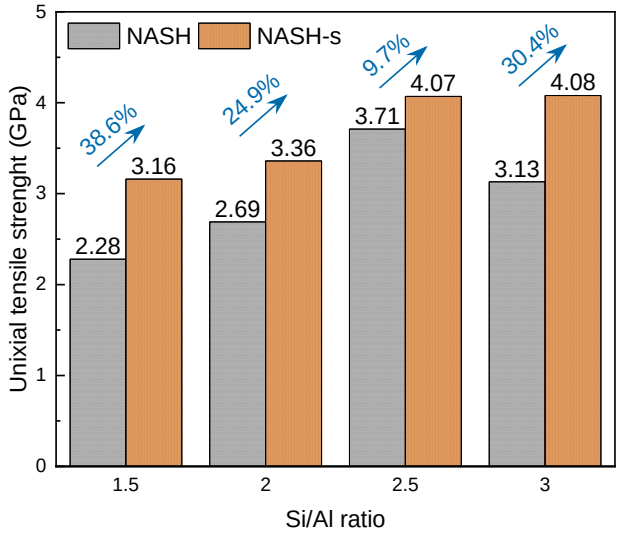

(b)

Figure 5.15 (a) Uniaxial tensile stress-strain curves for the NASH-silica composites with various Si/Al ratios of 1.5, 2.0, 2.5 and 3.0; (b) Uniaxial tensile strengths comparison of pure NASH gels and NASH gels generated on the amorphous silica substrate

Figure 5.15 shows the stress-strain curves of the four composite models and compares the calculated tensile strengths of the composites with the neat NASH gels. It can be found that the NASH gels' mechanical properties vary considerably after the incorporation of amorphous silica. As seen in **Figure 5.15(a)**, the four NASH-silica composites exhibit similar stress-strain behaviour. Their peak stresses are attained at a strain range of 0.1 to 0.2, and the structures totally fracture at a strain of 0.5. Moreover, the tensile strengths of all the composites are higher than those of the neat NASH gels, as shown in **Figure 5.15(b).** At a Si/Al ratio of 1.5, the incorporation of amorphous silica improves the tensile strength of the NASH gel from 2.28 to 3.16 GPa (i.e. 38.6%

enhancement). The neat NASH gel with a Si/Al ratio of 2.5 exhibits the highest tensile strength of 3.71 GPa, which is increased to 4.07 GPa (i.e. 9.7% enhancement) in the NASH-s with the same Si/Al ratio. In general, the incorporation of amorphous silica can improve the NASH gels' mechanical property, especially for those at a lower Si/Al ratio. The mechanical strength of various phases is in the order of ITZ > silica-modified NASH gel > neat NASH gel. Furthermore, the tensile strength of the composites generally increases with the Si/Al ratio, which is in line with that of the neat NASH gels. However, the NASH-s achieves the highest tensile strength of 4.1 GPa at a ratio of 2.5 and remains constant as the Si/Al ratio further increases. It indicates that incorporating amorphous silica can promote geopolymerisation reaction and subsequently improve the mechanical strength of NASH gel.

5.5 Concluding Remarks

In this study, the geopolymerisation reaction is simulated on the surface of the amorphous silica substrate based on a bottom-up reactive modelling approach. The composites of amorphous silica and NASH gel with various Si/Al ratios from 1.5 to 3.0 have been constructed. The NASH gel modified by silica is compared with the neat NASH gel (i.e. generated without amorphous silica), and the variation in atomic structure, dynamic properties and mechanical performances of the NASH gel is characterised. The interaction between amorphous silica and NASH gel is also explored and discussed. The following conclusions could be made based on the simulation results.

(1) The established molecular composite model can simulate the geopolymerisation reaction on the amorphous silica substrate. The chemical reaction between amorphous silica and NASH gel is observed by the RDF obtained from MD simulation. The average thickness of ITZ is found to be around 10 Å in the composite model. The ITZ has similar atomic structure and bond types as the neat NASH gel but has a much higher density and lower diffusion rate than the neat NASH gel.

(2) NASH gel modified by silica shows a higher reaction degree and skeleton complexity than the neat NASH gel. For the NASH gels with various Si/Al ratios, incorporating the amorphous silica can enhance the reaction degree and skeleton complexity of NASH gel by around 10% and 6%, respectively.

(3) The ions diffusion rate in the NASH gel modified by silica is lower than that in the neat NASH gel, indicating that the stability of NASH gel can be improved by the incorporation of amorphous silica. At a Si/Al ratio of 1.5, the diffusion coefficient of Na ions in the NASH gel modified by silica is 58% of that in the neat NASH gel.

(4) The mechanical strength in various phases is in the order of ITZ > silica-modified NASH gel > neat NASH gel. Moreover, the tensile strength of NASH gels is improved by 10~40% with the incorporation of amorphous silica, particularly for those with a lower Si/Al ratio. The silica-modified NASH gel can achieve the optimum tensile strength around 4.1 GPa at a Si/Al ratio of 2.5.

Chapter 6

Molecular Dynamics Simulations of Interfacial Interaction Mechanism between the NASH Gels and the Polyethene Fibre[‡]

6.1 Synopsis

Cementitious materials suffer from their inherent brittleness, and thus much research has been devoted to circumventing this problem. A promising approach is incorporating polymeric fibre to enhance the ductility of cementitious materials. Therefore, fibre-reinforced geopolymer composite (FRGC) has attracted much attention due to its ultra-high ductility and

[‡] The work in this chapter was published in:

Guan, X., Wu, J.-Q., Hernandez, A. G., Li, B.[*] & Do, H.[*] (2022). "Molecular dynamic simulations of interfacial interaction mechanism between the NASH gels and the polyethene fibre." *Construction and Building Materials*, 349, 128769.

environmentally friendly characteristics. The bonding between the fibre and matrix plays a critical role that impacts the FRGC's performance. However, the structure-property relationship of the composite is still unclear. In particular, the effect of matrix compositions, i.e. sodium aluminosilicate hydrated (NASH) gel, on the frictional bonding remains a mystery. In this paper, we employ molecular dynamics simulations to obtain a fundamental understanding of the interfacial interactions between NASH gels and polyethene fibre (PE) – a commonly found FRGC. The dynamic pull-out and the interfacial property characterization are conducted for several NASH/PE models with different Si/Al ratios and internal moisture contents. Our results reveal that the adhesive bonding between the NASH and PE is influenced by the interfacial interaction and the mechanical interlocking between the two materials. The interfacial interaction energies between NASH and PE are dominated by the short-range van der Waals interactions and the hydrogen bonding between hydrogen atoms in the polyethene chains and oxygen atoms in the NASH. In addition, the Si/Al ratio can significantly impact the shear bonding strength between PE and NASH. Moreover, the degradation of the adhesive properties of NASH/PE composite strongly correlates to the internal moisture of the NASH. Thus, our work reveals the sources of frictional bonding between PE fibre and NASH gels and relates the bonding performances with the Si/Al ratio and the internal moisture content of the matrix. Our results will provide valuable insights into the material design of FRGC and optimize their performances.

6.2 Introduction

Geopolymer, like the OPC material, also exhibits a high level of brittleness and a low tensile strength. To tackle these limitations, metallic and polymetric short fibres are introduced to reinforce the cementitious composites (Lyu et al. 2021). For example, the engineered cementitious composite (ECC), invented by Li and Leung in 1992 (Li and Leung 1992), is a plastic fibre reinforced cementitious material that exhibits pseudo strain-hardening behaviour and multiple-tight-cracking phenomena (Li 2003). The strain capacity of ECC is hundreds of times that of regular concrete (Li 2019), which is beneficial in enhancing the

infrastructure's durability (Lepech and Li 2009). Recently, fibre-reinforced geopolymer composite (FRGC) has been proposed as a substitution for ECC to enhance sustainability further (Lyu et al. 2021; Wang and Li 2007). In fibre reinforced materials, fibre bridging plays the most significant role in material performance. The excessive bonding between fibre and matrix, e.g. bonding strength higher than fibre strength, will cause fibre rupture, while the insufficient bonding, e.g. bridging strength smaller than the first-crack-strength of the cementitious matrix, leads to the fibre sliding under tensile loading (Li 2019). Therefore, the interfacial bonding between fibre and matrix is a crucial property for the micro-mechanical design of the FRGC.

Many types of fibres, such as polyvinyl alcohol (PVA) (Ohno and Li 2018), polyethene (PE) (Shaikh et al. 2018; Wang et al. 2022), polypropylene (PP) (Nguyen et al. 2018) and steel fibres (Bhutta et al. 2017), have been adopted to enhance the mechanical properties of FRGC. Among them, PE fibre is a suitable fibre reinforcement for superior tensile performance due to its high fibre modulus and elongation at break. For example, Nguyễn et al. (2021) employed 1.75 vol% of PE fibres into FA based geopolymer matrix, activated by sodium metasilicate pentahydrate and sodium hydroxide, and achieved a tensile strain capacity of 13.7% and a tensile strength of 6.8 MPa. Besides, Shaikh et al. (2018) compared the strain hardening and deflection hardening behaviours of heat/ambient cured geopolymer and OPC based composites, and found that both the FRGCs exhibit better performance than the OPC composite with the same volume fraction of PE fibre. Moreover, Wang et al. (2021) recommended an optimum geopolymer content in FRGC to enhance its properties. Also, Wu et al. (2022) investigated the interfacial behaviour of PE fibre and geopolymer incorporated with waste glass powder. They reported that the frictional bonding stress and slip hardening coefficient could be correlated to explain the tensile strain behaviours of FRGC. Consequently, many studies have reported that the PE reinforced geopolymer composite exhibits excellent performance and attracts increasing interest.

However, existing studies mainly focus on the property's enhancement and mechanical mechanism exploration of FRGC. It is reported that the bonding

between PE fibre and geopolymer material is dominated by frictional bonding (Choi et al. 2016; Li 2019). However, the influence of geopolymer composition on the bonding has not been reported yet. Few studies are devoted to discussing the atomic interaction between PE fibre and the NASH gel. It is not only because FRGC is a newly developed composite but also due to the limitation of current experimental techniques at the molecular level (Zhang et al. 2021).

With the development of computational technology, molecular dynamics (MD) simulation has shown its power to provide a complementary understanding of the atomic structure of cementitious materials and their interactions with other additives or composites (Xu et al. 2021b). Bahraq et al. (2022) reviewed studies related to the interaction between polymeric and cementitious materials at an atomic scale. They summarized that MD simulation could provide valuable information (e.g. interfacial mechanisms, structure, dynamics, energetics, mechanical properties) and aid in designing new composites. Wang et al. (2020b) used the 11 Å tobermorite crystal structure as a CSH model, and compared its interfacial shear strength with three different types of fibres by MD simulation. The study showed that the bonding is closely related to fibre types, where the Ca atoms at the interface play the key role and H-bonds between fibre and substrate also contribute to the bonding strength. Furthermore, Zhou et al. (2019b) investigated the bonding behaviour of the PVA/CSH composite, and revealed the existence of H-bonds between hydroxyl in PVA and non-bridging oxygen in CSH. Moreover, other studies reported the interaction of CSH matrix and modified PE fibres (Lu et al. 2021a; Lu et al. 2020), and concluded that surface treatment of oxidation and graphene oxide on PE fibre could significantly strengthen the interfacial bonding. Thus, MD simulation is an effective computational tool for characterizing the polymer/cement interactions at the molecular level, exploring the bonding mechanism and providing sight for better composites' design (Bahraq et al. 2022).

It can be found that MD simulations of fibre and geopolymer interaction are still rare. Only a few studies on the composites of geopolymer material with PVA or carbon nanotube (CNT) can be found. For instance, Zhang et al. (2021) studied the adhesion mechanism of PVA and alkali-activated slag/fly ash matrix.

Influences of Ca ions content and Al/Si ratio on the adsorption enthalpy and chemical bonding energy at the interfacial transition zone (ITZ) were evaluated. However, the matrix of alkali-activated slag/FA material contains a large content of Ca ions, which is different from geopolymer. On the other hand, Kai et al. (2020) and Sekkal and Zaoui. (2022) investigated the interaction between geopolymer and CNT by computing the composites' atomic information, mechanical strength and dynamic properties. To the author's knowledge, the molecular interaction between PE and NASH and the adhesion mechanism at the interface have not been reported yet.

To study the interface between PE and geopolymer, the first step is building the reasonable molecular models. The composite models are always derived by the combination of molecular models from the matrix and additives. The NASH models in this study are obtained by the same approach introduced in section 5.3.3.1. Specifically, it is based on the reactive MD simulation and geopolymerisation reaction. For PE models, Lu et al. (2020) has successfully built the orthorhombic layered structure with parallelly arranged straight polyethene chains to simulate the interaction between PE and CSH materials. It can be an effective method for model construction.

Moreover, the environmental humidity can influence the adhesion between PE fibre and the geopolymer substrate (Zahid and Shafiq 2020), which subsequently affects the mechanical properties of the fibre reinforced geopolymer. When used as the principal constituent for infrastructure, the construction material always suffers the attack from moisture, and the environmental humidity can impact the internal water content of the substrate. In this regard, some research has been carried out to investigate the effect of water content stay between the graphene oxide (GO) and CSH substrate (Wang et al. 2020a). It was reported that the water layer could prevent the bonding between GO and CSH, which works as a lubricant to reduce the pull-out strength. However, it considered the water only as of the interlayer between the substrate and GO. The effect of internal moisture content on the bonding between geopolymer matrix and polymetric fibre is seldom studied and the mechanism has not been reported yet.

In this work, we employ MD simulations to investigate the interfacial interaction between geopolymer material and PE fibre. The atomic model of NASH gel is developed based on an in-situ geopolymerisation reaction approach. The PE molecular model is employed as an interlayer of the NASH gel structures to build the composite model. The NASH structures with various internal water contents are generated by partially removing the water molecules. This approach represents a more realistic picture of the internal moisture of the substrate. Subsequently, the pull-out process of PE from NASH substrates is characterised. As the most significant composition parameters in the NASH model, the silicon to aluminium (Si/Al) ratio and internal water content in NASH are varied in the simulation, aiming to explore the relationship between the NASH constituents and adhesive behaviours. Afterwards, the adhesion mechanism between PE fibre and geopolymer is explored and explained from an atomic point of view. Hence, our work contributes to the instruction of material design for the fibre reinforced geopolymers.

6.3 Computational Methods

6.3.1 Model construction

6.3.1.1 NASH gels model

In this work, the seven types of oligomers mentioned in Chapter 4 are combined to develop NASH structures with Si/Al ratios from 1.5 to 3.0. The percentages of the oligomers are displayed in **Table 6.1**. The receipt for the NASH gel models are the same as that used in Chapter 5. Different percentages of oligomers with various Si/Al ratios (i.e. 1, 2 and 3) are used to achieve the targeting final Si/Al ratios. The same percentage is used for oligomers with the same Si/Al ratio by different configurations, i.e. linear and cyclic. By adding the equivalent number of sodium ions to the aluminium atoms, the negative charges are compensated and four cubic amorphous simulation cells with around 20,000 atoms each are obtained (i.e. C1.5, C2.0, C2.5 and C3.0 in **Table 6.1**). The sizes of the simulation cells are around 60×60×60 $Å^3$. Afterwards, the

simulation cells are subjected to the MD simulation for the reaction process, which is a melt-annealing-equilibrium simulation with a reactive force field. The bond in oligomers will be broken and form a new amorphous polymerized crosslinked structure. Simultaneously, water molecules will be generated by the polycondensation reaction. Moreover, to compare the properties of NASH structures with various internal water contents, some water molecules in the C2.5 composite system are removed in proportion. In the equilibrated structure of C2.5 composite, oxygen atoms with 2 hydrogen atoms surrounded within 2 Å radius are defined as water oxygen atoms. We search for these oxygen atoms and randomly delete the water molecules that contain them. The water reduced models are shown in **Table 6.1**, including C2.5w66, C2.5w33 and C2.5w0 (i.e. 66%, 33% and 0 water (dry) remain in NASH structures).

Table 6.1 The number and percentages of oligomers used for the initial model of NASH gels

NASH models	Numbers (percentages) of the oligomers							Si/Al ratio	Water molecules	Na ions	Total atoms
	Mo1	Mo2	Mo3	Mo4	Mo5	Mo6	Mo7				
C1.5	60%	15%	15%	2.5%	2.5%	2.5%	2.5%	1.5	1,878	1,080	19,791
C2.0	20%	30%	30%	5%	5%	5%	5%	2.0	1,646	960	19,824
C2.5	10%	15%	15%	15%	15%	15%	15%	2.5	1,549	860	19,952
C3.0	0	0	0	25%	25%	25%	25%	3.0	1,480	780	20,085
C2.5w66	10%	15%	15%	15%	15%	15%	15%	2.5	1,028	860	18,389
C2.5w33	10%	15%	15%	15%	15%	15%	15%	2.5	504	860	16,817
C2.5w0	10%	15%	15%	15%	15%	15%	15%	2.5	0	860	15,305

6.3.1.2 Model of the NASH gel and PE composite

To investigate the interaction between geopolymer and PE materials, the simulation boxes of equilibrated NASH models are split in the middle along the XY plane and separated for 20 Å. Afterwards, a PE simulation box with a thickness of 13.6 Å is inserted. The gap between the two systems is set as 3.2 Å. The PE model contains 4 layers of polyethylene chains along the x-direction, which includes 17 chains in each layer and consists of 48 CH_2 units in each chain. The distance between hydrogen atoms from the distinguished PE chain is 2.0 Å. The modelling procedure of NASH gels and composites of NASH gel and PE chains is displayed in **Figure 6.1**.

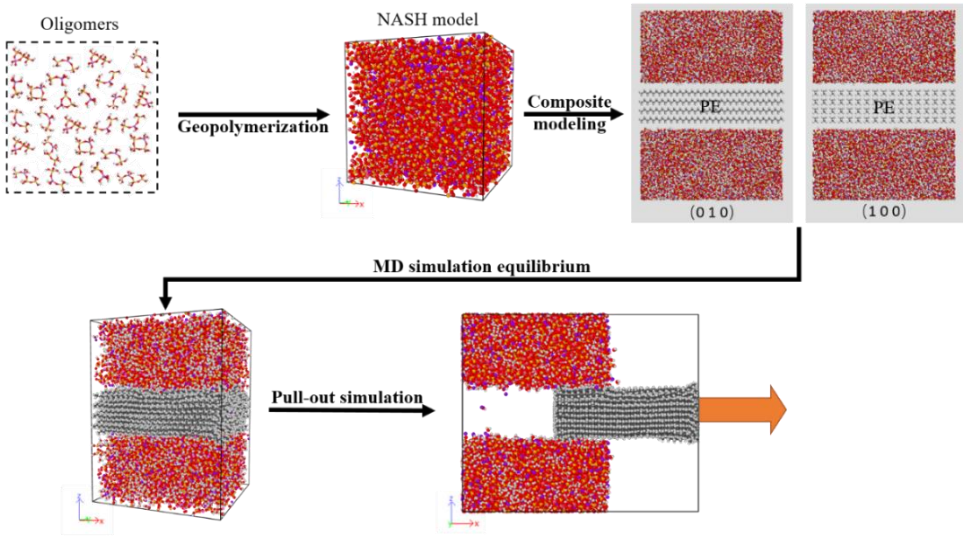

Figure 6.1 The diagram of modelling procedure of NASH gels, NASH/PE composite and the pull-out simulations

6.3.2 Force field

We have employed the reactive force field ReaxFF to simulate the geopolymerisation reaction and the interactions in the oligomers and NASH gels. However, the ReaxFF force field cannot distinguish the same element in various atom types, i.e. the different hydrogen atoms in NASH gel and polyethene chains. Thus, the atomic interaction at the interface cannot be simulated straightforwardly with the ReaxFF force field. Moreover, hybrid force fields have been successfully employed to describe the organic-inorganic interface (Wang et al. 2020b; Zhou et al. 2021). Regarding the composite system of NASH and PE, a hybrid force field of the ClayFF (Cygan et al. 2004) and the OPLS (Jorgensen et al. 1996) force field are employed to describe the interactions of NASH gel and polyethylene, respectively. ClayFF has been applied to various clay materials and cementitious materials, including NASH gel (Zhang et al. 2018c). It can successfully model the structure and interactions of aqueous species with oxide and hydroxide surfaces (Cygan et al. 2009). The OPLS force field has been proved to be appropriate to describe the interaction of organic molecules with diverse functional groups (Olsson et al. 2017). Therefore, this study has employed the hybrid ClayFF and OPLS force fields to conduct the MD simulation of the composite system of NASH gels and PE. The parameters for various species of atoms in this study can be referred to the Appendix I.

6.3.3 Simulation algorithm

6.3.3.1 Melt-annealing of NASH structure

The cubic simulation cells of NASH models are first relaxed by energy minimization using a conjugated gradient algorithm in LAMMPS (Plimpton et al. 2007) under the ReaxFF force field, followed by an equilibrium running at 300 K in the NVT ensemble for five ps with a timestep of 0.25 fs. Afterwards, the annealing procedure is started by heating the system to 2,100 K to remove any memory effects, followed by a cooling step with a temperature reducing rate of 3 K/ps until 300 K. The systems are subsequently equilibrated in the NPT ensemble for 200 ps 300 K and 1 atm to obtain an equilibrated density. Finally, the simulation cells are subject to NVT ensemble for another 200 ps for production.

6.3.3.2 Equilibrium of the NASH/PE composites

The NASH/PE composites are first subjected to energy minimization, followed by equilibration in the NVT ensemble at 300 K for 2.0 ns with a timestep of 1.0 fs. Afterwards, the systems are equilibrated in the NPT ensemble at 300 K and 1 atm in the z-direction for 3.0 ns to achieve the equilibrated density. This can maintain the same box lengths of PE and NASH in both x- and y-dimensions, and obtain the equilibrium NASH/PE interface. Finally, another NVT ensemble with 1.0 ns is employed for production.

6.3.3.3 Pull-out of PE layer from NASH substrate

To investigate the interaction between PE and NASH, a pull-out simulation of the PE layer from the NASH substrate has been performed to display the response of the composite system and directly calculate the required force for pulling out and the shear bonding strength at the interface. The pull-out simulation is performed along the x-direction, which is the direction of the polyethene chains (Lu et al. 2020). The boundary at the x-direction has been set as non-periodic and shrink-wrapped condition. This is done to eliminate the boundary limitation along the x-direction during the pull-out simulation process.

During the pull-out process, the PE part is subjected to a velocity of 0.001 Å/fs along the x-direction, while atoms belonging to the NASH layers (within a slab of 2 Å thickness), the top and bottom regions, are kept fixed. This pull-out simulation rate has been used in many studies and is widely suggested to investigate the reinforcement behaviour in nano-composites (Kai et al. 2020; Lu et al. 2018).

The systems are subjected to the NVT ensemble at 300 K for 60 ps with a timestep of 1.0 fs to achieve the complete pull-out of the PE layer from the NASH layers, as shown in **Figure 6.1**. The total force applied on all atoms in the PE part along the x-direction is computed to obtain the pull-out force-displacement curves, with atomic trajectories and force values recorded every 10 fs. Moreover, the interfacial shear bonding strength can be derived based on the highest force value in the smoothed force-displacement curves, defined as $\tau = \frac{F_{max}}{2ab}$, where F_{max} is the maximum force applied on PE, and a and b are the box length at x- and y-directions, respectively. The error bars are obtained from the fluctuation of force values in the original force-displacement curves.

6.4 Results and Discussion

This section first displays the NASH/PE composite models generated from the reactive MD simulation and analyses some physical properties of the models. Afterwards, the pull-out simulation of the interlayer PE structure from the NASH substrate is illustrated, and the mechanical performances of the models with various Si/Al ratios are characterised. Subsequently, the interfacial interaction mechanism between the NASH and PE is discussed by investigating molecular structural and energy properties. Finally, the effect of internal water content in the NASH structures on the pull-out bonding of PE and NASH has been revealed.

6.4.1 Physical and diffusion properties of the composites

To start with, four NASH models are generated from reactive MD simulations with different Si to Al atom ratios, increasing from 1.5 to 3.0. **Table 6.2**

summarizes the essential properties of the NASH models after the reaction. The reaction degree, which is represented by the reduction amount of OH radials, declines from 53.1% to 44.6% when the Si/Al ratio increases from 1.5 to 3.0. In oligomers with a higher Si/Al ratio, a smaller number of reactive hydroxyl groups can be found in their original structures, which is the nature of the original oligomers, as shown in **Figure 4.1**. The less OH group leads to a lower reaction probability. Consequently, the amount of yield product, that is water molecules, reduces as the reaction degree gets lower. The mass percentage of water is 13.56% in the C1.5 NASH structure, but it is reduced to 10.09% in C3.0. However, the skeleton network complexity of NASH structures generated from larger Si/Al ratios is higher than that from smaller Si/Al ratios. It also results from the nature of the oligomers: a larger Si/Al ratio indicates more original bridge oxygen atoms (O_b) in the molecules. The percentages of O_b in total oxygen atoms in each NASH system are also listed in **Table 6.2**, which increase gradually from 43.8% to 47.8% as the Si/Al ratio increases. It means more Si and Al tetrahedrons are connected and the skeleton complexity gets higher with the larger Si/Al ratio. It has been reported that the more complicated network structure can bring both better mechanical properties and stability to the NASH gel (Sadat et al. 2016b).

Moreover, the sodium ion content in the systems is correlated to the amount of Al atom in the skeleton. Thus, it also declines with the Si/Al ratio. The density of C1.5 is 1.77 g/cm^3, which is much lower than the others due to the low Si/Al ratio, lower structural complexity, and more water molecules in the system. All the other NASH structures have an equilibrium density larger than 2.0 g/cm^3, and the highest value is obtained at the Si/Al ratio of 2.5. The density range agrees with some previously reported experimental and simulation results (Sadat et al. 2018b; Wang et al. 2005). All of these constituents and structure properties would affect the interface interaction of NASH with PE fibres and the mechanical performances.

Table 6.2 Reaction degree and water and sodium content of the NASH models in reactive MD simulation

NASH	Reaction degree (%)	Na ion content (ms%)	Water content (ms%)	Bridge O in all O (%)	Bulk density (g/cm^3)
C1.5	53.1	9.95	13.56	43.8	1.77
C2.0	48.3	8.64	11.61	45.3	2.02
C2.5	46.2	7.60	10.73	46.8	2.05
C3.0	44.6	6.79	10.09	47.8	2.01

Figure 6.2 shows the density profile along the z-direction (perpendicular to the interface of NASH and PE layer) for the C2.5 NASH/PE system, computed using the trajectories sampled from the NVT production run after equilibrium with the hybrid force field. The local atom intensity is calculated by separating the simulation box into slabs of thickness 1 Å parallel to the interface (XY plane). The curves of densities versus z-coordinates show the atoms' distribution in the systems. The result is averaged over 100 trajectories during the simulation time of 20 ps. The distance ranging from 30 to 55 Å along the z-direction in the middle is the PE layer, and the two sides are NASH substrates. The density distribution curve shows that the bulk density of NASH and PE layers are around 2.0 and 1.0 g/cm^3, respectively. The density of NASH changes negligibly when force fields are switched from ReaxFF to ClayFF. The density of PE agrees with previously reported results (Pant et al. 1993). The densities of both NASH and PE do not show a noticeable change at their interfaces.

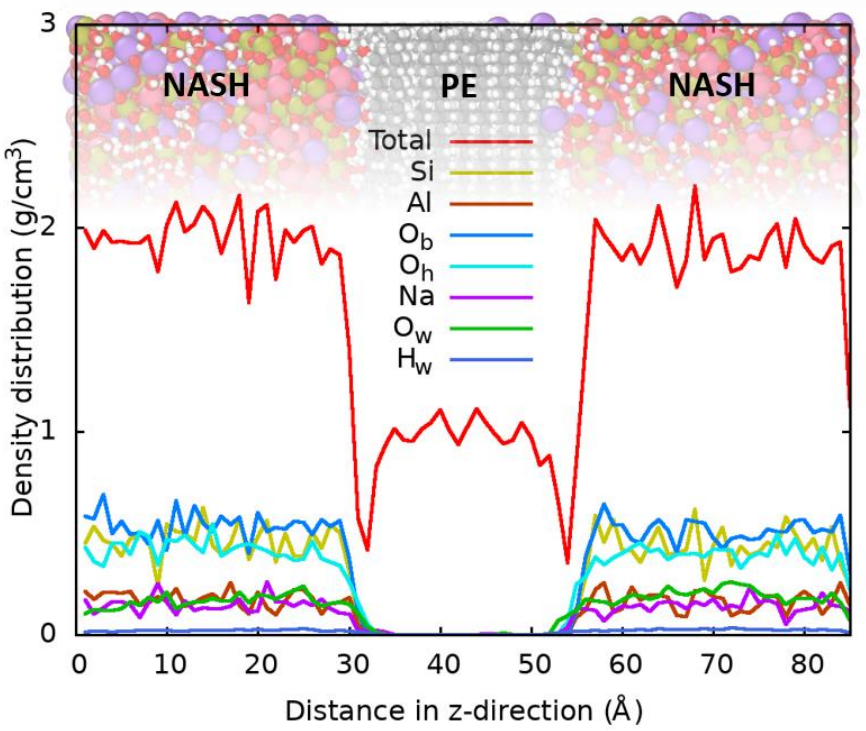

Figure 6.2 Density distribution of NASH/PE composite system with Si/Al ratio of 2.5 along z-direction: O_b is bridge oxygen atoms in the NASH skeleton, O_h is hydroxyl oxygen, O_w is water oxygen and H_w is water hydrogen

Figure 6.3 displays the equilibrated interface between PE and C2.5 NASH structure. At the bottom of the figure, the grey-white molecules represent the PE layer in the composite. The sodium ions and water molecules in the NASH part are represented by purple balls and red-white sticks, respectively, while the aluminosilicate skeleton is shown by lines. Some of the skeleton parts have been highlighted with ball and sticks to highlight the interaction. The figure depicts that sodium ions and water molecules can move freely and distribute in the amorphous structure of NASH at the interface. Some water molecules stay very close to the PE layer, and some tend to cluster together. Due to the hydrogen bond between water molecules, they can form clusters in the amorphous structure (Fukuda 1998). The larger rings and longer linear chain of aluminosilicate skeleton are found in the NASH structure, and some of the chain ends are also found getting close to and interacting with the PE layer.

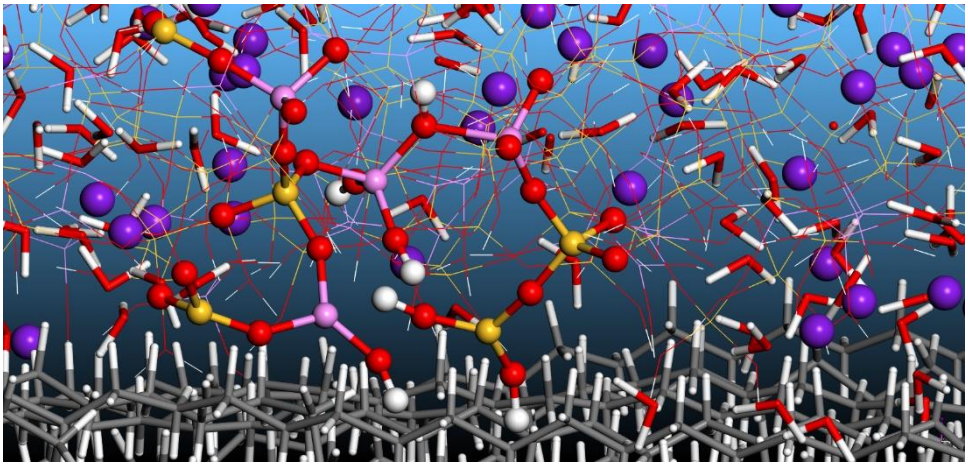

Figure 6.3 NASH/PE composites after the equilibrium stage: grey is carbon, yellow is silicon, pink is aluminium, red is oxygen, purple is sodium, and white is hydrogen.

The mean square displacement (MSD) characterizes the translational motion behaviours of atoms. The displacement of the atoms is computed per 1 ps and averaged over 2 ns to acquire the MSD curves. **Figure 6.4(a)** shows the MSD values of Si, Al, O_b, O_h, sodium ions, O_w and H_w atoms in the C2.5 NASH structure. The curves of Si, Al and O_b present an extremely low value of MSD. Since these three types of atoms represent the structural skeleton, the low MSD reveals the skeleton stability of the geopolymerised 3-D network structure. Sodium ions, the charge compensate cations in the NASH, show the higher mobility in the system. The ions can distribute in the vacancy of the network structure and interact with Al tetrahedrons by ionic bonds. Besides, the MSD curves of O_w and H_w show the highest level, which indicates the mobility of water molecules in the system.

The diffusion coefficients are calculated from the slope of MSD curves. **Figure 6.4(b)** shows the D values comparison of O_w and Na ions for the four NASH models with various Si/Al ratios. We can observe that the D value of O_w continually drops from 0.37 to 0.21 $Å^2$/ns when the Si/Al ratio increases from 1.5 to 3.0, and the decreasing rate at the ratio of 2.5 is particularly noticeable. The reduction of water mobility reveals the enhancement of structural complexity of the NASH with a higher Si/Al ratio. The steric hindrance effect restricts the mobility of water molecules. This result agrees with the physical properties and structure analysis depicted in **Figure 5.3**. On the other hand, the

Na ion curve shows a lower diffusion level with the D values less than 0.1 $Å^2$/ns. Like that of O_w, the value keeps decreasing with the Si/Al ratio.

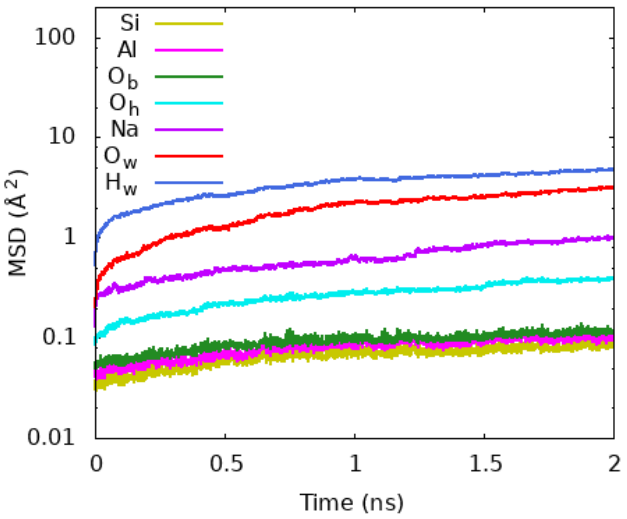

(a)

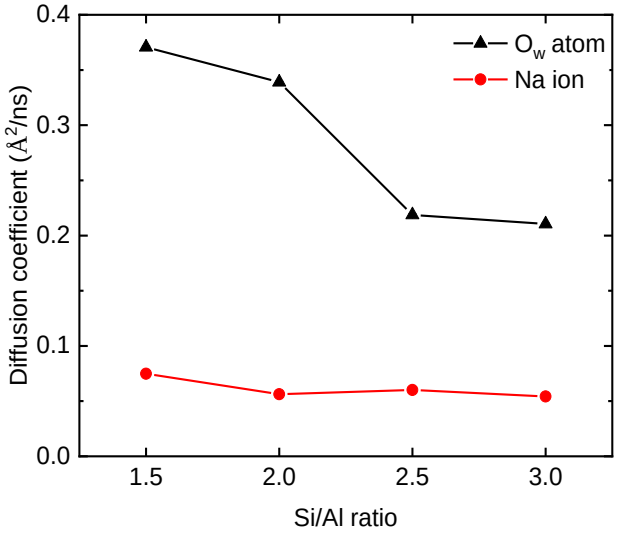

(b)

Figure 6.4 (a) Mean square displacement curves computed at ClayFF force field of composite system of NASH/PE with Si/Al ratio of 2.5; (b) calculated diffusion coefficient of O_w (water) and Na ions in the NASH/PE composite systems with various Si/Al ratios

6.4.2 Pull-out simulation of PE from NASH substrate

6.4.2.1 Shear bonding force-displacement curve

The dynamic pull-out simulation can provide a straightforward description of the structure change of the NASH/PE composite and reveal the interaction at the interface. The pull-out process of the PE layer from the NASH substrate with a Si/Al ratio of 2.5 is shown in **Figure 6.5**. The PE layer is moved along

the x-direction from the initial position until it is ultimately pulled out, and the total force applied in the x-direction is used to calculate the shear bonding force applied to the PE and plot the force-displacement curve. The points a, b, c and d represent simulation snapshots at 1 ps, 7 ps, 30 ps and 60 ps, respectively. The pull-out force is considered the response to the interaction between the NASH and PE layer, which is directly related to the interfacial stress transfer. A large number of discontinuous corrugations appear on the curve, as the PE is gradually pulled out from the NASH substrate. A similar phenomenon was also reported in reference (Fan et al. 2017). Firstly, the fluctuation of force-displacement curves comes from the dynamic force variation in MD simulation. Secondly, the shear bonding force between the NASH and the PE is contributed by the atomic interaction. The relative motion between atom pairs at the interface causes significant changes in pair distance. The force is weakened when the distance is stretched, while it is strengthened when new pairs interaction forms. Wang et al. (2020a) illustrated the "stick-slip" phenomenon by the repeated process of braking-reconnection of bonds when conducting MD pull-out simulation between graphene oxide and CSH substrate. Therefore, the interaction force fluctuates dramatically during the pull-out process.

For clarity, the curves in **Figure 6.5** are smoothed by approximating the data with a Bezier curve that connects the endpoint. The interface shear bonding strengths are derived based on the highest value in the force-displacement curves. We can observe that the shear bonding force of PE with the C2.5 NASH structure increases quickly to 30 nN at the initial stage of the pull-out process, before the first sharp drop to around 10 nN. The significant variation denotes that the interfacial adhesion properties have a large fluctuation when PE is pulled out from the NASH substrate. Afterwards, the force climbs discontinuously and reaches the peak value of approximately 35 nN at the displacement of 7 Å in the x-direction. Finally, the force value is lowered step by step, with some fluctuation emerging, until PE is completely pulled-out at the displacement of 60 Å.

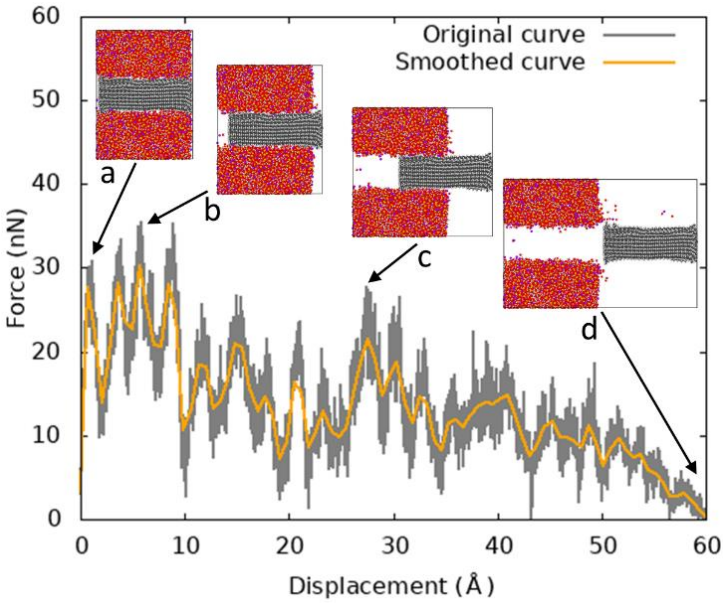

Figure 6.5 The pull-out force-displacement curves of NASH/PE system with Si/Al of 2.5 along x-direction

6.4.2.2 Effect of Si/Al ratio on the pull-out bonding

To investigate the bonding interaction between PE and NASH with various Si/Al ratios, the smoothed pull-out force-displacement curves of the four composite systems are compared in **Figure 6.6(a)**. All the four curves show the fluctuation of force during the pull-out process, and the highest values are obtained within the first 10 Å displacement. The composite C1.5 shows the lowest level of force, and the first peak is found at the very beginning of the pull-out process, with the ultimate force value of 14.2 nN. Afterwards, the force declines gradually. The other three curves show a higher level than C1.5 and reach the ultimate force values at the second or third peak (at a displacement of around 7 to 8 Å). It means that the atoms at the interface are rearranged and form new stronger interactions between NASH and PE when the PE layer is stretched out from the NASH substrate. It is the new interaction that brings the higher resistant force; therefore, the curves can get to a higher peak. The significant lower ultimate force of the C1.5 system is contributed by the lower density of its NASH substrate. Even if new interaction has been formed, the total force cannot reach a higher value. As the PE layer moves from the substrate, the interaction area between PE and NASH decreases. Moreover, the shear bonding strengths have been calculated from the ultimate force in the curves and compared in **Figure 6.6(b)**. The strengths of composites with Si/Al ratio of

1.5, 2.0 and 2.5 are 0.19 GPa, 0.29 GPa and 0.43 GPa, respectively. The maximum shear bonding strength between geopolymer and PE increases almost linearly with the Si/Al ratio. However, the computed shear bonding strengths decline to 0.38 GPa when the Si/Al ratio further increases to 3.0. The optimized bonding strength is found in the composite with a Si/Al ratio of 2.5.

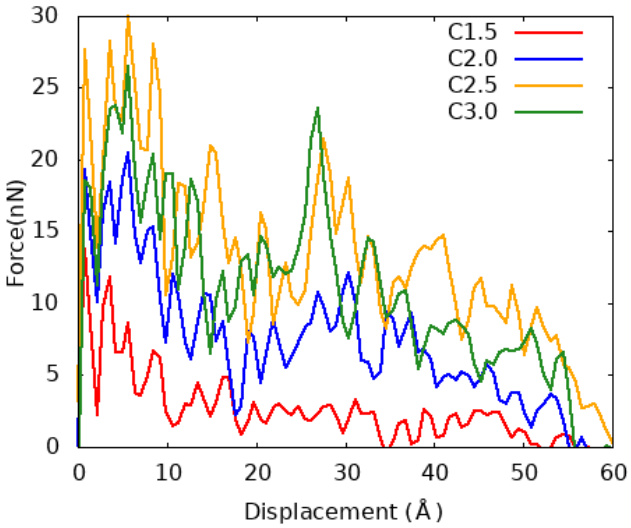

(a)

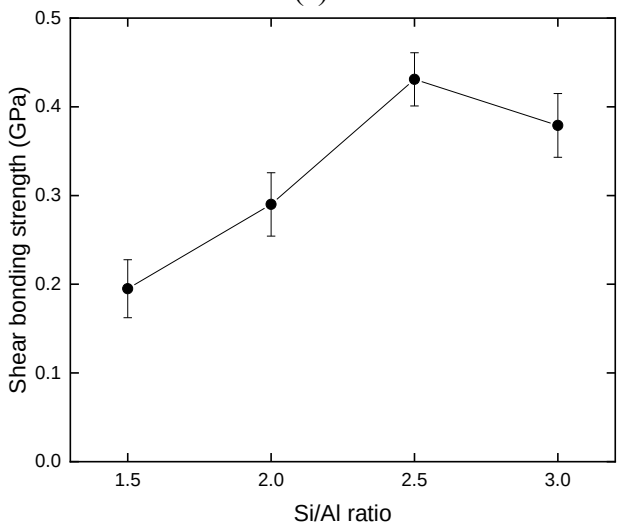

(b)

Figure 6.6 (a) The pull-out force-displacement curves of PE from NASH/PE systems with various Si/Al ratios from 1.5 to 3.0; (b) the shear bonding strengths of the interface between PE and NASH structures

The force acting on the PE layers comes from the interaction at the interface and is provided by the interfacial interaction energy. The interaction energies of two materials are calculated by the total pairwise energy between all atoms in the NASH group and all atoms in the PE group. The interaction energy result is averaged over 100 trajectories during the simulation time of 100 ps. **Figure 6.7**

compares the interface energies at the equilibrium stage of four composite systems with Si/Al ratios from 1.5 to 3.0. The result was computed based on only one interface in the composite system since we have two interfaces in each model. All the energies are negative, indicating the PE layer can be adsorbed by NASH structures (Zhou et al. 2019a). The adhesion energy contributes to the bonding strength between NASH and the PE fibre. The interfacial interaction energy of the C1.5 system is -276.1 Kcal/mole, while it continually increases to -518.5 Kcal/mole when the Si/Al ratio increases to 2.5. Afterwards, the energy of the C3.0 system drops to -416.5 Kcal/mole. The energy of the C2.5 has the greatest absolute value, and this trend is in good agreement with the shear bonding strength obtained from the pull-out simulation. However, the sources of the pull-out force between PE fibre and NASH substrate need further investigation. Two possible mechanisms influencing the pull-out behaviours between the NASH and PE will be discussed, including the interfacial atomic interaction or bonding between two systems, and the mechanical interlocking caused by the molecular configurations and the surface roughness (Bahraq et al. 2022; Wang et al. 2020a).

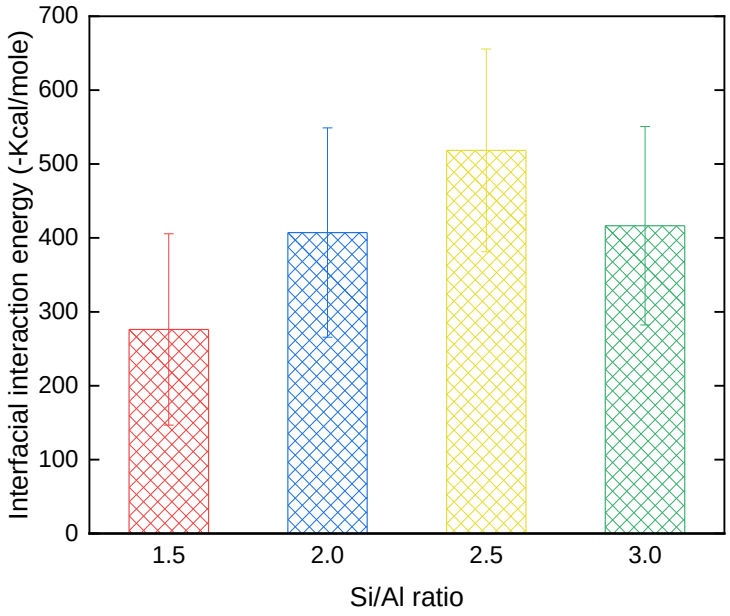

Figure 6.7 The dynamic equilibrated interfacial interaction energy of NASH and PE layer in the NASH/PE composites systems with Si/Al ratios of 1.5, 2.0, 2.5 and 3.0

6.4.3 Interfacial adhesion mechanism

6.4.3.1 Atomic interaction

To explain the atomic interaction at the interface between NASH and PE, the density distributions of different atoms along the z-direction in the composite are calculated as shown in **Figure 6.8**. PE layer locates within the distance ranging from around 30 to 55 Å in the z-direction, and the two sides are the C2.5 NASH. The atomic intensity curves show a roughly symmetrical shape, and the computed density values fluctuate due to the amorphous nature of the NASH structure. However, the curve for the hydroxyl oxygen atom (O_h) exhibits a sudden rise at the interface of NASH and PE, as shown in **Figure 6.8(a)**, while that for the Si atom represents the dynamic equilibrium trend. Moreover, the curve for the water oxygen atom (O_w) displays an even higher peak at the interface, as depicted in **Figure 6.8(b)**. It reveals that the presence probability of hydroxyl groups and water molecules at the interface is higher than that in the other part of the NASH structures, which is far away from the interfaces. It means that the hydroxyl groups and water molecules can be attracted by PE. The increased concentration of water molecules than hydroxyl groups at the interface results from their different mobility, as displayed in **Figure 6.4**. This means that water molecules in the NASH structure are easier to move and approach the NASH/PE interface. The motion of hydroxyl groups is restricted by the aluminosilicate skeleton, and only those near the interface can be attracted by the PE layer.

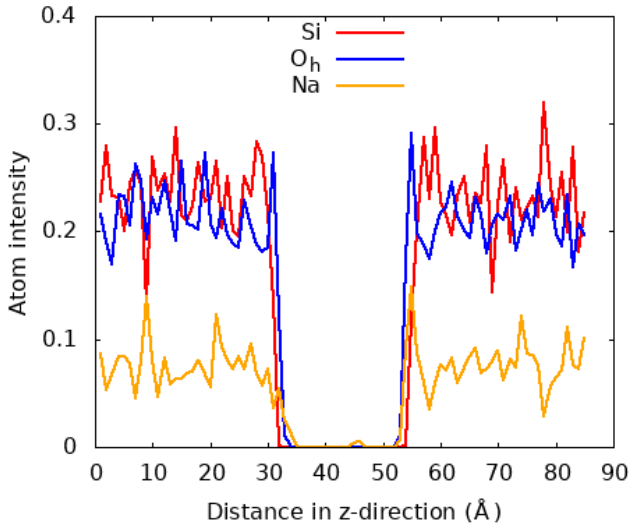

(a)

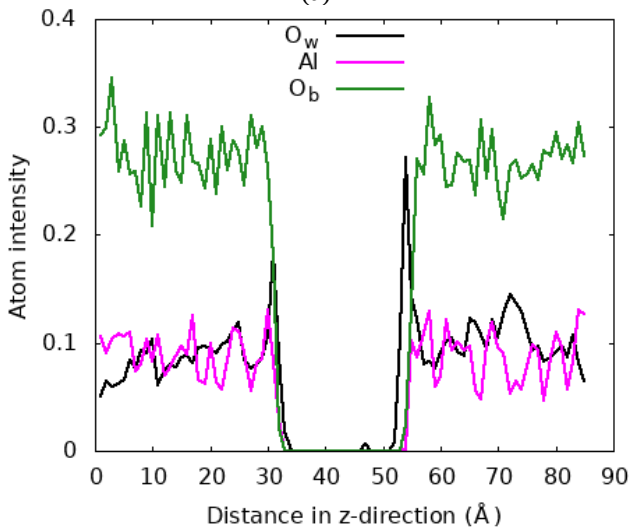

(b)

Figure 6.8 Atom intensity and distribution of NASH/PE composite system with Si/Al ratio of 2.5 along z-direction: (a) Si atom, hydroxyl O (O_h) atom and Na ion; (b) Al atom, water O (O_w) and bridge O (O_b) atoms

To further analyse the atomic interaction at the interface, the radial distribution function (RDF) among atoms between NASH and PE was computed (**Figure 6.9**). The function, *g(r)*, represents the probability of exhibit of other particles at the distance of the defined radius (*r*) of a centre particle. The result is computed based on the region with the thickness of 4 Å as the interface zone between NASH and PE in the simulation box. In the RDF curves, H_p represents the hydrogen atoms in polythene chains. In **Figure 6.9(a)**, at around 3 Å, a broad peak is found between H_p and O_w in the NASH. It means there is relatively a high probability that O_w atoms can be found in the distance range of 3-4 Å from H_p atoms. It indicates the existence of weak H-bonds between C-H and O (Desiraju and Steiner 2001). Lu et al. (2021b) also found similar weak H-bond

between PE fibre and CSH substrate. However, the interactions between H_p and O_h or O_b in NASH are not as obvious as that between H_p and O_w. It is because of the different mobility of various types of oxygen atoms. Water molecules with higher mobility are easier to move and contact the PE layer. On the other hand, O_b atoms are restricted in the skeleton, and seldom can interact with H_p. As seen in the atom distribution at the interface (**Figure 6.3**), there are more water molecules than O_h and O_b located near the surface. In addition, **Figure 6.9(b)** compares the RDF curves of the H_p-O_w pair in different NASH/PE composite systems. All the curves show a peak at the radius around 3 Å, which indicates that the weak H-bond between H_p and O_w generally exists at the interface of the NASH/PE composite with various Si/Al ratios. Due to the nonpolar properties of polyethene molecules, the coulombic interaction between PE chains and NASH substrate is weak. Thus, the interactions between the PE and NASH layers are dominated by the short-range van der Waals forces and hydrogen bonding between H_p and oxygen.

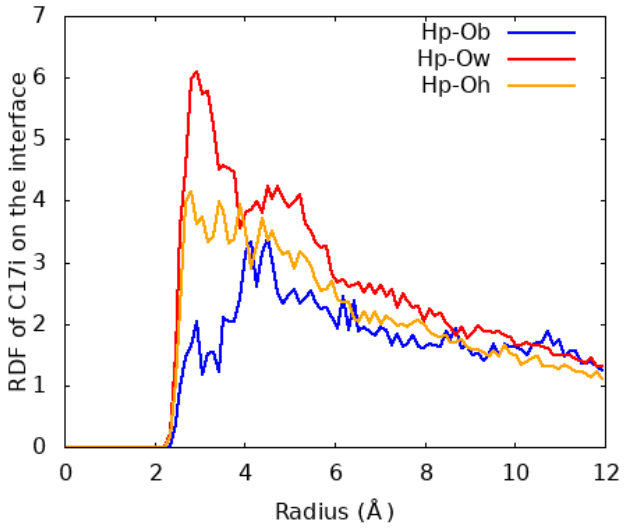

(a)

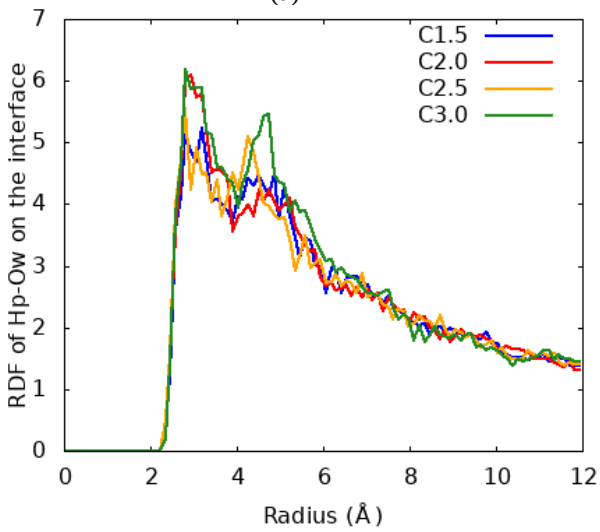

(b)

Figure 6.9 (a) RDF of the NASH with Si/Al ratio of 2.0 and PE materials on the interface (4 Å thickness): H_p refer to hydrogen in the PE, O_w, O_h and O_b refer to oxygen in the water molecule, hydroxyl group and NASH skeleton; (b) RDF comparison of H_p-O_w pair on the interface of NASH/PE composite systems with various Si/Al ratios

6.4.3.2 Van der Waals interaction

According to Van Oss surface energy theory, the interfacial intermolecular interaction can be distinguished as non-dispersive and dispersive components. The non-dispersive component relates to the permanent polar component on the surface, which has been discussed in the previous section. The dispersive component of the surface energy is from the van der Waals (vdW) force. It is distance-dependent and related to the temporary variation of electron densities that cause the attraction or repel between the surfaces (Ilango et al. 2021).

The vdW energy at the interface between the NASH and PE layer of the four composite systems has been computed from the trajectory data on the 2 ns after NVT equilibrium. **Figure 6.10** shows the vdW energy for the four systems with various Si/Al ratios. The computed vdW energy between NASH and PE for the C1.5 system is -280 Kcal/mole, which is lower than that of the other three systems. The others exhibit similar vdW energy around -330 Kcal/mole. Compared with the total interfacial interaction energy, the vdW accounts for more than 60% of the total interaction energy. This is in line with the findings reported by Ilango et al. (2021), in which the vdW force between organic polymer coating and hydrating cement is higher than their coulombic interactions. In particular, the vdW energy of the C1.5 composite takes the dominant part of the total interaction energy. This indicates that the coulombic interaction between NASH and PE in the C1.5 composite is relatively low.

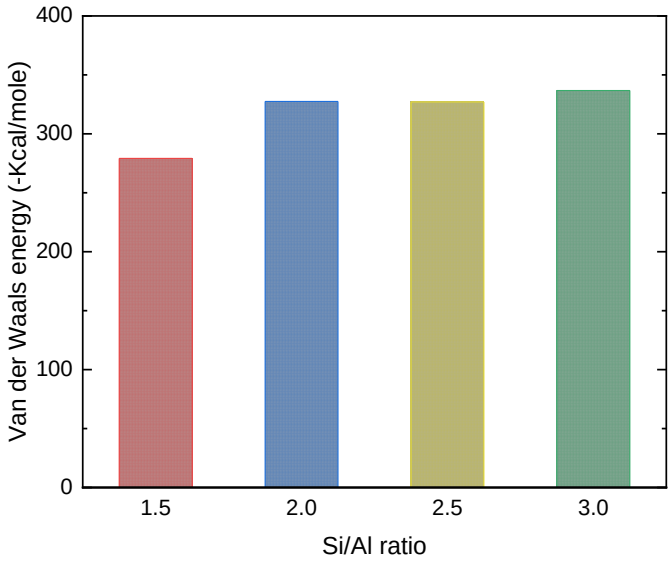

Figure 6.10 The van der Waals interaction energy between the NASH and the PE layer in the composite models with Si/Al ratios of 1.5, 2.0, 2.5 and 3.0

The vdW interaction is distance-dependent; thus, the averaged distances between the PE layer and the NASH part have also been calculated for comparison (**Figure 6.11**). The result is calculated from the equilibrium trajectory data of the four composite systems. The composite models have been separated into chunks with 2d spatial bins on the XY plane. The XY plane (around 60 Å × 60 Å) is first cut into 15×15 pieces with a square area of 4 Å × 4 Å, and then the models are separated into 225 pencil bins. In each bin, the maximum and minimum z-coordinate values in the PE and the NASH parts have

been extracted to calculate the gap distance between the two materials. Subsequently, the gap widths are the averaged distance between the centre of atoms at the interface along the z-direction. The gap distance in the C1.5 composite is much larger than that of the other models, which is around 3.2 Å while the others are all around 2.5 Å. The larger gap means a weaker interaction between NASH and PE, which is in line with the result of vdW energy (**Figure 6.10**). Moreover, the larger gap not only weakens the vdW energy, but also reduces the probability of the weak H-bond between H_p and O_w atoms.

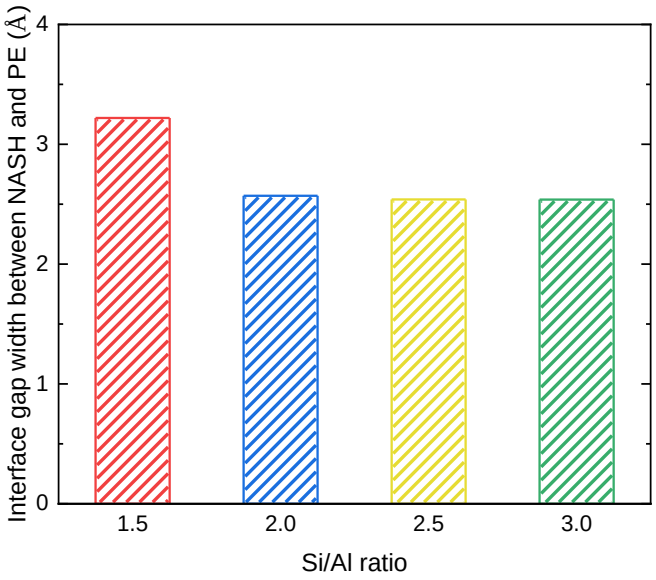

Figure 6.11 The averaged gap distance between the NASH part and the PE layer in the composite systems with Si/Al ratios of 1.5, 2.0, 2.5 and 3.0

6.4.4 Mechanical interlocking effect

The pull-out shear bonding strength is not only influenced by the interfacial atomic interaction between NASH and PE but is also impacted by the morphology of the interface. The surface roughness can cause the mechanical interlocking between two materials at the interface during the pull-out process (Gent and Lin 1990). Since the same PE model was used for all composite systems in this study, the surfaces of NASH substrates have been compared to reveal the influence of surface roughness on the pull-out strength. The NASH interface configurations of the lower layer of the NASH part in C1.5, C2.0, C2.5 and C3.0 systems have been extracted and shown in **Figure 6.12**. The XY planes in the graphs are the projection of the interface of the NASH configuration and various colours represent the variation of Z-coordinates. The

variation in the z-direction shows the roughness degree of the NASH surface. As seen in **Figure 6.12**, all the surfaces show many discontinuous corrugations. The influence of roughness on the pull-out strength has also been reported in previous studies to explain the mechanical interlocking effect (Wang et al. 2020a). Firstly, it can contribute to enlarging the interaction surface area between the NASH and the PE, further impacting the interaction energy. On the other hand, the corrugation leads to the interlocking and provides friction when PE is pulled out from the NASH substrate. For the four systems with various Si/Al ratios, there is no significant difference in surface roughness. For Si/Al ratios of 2.0, 2.5 and 3.0, the surfaces in **Figure 6.12** (b), (c) and (d) show a slightly increasing roughness degree. On the other hand, the graph for the C1.5 system shows a more apparent uneven surface. The lower coordinate level of the surface is relatively lower than the others and shows a darker colour on the graph. It should be contributed by the much lower density of the C1.5 NASH structure. Due to the looser atom distribution of NASH at the interface, more corrugations are found on the surface graph.

To sum up, the atomic weak H-bond interaction between H_p and O_w, vdW force between NASH and PE layer, and surface roughness combinedly affect the pull-out strengths of PE on NASH substrate with various Si/Al ratios. The general trend is that the vdW energy and surface roughness almost increase with the increase of the Si/Al ratio, which brings higher bonding strength. Although the composite with the lowest Si/Al ratio of 1.5 owns a rougher surface, its lower density and larger gap distance at the interface have weakened the mechanical interlocking effect. Consequently, C1.5 composite exhibits the lowest strength among the four composites. On the other hand, the weak H-bond on the interface also plays a non-negligible role. The decline of the strength of C3.0 composites is due to the less water content in the NASH structure, which has restricted the coulombic interaction between the two systems. As a result, the change of pull-out strength with Si/Al ratio (**Figure 6.6**) indicates that the composite with a Si/Al ratio of 2.5 presents the highest pull-out bonding strength between NASH and PE fibre.

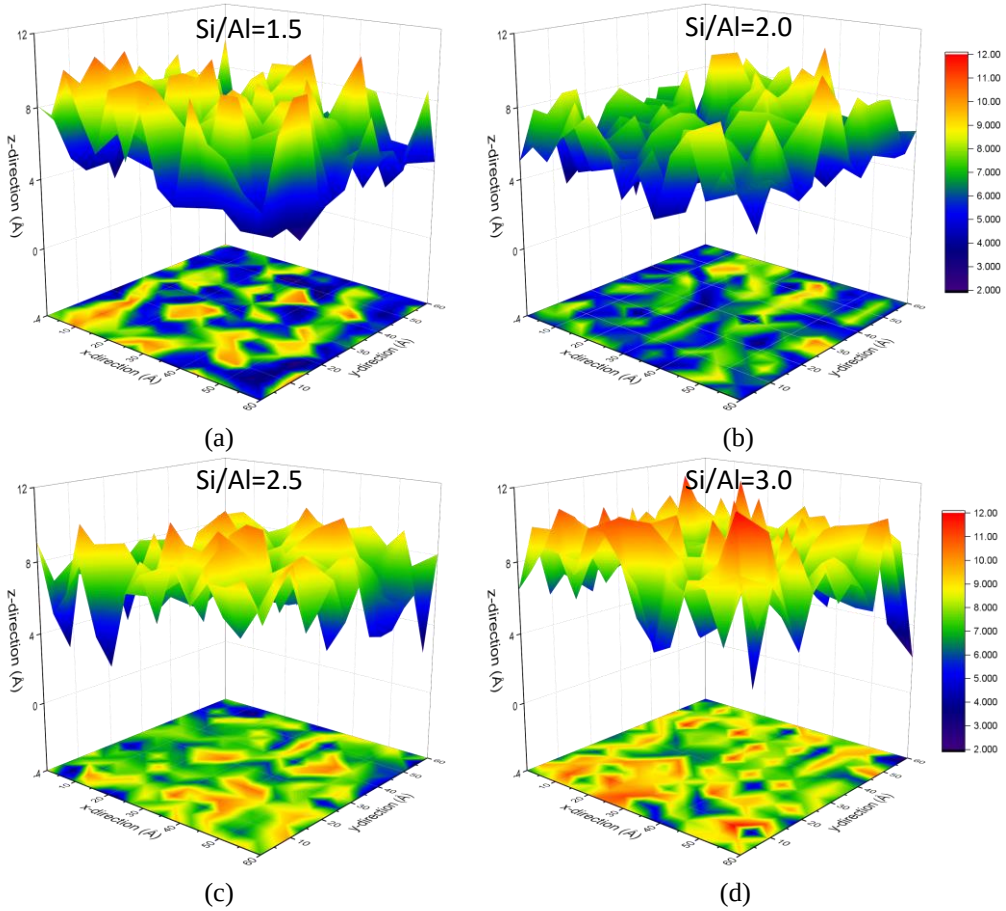

Figure 6.12 Contour map of the configuration of NASH/PE interface with various Si/Al ratios

6.4.5 Effect of water content in the NASH gel

This section presents the effect of internal water content in NASH on the bonding between PE and NASH. The smoothed pull-out force-displacement curves and the calculated shear bonding strengths are shown in **Figure 6.13**. Similar to the impact of Si/Al ratio variation, fluctuation of the pull-out force-displacement curves is observed. However, for the structures with less water content, the second and third force peaks of force-displacement curves are not as apparent as those of the full water curve. While the ultimate force value of the C2.5 (full water) system appears at the displacement of around 7 Å, those of water reduced ones appear much earlier (around 1 Å). The reason is that when fewer water molecules exit at the interface, fewer new interactions can be formed between the O_w in water and H_p in the polyethene chains during the pull-out process. Consequently, the rearrangement of atoms at the interface cannot bring a higher adhesion force between NASH and PE. In the force-displacement

curves of C2.5w66, C2.5w33 and C2.5w0 systems, the force values decline steadily until the complete pull-out of the PE layer.

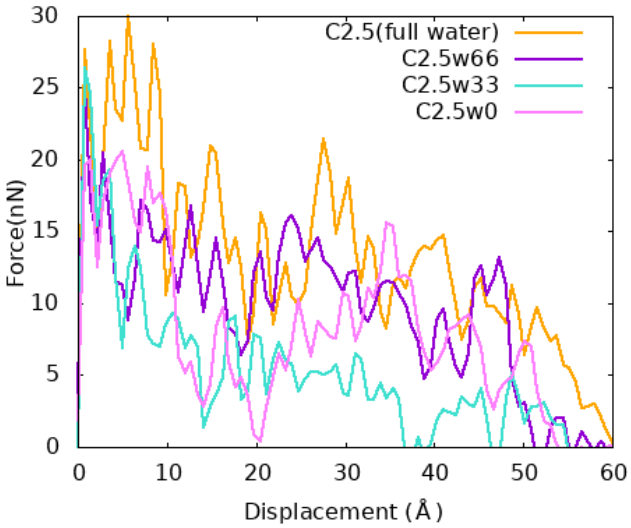

(a)

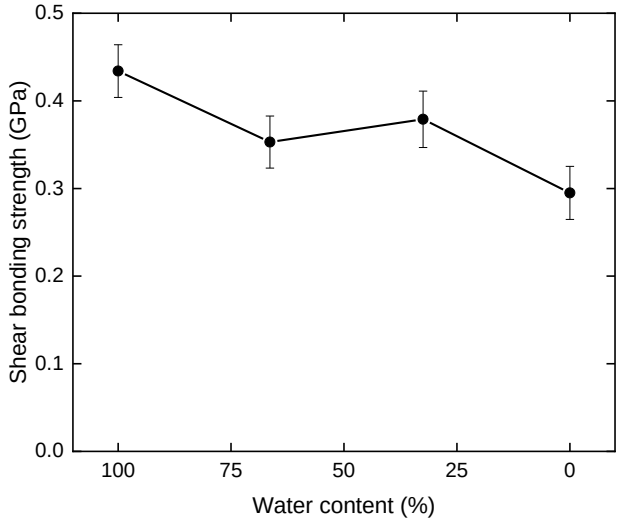

(b)

Figure 6.13 (a) The pull-out force-displacement curves of PE from NASH/PE systems (Si/Al=2.5) with various water contents (from 0 to full water content); (b) the shear bonding strengths at the interface between PE and NASH structures (Si/Al=2.5) with various water contents

Compared to the pull-out strength of C2.5 (full water), the strengths of the other three systems have been calculated and displayed in **Figure 6.13(b)**. With the reduction of water content, the pull-out strength decreases. The ultimate strength of C2.5 with full water is 0.43 GPa, while that of the dry structure C2.5w0 is only 0.30 GPa, which is only 70% of the full water one. The main reason is that less water content in the substrate reduces the probability of water molecules penetrating to the interface. Since water oxygen can form a weak H-

bond with hydrogens in the polyethene chains, less water causes a reduction in the coulombic interaction between the two sides. As a result, the strength declines.

The evidence is also found in the O_w atoms distribution curves shown in **Figure 6.14**. Atoms intensity of O_w along the z-direction in the composites of C2.5 (full water), C2.5w66, and C2.5w33 have been compared. The sharp peak at the interface is the most noticeable in the C2.5 system but much implicit in the system C2.5w66. When the water content has been reduced to 33% in system C2.5w33, the interface peak is hard to be observed. It indicates that more water molecules emerge at the interface of the composite of C2.5 with full water, which contributes to the more extensive coulombic interaction between NASH and PE and further enhances the pull-out shear bonding strength.

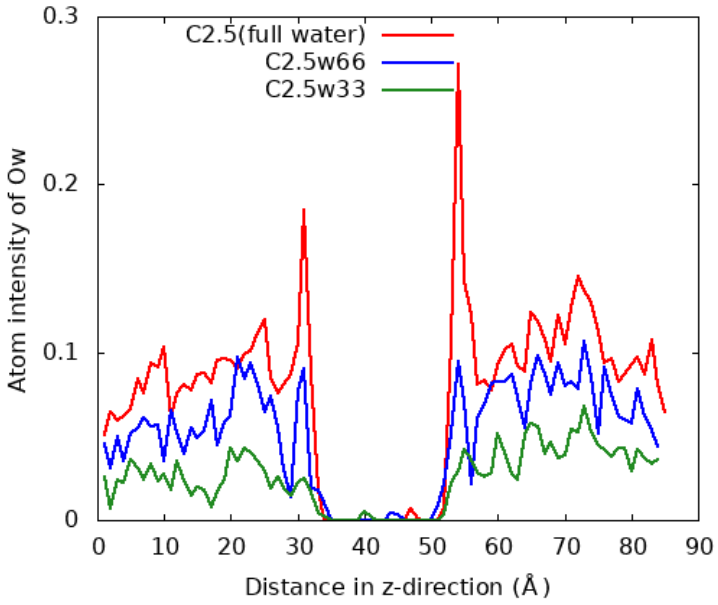

Figure 6.14 Normalized density distribution of O_w in NASH/PE systems with various water content along the z-direction

6.5 Concluding Remarks

In this work, NASH/PE composite models have been developed from the in-situ reactive geopolymerisation process to characterize the adhesive bonding between PE fibre and geopolymer materials. The dynamic pull-out simulation and the interfacial analysis have been conducted to explore the adhesion

mechanism and performances. Thus, the mechanism of the adhesion and impact of NASH compositions on the pull-out bonding have been explored and discussed. Based on the simulation results and analysis, the following conclusions could be made.

(1) The adhesive bonding between the NASH and PE is influenced by the interfacial interaction and the mechanical interlocking between two materials. The former contains the atomic pair interaction and the van der Waals force (vdW), while the latter is derived from the surface roughness. The vdW force contributes more than 60% of the interfacial interaction.
(2) The weak H-bond is found between H atoms in the polyethene chains and O atoms in the NASH, particularly the O atoms in water molecules. It provides the primary coulombic interaction between the polyethene chains and NASH.
(3) The Si/Al ratio in NASH can significantly impact the shear bonding strength between PE and NASH. The increase of the Si/Al ratio increases the vdW interaction energy at the interface between PE and NASH. The optimized shear bonding strength of 0.43 GPa is achieved at a Si/Al ratio of 2.5.
(4) The internal moisture in NASH structures degrades the adhesion properties by weakening the H-bond between PE and NASH. At the Si/Al ratio of 2.5, the bonding strength of a dry structure is only 70% of that of a full water one.

Chapter 7

Conclusions and Future Work

7.1 Conclusions

This thesis focuses on the MD simulation of NASH geopolymer and its composites, including investigating the structure-property relationships to provide more comprehensive knowledge of its structure at the nanoscale and exploring the interaction mechanism between NASH gels and other materials in its composites at the atomic level. To conduct MD simulation, it is vital that molecular models of NASH gels should be reliable and can provide sufficient information about the geopolymer system. Thus, this study is first dedicated to developing a suitable model for NASH gels. Afterwards, the reliable NASH gel models are employed in MD simulation to explore the structural, dynamics and mechanical properties, and simulate the NASH gel composites.

From the overview of existing research and development of geopolymers at the molecular or atomic level, it is found that MD simulation can be an effective approach to study the molecular structure of NASH gels. Thus, it is urgent to develop a reliable amorphous molecular model of NASH gels to deeply investigate its structure-property relationships and explore the interaction mechanism of NASH gels with organic and inorganic additives in geopolymer composites at the molecular level. Therefore, this MD simulation of NASH gels and their composites has been conducted.

Firstly, the NASH gel's microscopic structures, reaction process, and mechanical properties are studied using reactive MD. The major conclusions contain:

- The geopolymerisation reaction has been simulated based on a realistic bottom-up modelling method from oligomers with various Si/Al ratios and configurations.
- The estimated geopolymerisation degree indicates that 50% of the hydroxyls in oligomers are consumed; Besides, a higher Si/Al ratio and linear configuration can enhance the reaction degree, while those with cyclic oligomers exhibit a higher complexity network structure.
- Decreasing the Si/Al ratio can reduce the bond angle of aluminosilicate chains, decrease the structure's stability, and restrict the dynamic water diffusion.
- Around 2.5% of the generated water molecules can be dissociated during tensile deformation, reflecting the number of breakage chains; Besides, more broken Al-O than Si-O bonds are found, indicating the weaker nature of Al-O bonds.
- Larger Si/Al ratios and cyclic configuration enhance both tensile strength and elastic modulus, while the increase of elastic modulus is mainly attributed to the reduction in hydroxyl radicals and enhanced network complexity of NASH gels.

In the MD simulation of nano-silica modified NASH gel composites, the NASH-silica systems with various Si/Al ratios from 1.5 to 3.0 have been constructed, and the composites are compared with the neat NASH gels generated without amorphous silica. It is found that:

- The chemical reaction between amorphous silica and NASH gel is observed by the RDF obtained, with the 10 Å-thick ITZ in the composites. The ITZ has similar atomic structure and bond types as NASH gel, but has a much higher density and lower diffusion rate.
- Amorphous silica can enhance reaction degree and skeleton complexity: the reaction degree is improved by around 10%, and the bridge oxygen percentage is increased by around 6%.

- Amorphous silica can improve the stability of NASH gel: at Si/Al ratio of 1.5, the diffusion coefficient of Na ions in NASH gel with amorphous silica is only 58% of that in neat NASH gel.
- In various phases, the mechanical strength is in the order of ITZ > NASH-s > neat NASH gel. The tensile strength of NASH gels is improved by 10~40% with the incorporation of amorphous silica, and the optimum UTS of the composites is obtained as 4.1 GPa at Si/Al ratios of 2.5 and 3.0.

In the MD simulation of FRGC, NASH-PE composite models have been built. Based on the structure analysis, energy and dynamics characterization, and pull-out simulation, it is found that:

- The interfacial interaction and the mechanical interlocking between two materials constitute adhesive bonding. The interfacial interaction mainly comes from the atomic pair interaction and the vdW force, while the mechanical interlocking is derived from the surface roughness. The vdW force contributes more than 60% of the interfacial interaction.
- A weak H-bond is observed between PE and NASH, which provides the primary coulombic interaction.
- The shear bonding strength is significantly impacted by Si/Al ratio in NASH, which can vary the vdW interaction energy at the interface. At an optimized Si/Al ratio of 2.5, the shear bonding strength is 0.43 GPa.
- The adhesion property is also influenced by the internal moisture in NASH, since the H-bond numbers can be changed. At the Si/Al ratio of 2.5, the bonding strength of a dry structure is only 70% of that of a full water one.

The thesis proposes a feasible methodology for MD simulations of in-situ geopolymerised NASH gels and their composites. Subsequently, reliable NASH gel models with various Si/Al ratios have been generated from a reactive MD simulation. With these models, the effect of nano-silica in geopolymers has been explained by observing the reaction between silica and NASH gel at the molecular level; the adhesive bonding between geopolymers and PE fibre has been characterized by MD simulation of the interface of the nano-composites.

MD simulations of NASH gels and their composites provide insights into structural information and interaction mechanism of geopolymers at the molecular level, which is valuable for further materials design.

7.2 Major Contributions

The major contributions of this study are:

- A bottom-up reactive MD simulation approach has been proposed to obtain NASH gel molecular models from realistic oligomers. Geopolymerisation has been simulated to investigate the effect of Si/Al ratios in the systems on the properties of NASH gel.
- The structure-property relationships of NASH gels have been characterized as the function of the Si/Al ratio and oligomers' configuration. The results provide valuable insights into the design of geopolymer at the macro-scale level.
- The reaction between nano-silica and NASH gel has been observed with MD simulations. The enhancement in NASH gels' performances by incorporating nano-silica has been explained at the molecular level.
- The interaction mechanism between NASH gel and PE fibres has been characterized by MD simulation. The effects of NASH gel compositions on interfacial bonding are explored.

7.3 Future Work

Geopolymer, considered as a sustainable material, is believed to be promising for multi-functional applications in the construction industry. The MD simulation has enhanced the understanding of structural information, reaction mechanism, thermodynamic properties, mechanical performances, and dynamics of geopolymers. However, the MD simulation on geopolymers is still relatively new at this stage. The following research directions in MD simulation of geopolymers are recommended for future study.

- The existing modelling methods of NASH gels, including modification from zeolites or NAS glass models, bottom-up modelling by types of atoms or monomers, and the in-situ reactive simulation of geopolymerisation, are all generating NASH gel models with box sizes with the scale of a few nanometres. This cannot explain the actual pores and defects inside geopolymers. It is mainly due to the expensive simulation time required for larger systems and the limitation of computational resources. There is still a vast difference between simulation and experimental results. However, it is valuable to develop larger and more accurate MD models for geopolymer as well as to conjugate with other simulation technology for the development of a multi-scaled modelling system.
- The simulation studies of geopolymers mainly focus on NASH gels. However, potassium or lithium-based geopolymers also show attractive features. The KASH and LASH structures can be established to investigate their properties. In addition, properties of geopolymer highly depend on the precursors. Effects of various elements and ions in different types of precursors on the properties of geopolymer need to be further investigated by MD simulation, e.g. Ca ions in GGBS, Fe element in GGBS and MK, the carbon content in FA, heavy metals in tail mineral slag, etc. These elements may modify the molecular structure of the reaction products, as well as impact the simulation results. Thus, more in-depth MD simulations are suggested to reflect the actual compositions of geopolymer.
- There are still limited studies focusing on the MD simulation of geopolymer composites. A variety of additives have been added to the construction materials in practice. MD simulation can be a useful tool for materials selection and optimization. For instance, the use of retarder, water reducer and thixotropy modifier in geopolymer is still a mystery. It is essential to reveal the impact of incorporating additives on the quality control of geopolymers
- The selection of force field in the MD simulation of geopolymer materials remains unclear. It has been recognized that the MD results

vary in the force fields adopted in the simulation. The most common force fields include general force fields, ClayFF and ReaxFF force fields. With the further development of geopolymer MD simulation, it is necessary to develop a specific force field or explore the more accurate force field parameters for geopolymers. This is beneficial to narrow the difference between simulation results obtained in various studies and makes the simulation results more comparable to the experimental results.

References

Adak, D., Sarkar, M., and Mandal, S. (2017). "Structural performance of nano-silica modified fly-ash based geopolymer concrete." *Construction and Building Materials*, 135, 430-439.

Ahmed, H. U. A., Mohammed, A. S., and Mohammed, A. (2022). "The role of nanomaterials in geopolymer concrete composites: A state-of-the-art review." *Journal of Building Engineering*, 49.

Amran, Y. M., Alyousef, R., Alabduljabbar, H., and El-Zeadani, M. (2020). "Clean production and properties of geopolymer concrete; A review." *Journal of Cleaner Production*, 251, 119679.

Assi, L. N., Deaver, E. E., and Ziehl, P. (2018). "Effect of source and particle size distribution on the mechanical and microstructural properties of fly Ash-Based geopolymer concrete." *Construction and Building Materials*, 167, 372-380.

Bagheri, A., Nazari, A., Sanjayan, J. G., and Duan, W. (2018). "Molecular simulation of water and chloride ion diffusion in nanopores of alkali-activated aluminosilicate structures." *Ceramics International*, 44(17), 20723-20731.

Bagheri, A., Nazari, A., Sanjayan, J. G., Rajeev, P., and Duan, W. (2017). "Fly ash-based boroaluminosilicate geopolymers: Experimental and molecular simulations." *Ceramics International*, 43(5), 4119-4126.

Bahraq, A. A., Al-Osta, M. A., Al-Amoudi, O. S. B., Saleh, T. A., and Obot, I. (2022). "Atomistic simulation of polymer-cement interactions: Progress and research challenges." *Construction and Building Materials*, 327, 126881.

Bai, C., Liu, L., and Sun, H. (2012). "Molecular dynamics simulations of methanol to olefin reactions in HZSM-5 zeolite using a ReaxFF force field." *The Journal of Physical Chemistry C*, 116(12), 7029-7039.

Beleña, I., and Zhu, W. (2009). "Nanoindentation study of Na-geopolymers exposed to high temperatures", *Nanotechnology in Construction 3*. Springer, pp. 169-174.

Bhutta, A., Borges, P. H., Zanotti, C., Farooq, M., and Banthia, N. (2017). "Flexural behavior of geopolymer composites reinforced with steel and polypropylene macro fibers." *Cement and Concrete Composites*, 80, 31-40.

Botan, A., Marry, V., Rotenberg, B., Turq, P., and Noetinger, B. (2013). "How Electrostatics Influences Hydrodynamic Boundary Conditions: Poiseuille and Electro-osmostic Flows in Clay Nanopores." *The Journal of Physical Chemistry C*, 117(2), 978-985.

Chindaprasirt, P., De Silva, P., Sagoe-Crentsil, K., and Hanjitsuwan, S. (2012). "Effect of SiO2 and Al2O3 on the setting and hardening of high calcium fly ash-based geopolymer systems." *Journal of Materials Science*, 47(12), 4876-4883.

Chitsaz, S., and Tarighat, A. (2020). "Molecular dynamics simulation of N-A-S-H geopolymer macro molecule model for prediction of its modulus of elasticity." *Construction and Building Materials*, 243.

Choi, J.-I., Lee, B. Y., Ranade, R., Li, V. C., and Lee, Y. (2016). "Ultra-high-ductile behavior of a polyethylene fiber-reinforced alkali-activated slag-based composite." *Cement and Concrete Composites*, 70, 153-158.

Criado, M., Fernández-Jiménez, A., Palomo, A., Sobrados, I., and Sanz, J. (2008). "Effect of the SiO2/Na2O ratio on the alkali activation of fly ash. Part II: 29Si MAS-NMR Survey." *Microporous and Mesoporous Materials*, 109(1-3), 525-534.

Cygan, R. T., Greathouse, J. A., Heinz, H., and Kalinichev, A. G. (2009). "Molecular models and simulations of layered materials." *Journal of Materials Chemistry*, 19(17), 2470-2481.

Cygan, R. T., Greathouse, J. A., and Kalinichev, A. G. (2021). "Advances in Clayff molecular simulation of layered and nanoporous materials and their aqueous interfaces." *The Journal of Physical Chemistry C*, 125(32), 17573-17589.

Cygan, R. T., Liang, J.-J., and Kalinichev, A. G. (2004). "Molecular models of hydroxide, oxyhydroxide, and clay phases and the development of a general force field." *The Journal of Physical Chemistry B*, 108(4), 1255-1266.

Das, S., Yang, P., Singh, S. S., Mertens, J. C. E., Xiao, X., Chawla, N., and Neithalath, N. (2015). "Effective properties of a fly ash geopolymer: Synergistic application of X-ray synchrotron tomography, nanoindentation, and homogenization models." *Cement and Concrete Research*, 78, 252-262.

Davidovits, J. (1991). "Geopolymers - Inorganic Polymeric New Materials." *Journal of Thermal Analysis*, 37(8), 1633-1656.

Davidovits, J. "Properties of geopolymer cements." *Presented at First international conference on alkaline cements and concretes*.

Deb, P. S., Sarker, P. K., and Barbhuiya, S. (2015). "Effects of nano-silica on the strength development of geopolymer cured at room temperature." *Construction and Building Materials*, 101, 675-683.

Deb, P. S., Sarker, P. K., and Barbhuiya, S. (2016). "Sorptivity and acid resistance of ambient-cured geopolymer mortars containing nano-silica." *Cement & Concrete Composites*, 72, 235-245.

Desiraju, G. R., and Steiner, T. (2001). *The weak hydrogen bond: in structural chemistry and biology*: International Union of Crystal.

Dimas, D., Giannopoulou, I., and Panias, D. (2009). "Polymerization in sodium silicate solutions: a fundamental process in geopolymerization technology." *Journal of Materials Science*, 44(14), 3719-3730.

Duxson, P., Fernández-Jiménez, A., Provis, J. L., Lukey, G. C., Palomo, A., and van Deventer, J. S. J. (2006a). "Geopolymer technology: the current state of the art." *Journal of Materials Science*, 42(9), 2917-2933.

Duxson, P., Lukey, G. C., and van Deventer, J. S. J. (2006b). "Thermal conductivity of metakaolin geopolymers used as a first approximation for determining gel interconnectivity." *Industrial & Engineering Chemistry Research*, 45(23), 7781-7788.

Duxson, P., Provis, J. L., Lukey, G. C., Mallicoat, S. W., Kriven, W. M., and van Deventer, J. S. J. (2005). "Understanding the relationship between

geopolymer composition, microstructure and mechanical properties." *Colloids and Surfaces A: Physicochemical and Engineering Aspects*, 269(1-3), 47-58.

Fan, D., Lue, L., and Yang, S. (2017). "Molecular dynamics study of interfacial stress transfer in graphene-oxide cementitious composites." *Computational Materials Science*, 139, 56-64.

Fan, D., and Yang, S. (2018). "Mechanical properties of C-S-H globules and interfaces by molecular dynamics simulation." *Construction and Building Materials*, 176, 573-582.

Fukuda, M. (1998). "Clustering of water in polyethylene: A molecular-dynamics simulation." *The Journal of chemical physics*, 109(15), 6476-6485.

Garside, M. (2022). "Global cement production 1995-2021." ***US Geological survey (USGS) mineral commodity summaries***.

Gent, A., and Lin, C.-W. (1990). "Model studies of the effect of surface roughness and mechanical interlocking on adhesion." *The Journal of Adhesion*, 32(2-3), 113-125.

Guan, X., Jiang, L., Fan, D., Hernandez, A. G., Li, B., and Do, H. (2022). "Molecular simulations of the structure-property relationships of NASH gels." *Construction and Building Materials*, 329, 127166.

Hahn, S. H., Rimsza, J., Criscenti, L., Sun, W., Deng, L., Du, J., Liang, T., Sinnott, S. B., and Van Duin, A. C. (2018). "Development of a ReaxFF reactive force field for NaSiO x/water systems and its application to sodium and proton self-diffusion." *The Journal of Physical Chemistry C*, 122(34), 19613-19624.

Henderson, G. S., Neuville, D. R., Cochain, B., and Cormier, L. (2009). "The structure of GeO2–SiO2 glasses and melts: A Raman spectroscopy study." *Journal of Non-Crystalline Solids*, 355(8), 468-474.

Hosan, A., Shaikh, F. U. A., Sarker, P., and Aslani, F. (2021). "Nano- and micro-scale characterisation of interfacial transition zone (ITZ) of high volume slag and slag-fly ash blended concretes containing nano SiO2 and nano CaCO3." *Construction and Building Materials*, 269.

Hou, D. (2014). *Molecular simulation on the calcium silicate hydrate (CSH) gel*: Hong Kong University of Science and Technology (Hong Kong).

Hou, D., Yu, J., and Wang, P. (2019). "Molecular dynamics modeling of the structure, dynamics, energetics and mechanical properties of cement-polymer nanocomposite." *Composites Part B: Engineering*, 162, 433-444.

Hou, D., Zhang, J., Pan, W., Zhang, Y., and Zhang, Z. (2020). "Nanoscale mechanism of ions immobilized by the geopolymer: A molecular dynamics study." *Journal of Nuclear Materials*, 528.

Hou, D., Zhang, Y., Yang, T., Zhang, J., Pei, H., Zhang, J., Jiang, J., and Li, T. (2018). "Molecular structure, dynamics, and mechanical behavior of sodium aluminosilicate hydrate (NASH) gel at elevated temperature: a molecular dynamics study." *Phys Chem Chem Phys*, 20(31), 20695-20711.

Ibrahim, M., Johari, M. A. M., Maslehuddin, M., and Rahman, M. K. (2018). "Influence of nano-SiO2 on the strength and microstructure of natural pozzolan based alkali activated concrete." *Construction and Building Materials*, 173, 573-585.

Ilango, N. K., Gujar, P., Nagesh, A. K., Alex, A., and Ghosh, P. (2021). "Interfacial adhesion mechanism between organic polymer coating and hydrating cement paste." *Cement and Concrete Composites*, 115, 103856.

Ismail, I., Bernal, S. A., Provis, J. L., Nicolas, R. S., Hamdan, S., and van Deventer, J. S. J. (2014). "Modification of phase evolution in alkali-activated blast furnace slag by the incorporation of fly ash." *Cement & Concrete Composites*, 45, 125-135.

Issa, H. K., Taherizadeh, A., and Maleki, A. (2020). "Atomistic-level study of the mechanical behavior of amorphous and crystalline silica nanoparticles." *Ceramics International*, 46(13), 21647-21656.

J.Davidovits. (1989). "Geopolymers and geopolymeric materials." *Journal of Thermal Analysis and Calorimetry*, 35(2), 429-441.

J.Davidovits. (1991). "<Geopolymers: inorganic polymeric new materials>." *Journal ofThamalAnalysis*, 37, 1633-1656.

Jindal, B. B., and Sharma, R. (2020). "The effect of nanomaterials on properties of geopolymers derived from industrial by-products: A state-of-the-art review." *Construction and Building Materials*, 252.

Jorgensen, W. L., Maxwell, D. S., and Tirado-Rives, J. (1996). "Development and Testing of the OPLS All-Atom Force Field on Conformational Energetics and Properties of Organic Liquids." *Journal of the American Chemical Society*, 118(45), 11225-11236.

Kai, M. F., and Dai, J. G. (2021). "Understanding geopolymer binder-aggregate interfacial characteristics at molecular level." *Cement and Concrete Research*, 149.

Kai, M. F., Zhang, L. W., and Liew, K. M. (2020). "Carbon nanotube-geopolymer nanocomposites: A molecular dynamics study of the influence of interfacial chemical bonding upon the structural and mechanical properties." *Carbon*, 161, 772-783.

Kajaste, R., and Hurme, M. (2016). "Cement industry greenhouse gas emissions – management options and abatement cost." *Journal of Cleaner Production*, 112, 4041-4052.

Kani, E. N., Allahverdi, A., and Provis, J. L. (2012). "Efflorescence control in geopolymer binders based on natural pozzolan." *Cement & Concrete Composites*, 34(1), 25-33.

Khan, M. Z. N., Shaikh, F. U. A., Hao, Y. F., and Hao, H. (2016). "Synthesis of high strength ambient cured geopolymer composite by using low calcium fly ash." *Construction and Building Materials*, 125, 809-820.

Khater, H. M. (2016). "Nano-Silica effect on the physicomechanical properties of geopolymer composites." *Advances in Nano Research*, 4(3), 181-195.

Kinrade, S. D., and Swaddle, T. W. J. I. C. (1989). "Direct detection of aluminosilicate species in aqueous solution by silicon-29 and aluminum-27 NMR spectroscopy." 28(10), 1952-1954.

Kong, D. L. Y., and Sanjayan, J. G. (2010). "Effect of elevated temperatures on geopolymer paste, mortar and concrete." *Cement and Concrete Research*, 40(2), 334-339.

Kotop, M. A., El-Feky, M. S., Alharbi, Y. R., Abadel, A. A., and Binyahya, A. S. (2021). "Engineering properties of geopolymer concrete incorporating hybrid nano-materials." *Ain Shams Engineering Journal*, 12(4), 3641-3647.

Lazaro, A., Yu, Q. L., and Brouwers, H. J. H. (2016). "Nanotechnologies for sustainable construction." *Sustainability of Construction Materials, 2nd Edition*, 70, 55-78.

Le Roux, S., and Jund, P. (2010). "Ring statistics analysis of topological networks: New approach and application to amorphous GeS2 and SiO2 systems." *Computational Materials Science*, 49(1), 70-83.

Lehne, J., and Preston, F. (2018). "Making concrete change: Innovation in low-carbon cement and concrete."

Lepech, M. D., and Li, V. C. (2009). "Water permeability of engineered cementitious composites." *Cement and concrete composites*, 31(10), 744-753.

Li, T., Tang, Z. A., Huang, Z. X., and Yu, J. (2017). "Thermal boundary resistance between the polycrystalline graphene and the amorphous SiO2 substrate." *Chemical Physics Letters*, 685, 349-353.

Li, V. C. (2003). "On engineered cementitious composites (ECC) a review of the material and its applications." *Journal of advanced concrete technology*, 1(3), 215-230.

Li, V. C. (2019). *Engineered cementitious composites (ECC): bendable concrete for sustainable and resilient infrastructure*: Springer.

Li, V. C., and Leung, C. K. (1992). "Steady-state and multiple cracking of short random fiber composites." *Journal of engineering mechanics*, 118(11), 2246-2264.

Li, Z. P., Fei, M. E., Huyan, C. X., and Shi, X. M. (2021). "Nano-engineered, Fly Ash-Based Geopolymer Composites: An Overview." *Resources Conservation and Recycling*, 168.

Lo, K. W., Lin, K. L., Cheng, T. W., Chang, Y. M., and Lan, J. Y. (2017). "Effect of nano-SiO2 on the alkali-activated characteristics of spent catalyst metakaolin-based geopolymers." *Construction and Building Materials*, 143, 455-463.

Lolli, F., Manzano, H., Provis, J. L., Bignozzi, M. C., and Masoero, E. (2018). "Atomistic Simulations of Geopolymer Models: The Impact of Disorder on Structure and Mechanics." *ACS Appl Mater Interfaces*, 10(26), 22809-22820.

Lu, J., Luo, M., and Yakobson, B. I. (2018). "Glass composites reinforced with silicon-doped carbon nanotubes." *Carbon*, 128, 231-236.

Lu, Z., Yin, R., Yao, J., and Zhao, B. (2021a). "Experimental and molecular dynamic study on the interfacial strengthening mechanism of PE fiber/cement mortar using advanced oxidation processes." *Construction and Building Materials*, 309, 125144.

Lu, Z. Y., Yin, R., Yao, J., and Zhao, B. J. (2021b). "Experimental and molecular dynamic study on the interfacial strengthening mechanism of PE fiber/cement mortar using advanced oxidation processes." *Construction and Building Materials*, 309.

Lu, Z. Y., Yu, J., Yao, J., and Hou, D. S. (2020). "Experimental and molecular modeling of polyethylene fiber/cement interface strengthened by graphene oxide." *Cement & Concrete Composites*, 112.

Luo, Z., Li, W., Gan, Y., Mendu, K., and Shah, S. P. (2020). "Applying grid nanoindentation and maximum likelihood estimation for N-A-S-H gel in geopolymer paste: Investigation and discussion." *Cement and Concrete Research*, 135.

Lyngdoh, G. A., Kumar, R., Krishnan, N. M. A., and Das, S. (2019). "Realistic atomic structure of fly ash-based geopolymer gels: Insights from molecular dynamics simulations." *The Journal of Chemical Physics*, 151(6).

Lyngdoh, G. A., Nayak, S., Krishnan, N. M. A., and Das, S. (2020a). "Fracture toughness of fly ash-based geopolymer gels: Evaluations using nanoindentation experiment and molecular dynamics simulation." *Construction and Building Materials*, 262.

Lyngdoh, G. A., Nayak, S., Kumar, R., Anoop Krishnan, N., and Das, S. (2020b). "Fracture toughness of sodium aluminosilicate hydrate (NASH) gels: Insights from molecular dynamics simulations." *Journal of Applied Physics*, 127(16), 165107.

Lyu, B.-C., Ding, C., Guo, L.-P., Chen, B., and Wang, A.-g. (2021). "Basic performances and potential research problems of strain hardening geopolymer composites: A critical review." *Construction and Building Materials*, 287, 123030.

Lyu, S.-J., Wang, T.-T., Cheng, T.-W., and Ueng, T.-H. (2013). "Main factors affecting mechanical characteristics of geopolymer revealed by experimental design and associated statistical analysis." *Construction and Building Materials*, 43, 589-597.

Majidi, B. (2009). "Geopolymer technology, from fundamentals to advanced applications: a review." *Materials Technology*, 24(2), 79-87.

Mantisi, B., Tanguy, A., Kermouche, G., and Barthel, E. (2012). "Atomistic response of a model silica glass under shear and pressure." *The European Physical Journal B*, 85(9), 304.

Mauri, F., Pasquarello, A., Pfrommer, B. G., Yoon, Y.-G., and Louie, S. G. (2000). "Si-O-Si bond-angle distribution in vitreous silica from first-principles 29 Si NMR analysis." *Physical Review B*, 62(8), R4786.

McLellan, B. C., Williams, R. P., Lay, J., van Riessen, A., and Corder, G. D. (2011). "Costs and carbon emissions for geopolymer pastes in comparison to ordinary portland cement." *Journal of Cleaner Production*, 19(9), 1080-1090.

Monteiro, P. J. M., Miller, S. A., and Horvath, A. (2017). "Towards sustainable concrete." *Nat Mater*, 16(7), 698-699.

Mustakim, S. M., Das, S. K., Mishra, J., Aftab, A., Alomayri, T. S., Assaedi, H. S., and Kaze, C. R. (2021). "Improvement in Fresh, Mechanical and Microstructural Properties of Fly Ash- Blast Furnace Slag Based Geopolymer Concrete By Addition of Nano and Micro Silica." *Silicon*, 13(8), 2415-2428.

Nematollahi, B., Sanjayan, J., and Shaikh, F. U. A. (2015). "Synthesis of heat and ambient cured one-part geopolymer mixes with different grades of sodium silicate." *Ceramics International*, 41(4), 5696-5704.

Němeček, J., Šmilauer, V., and Kopecký, L. (2011). "Nanoindentation characteristics of alkali-activated aluminosilicate materials." *Cement and Concrete Composites*, 33(2), 163-170.

Ng, C., Alengaram, U. J., Wong, L. S., Mo, K. H., Jumaat, M. Z., and Ramesh, S. (2018). "A review on microstructural study and compressive strength of geopolymer mortar, paste and concrete." *Construction and Building Materials*, 186, 550-576.

Nguyen, H., Carvelli, V., Adesanya, E., Kinnunen, P., and Illikainen, M. (2018). "High performance cementitious composite from alkali-activated ladle slag reinforced with polypropylene fibers." *Cement and Concrete Composites*, 90, 150-160.

Nguyễn, H. H., Lương, Q.-H., Choi, J.-I., Ranade, R., Li, V. C., and Lee, B. Y. (2021). "Ultra-ductile behavior of fly ash-based engineered geopolymer composites with a tensile strain capacity up to 13.7%." *Cement and Concrete Composites*, 122, 104133.

Nicholson, C., Fletcher, R., Miller, N., Stirling, C., Morris, J., Hodges, S., MacKenzie, K., and Schmucker, M. (2005). "Building innovation through geopolymer technology." *Chemistry in New Zealand*, 69(3), 10.

North, M. R., and Swaddle, T. W. J. I. c. (2000). "Kinetics of silicate exchange in alkaline aluminosilicate solutions." 39(12), 2661-2665.

Nuaklong, P., Jongvivatsakul, P., Pothisiri, T., Sata, V., and Chindaprasirt, P. (2020). "Influence of rice husk ash on mechanical properties and fire resistance of recycled aggregate high-calcium fly ash geopolymer concrete." *Journal of Cleaner Production*, 252.

Nuaklong, P., Sata, V., Wongsa, A., Srinavin, K., and Chindaprasirt, P. (2018). "Recycled aggregate high calcium fly ash geopolymer concrete with inclusion of OPC and nano-SiO2." *Construction and Building Materials*, 174, 244-252.

Ohno, M., and Li, V. C. (2018). "An integrated design method of Engineered Geopolymer Composite." *Cement and Concrete Composites*, 88, 73-85.

Olsson, P. A., Schröder, E., Hyldgaard, P., Kroon, M., Andreasson, E., and Bergvall, E. (2017). "Ab initio and classical atomistic modelling of structure and defects in crystalline orthorhombic polyethylene: Twin boundaries, slip interfaces, and nature of barriers." *Polymer*, 121, 234-246.

Pacheco-Torgal, F. (2015). "Handbook of Alkali-activated Cements, Mortars and Concretes", in F. Pacheco-Torgal, J. A. Labrincha, C. Leonelli, A. Palomo, and P. Chindaprasirt, (eds.), *Handbook of Alkali-Activated Cements, Mortars and Concretes*. Oxford: Woodhead Publishing, pp. 1-16.

Pacheco-Torgal, F., Abdollahnejad, Z., Camões, A. F., Jamshidi, M., and Ding, Y. (2012). "Durability of alkali-activated binders: A clear advantage over Portland cement or an unproven issue?" *Construction and Building Materials*, 30, 400-405.

Palomo, A., Blanco-Varela, M. T., Granizo, M. L., Puertas, F., Vazquez, T., and Grutzeck, M. W. (1999). "Chemical stability of cementitious materials based on metakaolin." *Cement and Concrete Research*, 29(7), 997-1004.

Pant, P. K., Han, J., Smith, G. D., and Boyd, R. H. (1993). "A molecular dynamics simulation of polyethylene." *The Journal of chemical physics*, 99(1), 597-604.

Phoo-ngernkham, T., Chindaprasirt, P., Sata, V., Pangdaeng, S., and Sinsiri, T. (2013). "Properties of high calcium fly ash geopolymer pastes with Portland cement as an additive." *International Journal of Minerals Metallurgy and Materials*, 20(2), 214-220.

Plimpton, S., Crozier, P., and Thompson, A. (2007). "LAMMPS-large-scale atomic/molecular massively parallel simulator." *Sandia National Laboratories*, 18, 43.

Provis, J. L., Duxson, P., Van Deventer, J. S. J., and Lukey, G. C. (2005). "The Role of Mathematical Modelling and Gel Chemistry in Advancing Geopolymer Technology." *Chemical Engineering Research and Design*, 83(7), 853-860.

Quercia, G., and Brouwers, H. "Application of nano-silica (nS) in concrete mixtures." *Presented at 8th fib PhD symposium in Kgs, Lyngby, Denmark*.

Rabiaa, E., Mohamed, R. A. S., Sofi, W. H., and Tawfik, T. A. (2020). "Developing Geopolymer Concrete Properties by Using Nanomaterials and Steel Fibers." *Advances in Materials Science and Engineering*, 2020.

Rasaki, S. A., Bingxue, Z., Guarecuco, R., Thomas, T., and Minghui, Y. (2019). "Geopolymer for use in heavy metals adsorption, and advanced oxidative processes: A critical review." *Journal of Cleaner Production*, 213, 42-58.

Rees, C. A., Provis, J. L., Lukey, G. C., and van Deventer, J. S. (2007a). "Attenuated total reflectance fourier transform infrared analysis of fly ash geopolymer gel aging." *Langmuir*, 23(15), 8170-8179.

Rees, C. A., Provis, J. L., Lukey, G. C., and Van Deventer, J. S. (2007b). "In situ ATR-FTIR study of the early stages of fly ash geopolymer gel formation." *Langmuir*, 23(17), 9076-9082.

Revathi, T., Jeyalakshmi, R., and Rajamane, N. P. (2018). "Study on the role of n-SiO2 incorporation in thermo-mechanical and microstructural properties of ambient cured FA-GGBS geopolymer matrix." *Applied Surface Science*, 449, 322-331.

Sadat, M. R., Bringuier, S., Asaduzzaman, A., Muralidharan, K., and Zhang, L. (2016a). "A molecular dynamics study of the role of molecular water on the structure and mechanics of amorphous geopolymer binders." *J Chem Phys*, 145(13), 134706.

Sadat, M. R., Bringuier, S., Muralidharan, K., Frantziskonis, G., and Zhang, L. (2018a). "Atomic-scale dynamics and mechanical response of geopolymer binder under nanoindentation." *Computational Materials Science*, 142, 227-236.

Sadat, M. R., Bringuier, S., Muralidharan, K., Runge, K., Asaduzzaman, A., and Zhang, L. (2016b). "An atomistic characterization of the interplay between composition, structure and mechanical properties of amorphous geopolymer binders." *Journal of Non-Crystalline Solids*, 434, 53-61.

Sadat, M. R., Muralidharan, K., and Zhang, L. (2018b). "Reactive molecular dynamics simulation of the mechanical behavior of sodium aluminosilicate geopolymer and calcium silicate hydrate composites." *Computational Materials Science*, 150, 500-509.

Sekkal, W., and Zaoui, A. (2022). "High strength metakaolin-based geopolymer reinforced by pristine and covalent functionalized carbon nanotubes." *Construction and Building Materials*, 327, 126910.

Shahrajabian, F., and Behfarnia, K. (2018). "The effects of nano particles on freeze and thaw resistance of alkali-activated slag concrete." *Construction and Building Materials*, 176, 172-178.

Shaikh, F. U. A., Fairchild, A., and Zammar, R. (2018). "Comparative strain and deflection hardening behaviour of polyethylene fibre reinforced ambient air and heat cured geopolymer composites." *Construction and Building Materials*, 163, 890-900.

Shinoda, W., Shiga, M., and Mikami, M. (2004). "Rapid estimation of elastic constants by molecular dynamics simulation under constant stress." *Physical Review B*, 69(13), 134103.

Singh, P. S., Trigg, M., Burgar, I., and Bastow, T. (2005). "Geopolymer formation processes at room temperature studied by 29Si and 27Al MAS-NMR." *Materials Science and Engineering: A*, 396(1-2), 392-402.

Soper, A. K., and Benmore, C. J. (2008). "Quantum Differences between Heavy and Light Water." *Phys Rev Lett*, 101(6), 065502.

Sun, K. K., Peng, X. Q., Wang, S. P., Zeng, L., Ran, P., and Ji, G. X. (2020). "Effect of nano-SiO2 on the efflorescence of an alkali-activated metakaolin mortar." *Construction and Building Materials*, 253.

Teleman, O., Jönsson, B., and Engström, S. (1987). "A molecular dynamics simulation of a water model with intramolecular degrees of freedom." *Molecular Physics*, 60(1), 193-203.

Tuckerman, M. E., Alejandre, J., López-Rendón, R., Jochim, A. L., and Martyna, G. J. (2006). "A Liouville-operator derived measure-preserving integrator for molecular dynamics simulations in the isothermal–isobaric ensemble." *Journal of Physics A: Mathematical and General*, 39(19), 5629.

Turner, L. K., and Collins, F. G. (2013). "Carbon dioxide equivalent (CO2-e) emissions: A comparison between geopolymer and OPC cement concrete." *Construction and Building Materials*, 43, 125-130.

Van Duin, A. C., Dasgupta, S., Lorant, F., and Goddard, W. A. (2001). "ReaxFF: a reactive force field for hydrocarbons." *The Journal of Physical Chemistry A*, 105(41), 9396-9409.

van Duin, A. C. T., Strachan, A., Stewman, S., Zhang, Q. S., Xu, X., and Goddard, W. A. (2003). "ReaxFF(SiO) reactive force field for silicon and silicon oxide systems." *Journal of Physical Chemistry A*, 107(19), 3803-3811.

Van Oss, H. (2009). "US Geological survey (USGS) mineral commodity summaries: Cement". City.

Verlet, L. (1967). "Computer" experiments" on classical fluids. I. Thermodynamical properties of Lennard-Jones molecules." *Physical review*, 159(1), 98.

Vo, T., He, B., Blum, M., Damone, A., and Newell, P. (2020). "Molecular scale insight of pore morphology relation with mechanical properties of amorphous silica using ReaxFF." *Computational Materials Science*, 183.

Walkley, B., Rees, G. J., San Nicolas, R., van Deventer, J. S. J., Hanna, J. V., and Provis, J. L. (2018). "New Structural Model of Hydrous Sodium Aluminosilicate Gels and the Role of Charge-Balancing Extra-Framework Al." *The Journal of Physical Chemistry C*, 122(10), 5673-5685.

Wang, H. L., Li, H. H., and Yan, F. Y. (2005). "Synthesis and mechanical properties of metakaolinite-based geopolymer." *Colloids and Surfaces a-Physicochemical and Engineering Aspects*, 268(1-3), 1-6.

Wang, P., Qiao, G., Guo, Y., Zhang, Y., Hou, D., Jin, Z., Zhang, J., Wang, M., and Hu, X. (2020a). "Molecular dynamics simulation of the interfacial bonding properties between graphene oxide and calcium silicate hydrate." *Construction and Building Materials*, 260, 119927.

Wang, P., Qiao, G., Zhang, Y., Hou, D. S., Zhang, J. R., Wang, M. H., Wang, X. P., and Hu, X. X. (2020b). "Molecular dynamics simulation study on interfacial shear strength between calcium-silicate-hydrate and polymer fibers." *Construction and Building Materials*, 257.

Wang, R., Wang, J., Dong, T., and Ouyang, G. (2020c). "Structural and mechanical properties of geopolymers made of aluminosilicate powder with different SiO2/Al2O3 ratio: Molecular dynamics simulation and microstructural experimental study." *Construction and Building Materials*, 240.

Wang, S., and Li, V. C. (2007). "Engineered cementitious composites with high-volume fly ash." *ACI materials journal*, 104(3), 233.

Wang, Y., Wang, Y., and Zhang, M. (2021). "Effect of sand content on engineering properties of fly ash-slag based strain hardening geopolymer composites." *Journal of Building Engineering*, 34, 101951.

Wang, Y., Zhong, H., and Zhang, M. (2022). "Experimental study on static and dynamic properties of fly ash-slag based strain-hardening geopolymer composites." *Cement and Concrete Composites*, 104481.

White, C. E., Page, K., Henson, N. J., and Provis, J. L. (2013a). "In situ synchrotron X-ray pair distribution function analysis of the early stages of gel formation in metakaolin-based geopolymers." *Applied Clay Science*, 73, 17-25.

White, C. E., Provis, J. L., Bloomer, B., Henson, N. J., and Page, K. (2013b). "In situ X-ray pair distribution function analysis of geopolymer gel nanostructure formation kinetics." *Phys Chem Chem Phys*, 15(22), 8573-82.

White, C. E., Provis, J. L., Llobet, A., Proffen, T., and van Deventer, J. S. J. (2011). "Evolution of Local Structure in Geopolymer Gels: AnIn SituNeutron Pair Distribution Function Analysis." *Journal of the American Ceramic Society*, 94(10), 3532-3539.

White, C. E., Provis, J. L., Proffen, T., and Van Deventer, J. S. J. (2010). "The Effects of Temperature on the Local Structure of Metakaolin-Based Geopolymer Binder: A Neutron Pair Distribution Function Investigation." *Journal of the American Ceramic Society*, 93(10), 3486-3492.

Williams, R. P., Hart, R. D., and van Riessen, A. (2011). "Quantification of the Extent of Reaction of Metakaolin-Based Geopolymers Using X-Ray Diffraction, Scanning Electron Microscopy, and Energy-Dispersive Spectroscopy." *Journal of the American Ceramic Society*, 94(8), 2663-2670.

Wu, J.-D., Guo, L.-P., Cao, Y.-Z., and Lyu, B.-C. (2022). "Mechanical and fiber/matrix interfacial behavior of ultra-high-strength and high-ductility cementitious composites incorporating waste glass powder." *Cement and Concrete Composites*, 126, 104371.

Xiang, Y., Du, J., Smedskjaer, M. M., and Mauro, J. C. (2013). "Structure and properties of sodium aluminosilicate glasses from molecular dynamics simulations." *The Journal of chemical physics*, 139(4), 044507.

Xu, J., Chen, X., Yang, G., Niu, X. L., Chang, F. J., and Lacidogna, G. (2021a). "Review of research on micromechanical properties of cement-based materials based on molecular dynamics simulation." *Construction and Building Materials*, 312.

Xu, L.-Y., Alrefaei, Y., Wang, Y.-S., and Dai, J.-G. (2021b). "Recent advances in molecular dynamics simulation of the N-A-S-H geopolymer system: modeling, structural analysis, and dynamics." *Construction and Building Materials*, 276.

Yeon, J., and van Duin, A. C. T. (2016). "ReaxFF Molecular Dynamics Simulations of Hydroxylation Kinetics for Amorphous and Nano-Silica Structure, and Its Relations with Atomic Strain Energy." *Journal of Physical Chemistry C*, 120(1), 305-317.

Yuan, F. L., and Huang, L. P. (2012). "Molecular dynamics simulation of amorphous silica under uniaxial tension: From bulk to nanowire." *Journal of Non-Crystalline Solids*, 358(24), 3481-3487.

Zahid, M., and Shafiq, N. (2020). "Effects of sand/fly ash and the water/solid ratio on the mechanical properties of engineered geopolymer composite and mix design optimization." *Minerals*, 10(4), 333.

Zhang, J., Hou, D., Hafiz, R. B., Han, Q., and Ma, H. (2018a). "Effects of internally introduced sulfate on early age concrete properties: Active acoustic monitoring and molecular dynamics simulation." *Construction and Building Materials*, 188, 1014-1024.

Zhang, M., Deskins, N. A., Zhang, G., Cygan, R. T., and Tao, M. (2018b). "Modeling the Polymerization Process for Geopolymer Synthesis through Reactive Molecular Dynamics Simulations." *The Journal of Physical Chemistry C*, 122(12), 6760-6773.

Zhang, S. Z., Duque-Redondo, E., Kostiuchenko, A., Dolado, J. S., and Ye, G. (2021). "Molecular dynamics and experimental study on the adhesion mechanism of polyvinyl alcohol (PVA) fiber in alkali-activated slag/fly ash." *Cement and Concrete Research*, 145.

Zhang, Y., Li, T., Hou, D., Zhang, J., and Jiang, J. (2018c). "Insights on magnesium and sulfate ions' adsorption on the surface of sodium alumino-silicate hydrate (NASH) gel: a molecular dynamics study." *Phys Chem Chem Phys*, 20(27), 18297-18310.

Zhao, J. H., Tong, L. Y., Li, B. E., Chen, T. H., Wang, C. P., Yang, G. Q., and Zheng, Y. (2021). "Eco-friendly geopolymer materials: A review of performance improvement, potential application and sustainability assessment." *Journal of Cleaner Production*, 307.

Zhou, S., Vu-Bac, N., Arash, B., Zhu, H., and Zhuang, X. (2019a). "Interface characterization between polyethylene/silica in engineered cementitious composites by molecular dynamics simulation." *Molecules*, 24(8), 1497.

Zhou, Y., Hou, D., Jiang, J., She, W., and Yu, J. (2017a). "Reactive molecular simulation on the calcium silicate hydrates/polyethylene glycol composites." *Chemical Physics Letters*, 687, 184-187.

Zhou, Y., Hou, D., Manzano, H., Orozco, C. A., Geng, G., Monteiro, P. J., and Liu, J. (2017b). "Interfacial connection mechanisms in calcium–silicate–hydrates/polymer nanocomposites: a molecular dynamics study." *ACS applied materials & interfaces*, 9(46), 41014-41025.

Zhou, Y., Huang, J., Yang, X., Dong, Y., Feng, T., and Liu, J. (2021). "Enhancing the PVA fiber-matrix interface properties in ultra high performance concrete: An experimental and molecular dynamics study." *Construction and Building Materials*, 285, 122862.

Zhou, Y., Tang, L., Liu, J., and Miao, C. (2019b). "Interaction mechanisms between organic and inorganic phases in calcium silicate hydrates/poly

(vinyl alcohol) composites." *Cement and Concrete Research*, 125, 105891.
Zidi, Z., Ltifi, M., and Zafar, I. (2021). "Synthesis and attributes of nano-SiO2 local metakaolin based-geopolymer." *Journal of Building Engineering*, 33.

Appendix I

Force Field Parameters

I.a. ReaxFF force field

Table I.1 Parameters for reactive force field

```
39 ! Number of general parameters
   50.0000 !Overcoordination parameter
    9.5469 !Overcoordination parameter
   26.5405 !Valency angle conjugation parameter
    1.7224 !Triple bond stabilisation parameter
    6.8702 !Triple bond stabilisation parameter
   60.4850 !C2-correction
    1.0588 !Undercoordination parameter
    4.6000 !Triple bond stabilisation parameter
   12.1176 !Undercoordination parameter
   13.3056 !Undercoordination parameter
  -70.5044 !Triple bond stabilization energy
    0.0000 !Lower Taper-radius
   10.0000 !Upper Taper-radius
    2.8793 !Not used
   33.8667 !Valency undercoordination
    6.0891 !Valency angle/lone pair parameter
    1.0563 !Valency angle
    2.0384 !Valency angle parameter
    6.1431 !Not used
    6.9290 !Double bond/angle parameter
    0.3989 !Double bond/angle parameter: overcoord
    3.9954 !Double bond/angle parameter: overcoord
   -2.4837 !Not used
    5.7796 !Torsion/BO parameter
   10.0000 !Torsion overcoordination
    1.9487 !Torsion overcoordination
   -1.2327 !Conjugation 0 (not used)
    2.1645 !Conjugation
    1.5591 !vdWaals shielding
```

```
  0.1000 !Cutoff for bond order (*100)
  2.1365 !Valency angle conjugation parameter
  0.6991 !Overcoordination parameter
 50.0000 !Overcoordination parameter
  1.8512 !Valency/lone pair parameter
  0.5000 !Not used
 20.0000 !Not used
  5.0000 !Molecular energy (not used)
  0.0000 !Molecular energy (not used)
  2.6962 !Valency angle conjugation parameter
 9 ! Nr of atoms; cov.r; valency;a.m;Rvdw;Evdw;gammaEEM;cov.r2;#
                alfa;gammavdW;valency;Eunder;Eover;chiEEM;etaEEM;n.u.
                cov r3;Elp;Heat inc.;n.u.;n.u.;n.u.;n.u.
                ov/un;val1;n.u.;val3,vval4
C    1.3674   4.0000  12.0000   2.0453   0.1444   0.7920   1.1706   4.0000
     9.0000   1.5000   4.0000  27.5134  79.5548   6.7897   6.0000   0.0000
     1.1168   0.0000 181.0000  14.2732  24.4406   6.7313   0.8563   0.0000
    -4.1021   5.0000   1.0564   4.0000   2.9663   0.0000   0.0000   0.0000
H    0.8930   1.0000   1.0080   1.3550   0.0930   0.8203  -0.1000   1.0000
     8.2230  33.2894   1.0000   0.0000 121.1250   3.7248   9.6093   1.0000
    -0.1000   0.0000  61.6606   3.0408   2.4197   0.0003   1.0698   0.0000
   -19.4571   4.2733   1.0338   1.0000   2.8793   0.0000   0.0000   0.0000
O    1.2450   2.0000  15.9990   2.3890   0.1000   1.0898   1.0548   6.0000
     9.7300  13.8449   4.0000  37.5000 116.0768   8.5000   8.3122   2.0000
     0.9049   0.4056  59.0626   3.5027   0.7640   0.0021   0.9745   0.0000
    -3.5500   2.9000   1.0493   4.0000   2.9225   0.0000   0.0000   0.0000
Ca   1.9535   2.0000  40.0870   2.7142   0.1886   1.0000   1.0000   2.0000
    10.5235  27.5993   3.0000  38.0000   0.0000  -1.7130   6.5096   0.0000
    -1.3000   0.0000 220.0000  49.9248   0.3370   0.0000   0.0000   0.0000
    -2.0000   3.8301   1.0564   8.0000   2.9663   0.0000   0.0000   0.0000
Si   2.1932   4.0000  28.0600   1.8951   0.1737   0.5947   1.2962   4.0000
    11.3429   5.2054   4.0000  21.7115 139.9309   4.2033   5.5558   0.0000
    -1.0000   0.0000 128.2031   9.0751  23.8188   0.8381   0.8563   0.0000
    -4.1684   2.0754   1.0338   4.0000   2.5791   1.4000   0.2000  13.0000
Al   2.1967   3.0000  26.9820   2.3738   0.2328   0.4265  -1.6836   3.0000
     9.4002   3.9009   3.0000   0.0076  16.5151   1.7429   6.8319   0.0000
    -1.0000   0.0000  78.4675  20.0000   0.2500   0.0000   0.8563   0.0000
   -22.7101   1.7045   1.0338   8.0000   2.5791   0.0000   0.0000   0.0000
S    1.9405   2.0000  32.0600   2.0677   0.2099   1.0336   1.5479   6.0000
     9.9575   4.9055   4.0000  52.9998 112.1416   5.8284   8.2545   2.0000
     1.4601   9.7177  71.1843   5.7487  23.2859  12.7147   0.9745   0.0000
   -11.0000   2.7466   1.0338   6.2998   2.8793   0.0000   0.0000   0.0000
Na   1.7878   1.0000  22.9898   2.6441   0.2588   0.8476  -1.0000   1.0000
     9.0003   2.5000   1.0000   0.0000   0.0000  -3.4731   8.1298   0.0000
    -1.0000gz 0.0000  23.0445 100.0000   1.0000   0.0000   0.8563   0.0000
    -4.1479   3.9900   1.0338   8.0000   2.5791   0.0000   0.0000   0.0000
X   -0.1000   2.0000   1.0080   2.0000   0.0000   1.0000  -0.1000   6.0000
    10.0000   2.5000   4.0000   0.0000   0.0000   8.5000   1.5000   0.0000
    -0.1000   0.0000  -2.3700   8.7410  13.3640   0.6690   0.9745   0.0000
   -11.0000   2.7466   1.0338   2.0000   2.8793   0.0000   0.0000   0.000
```

```
30 ! Nr of bonds; Edis1;LPpen;n.u.;pbe1;pbo5;13corr;pbo6
                  pbe2;pbo3;pbo4;n.u.;pbo1;pbo2;ovcorr
 1  1  80.8865 107.9944  52.0636   0.5218  -0.3636   1.0000  34.9876   0.7769
        6.1244  -0.1693   8.0804   1.0000  -0.0586   8.1850   1.0000   0.0000
 1  2 169.4760   0.0000   0.0000  -0.6083   0.0000   1.0000   6.0000   0.7652
        5.2290   1.0000   0.0000   1.0000  -0.0500   6.9136   0.0000   0.0000
 2  2 153.3934   0.0000   0.0000  -0.4600   0.0000   1.0000   6.0000   0.7300
        6.2500   1.0000   0.0000   1.0000  -0.0790   6.0552   0.0000   0.0000
 1  3 158.6946 107.4583  23.3136  -0.4240  -0.1743   1.0000  10.8209   1.0000
        0.5322  -0.3113   7.0000   1.0000  -0.1447   5.2450   0.0000   0.0000
 3  3 142.2858 145.0000  50.8293   0.2506  -0.1000   1.0000   9.7503   0.6051
        0.3451  -0.1055   9.0000   1.0000  -0.1225   5.5000   1.0000   0.0000
 2  3 160.0000   0.0000   0.0000  -0.5725   0.0000   1.0000   6.0000   0.5626
        1.1150   1.0000   0.0000   1.0000  -0.0920   4.2790   0.0000   0.0000
 2  4   0.0000   0.0000   0.0000  -0.0203  -0.1418   1.0000  13.1260   0.0230
        8.2136  -0.1310   0.0000   1.0000  -0.2692   6.4254   0.0000  24.4461
 3  4  49.2298   0.0000  43.3991   0.9186  -0.3000   1.0000  36.0000   0.0025
        0.8319  -0.2500  12.0000   1.0000  -0.0569   9.1331   1.0000  24.4461
 4  4  39.2866   0.0000   0.0000  -0.2437  -0.2000   0.0000  16.0000   0.3235
        0.1112  -0.2000  10.0000   1.0000  -0.0806   4.1233   0.0000   0.0000
 2  5 250.0000   0.0000   0.0000  -0.7128   0.0000   1.0000   6.0000   0.1186
       18.5790   1.0000   0.0000   1.0000  -0.0731   7.4983   0.0000   0.0000
 3  5 274.8339   5.0000   0.0000  -0.5884  -0.3000   1.0000  36.0000   0.2131
        9.9772  -0.2572  28.8153   1.0000  -0.1130   8.4790   6.0658   0.0000
 4  5   0.0000   0.0000   0.0000   0.5000  -0.3000   1.0000  16.0000   0.5000
        0.5000  -0.2500  15.0000   1.0000  -0.1000   9.0000   0.0000   0.0000
 5  5  70.9120  54.0531  30.0000   0.4931  -0.3000   1.0000  16.0000   0.0392
        0.2476  -0.8055   7.1248   1.0000  -0.1009   8.7229   0.0000   0.0000
 1  6   0.0000   0.0000   0.0000  -0.6528  -0.3000   0.0000  36.0000   0.5000
       10.0663  -0.3500  25.0000   1.0000  -0.1000  10.0000   0.0000   0.0000
 2  6  92.8579   0.0000   0.0000  -0.6528  -0.3000   0.0000  36.0000   0.1551
       10.0663  -0.3500  25.0000   1.0000  -0.3842  13.1758   0.0000   0.0000
 3  6 227.9327   0.0000   0.0000  -0.8375  -0.3000   0.0000  36.0000   0.1286
        0.3686  -0.3500  25.0000   1.0000  -0.1740   5.2057   0.0000   0.0000
 4  6   0.0000   0.0000   0.0000   1.0000   0.3000   0.0000  26.0000   1.0000
        0.5000   0.0000  12.0000   1.0000  -0.2000  10.0000   0.0000   0.0000
 5  6   0.0000   0.0000   0.0000   1.0000   0.3000   0.0000  26.0000   1.0000
        0.5000   0.0000  12.0000   1.0000  -0.2000  10.0000   0.0000   0.0000
 6  6  34.0777   0.0000   0.0000   0.4832  -0.3000   0.0000  16.0000   0.5154
        6.4631  -0.4197  14.3085   1.0000  -0.1463   6.1608   0.0000   0.0000
 1  7 128.7959  56.4134  39.0716   0.0688  -0.4463   1.0000  31.1766   0.4530
        0.1955  -0.3587   6.2148   1.0000  -0.0770   6.6386   1.0000   0.0000
 2  7 136.1049   0.0000   0.0000  -0.4669   0.0000   1.0000   6.0000   0.3803
       10.5730   1.0000   0.0000   1.0000  -0.1000   7.0000   1.0000   0.0000
 3  7 161.0562 220.0000  40.0000   0.6070  -0.2406   1.0000  22.1005   0.2476
        0.7150  -0.2741   8.3216   1.0000  -0.1109   5.4501   1.0000   0.0000
 4  7   0.0000   0.0000   0.0000   0.5000  -0.5000   1.0000  50.0000   0.6000
        0.5000  -0.2500  10.0000   1.0000  -0.2000  10.0000   1.0000   0.0000
 5  7   0.0000   0.0000   0.0000   0.5000  -0.5000   1.0000  50.0000   0.6000
        0.5000  -0.2500  10.0000   1.0000  -0.2000  10.0000   1.0000   0.0000
```

```
 6  7   0.0000   0.0000   0.0000   0.5000  -0.5000   1.0000  50.0000   0.6000
         0.5000  -0.2500  10.0000   1.0000  -0.2000  10.0000   1.0000   0.0000
 7  7  96.1871  93.7006  68.6860   0.0955  -0.4781   1.0000  17.8574   0.6000
         0.2723  -0.2373   9.7875   1.0000  -0.0950   6.4757   1.0000   0.0000
 2  8  26.7569   0.0000   0.0000   1.0000  -0.3000   1.0000  36.0000   0.0100
         0.5785  -0.3500  25.0000   1.0000  -0.2601   6.6137   1.0000   0.0000
 3  8  28.0000   0.0000   0.0000   0.4351  -0.3000   1.0000  36.0000   0.0656
        18.6859  -0.3500  25.0000   1.0000  -0.1391   7.4280   1.0000   0.0000
 5  8   0.1000   0.0000   0.0000   0.2500  -0.5000   1.0000  35.0000   0.6000
         0.5000  -0.5000  20.0000   1.0000  -0.2000  10.0000   1.0000   0.0000
 8  8   72.6003  0.0000   0.0000  -0.7273   0.3000   0.0000  25.0000   0.1919
         6.6441 -0.4000  12.0000   1.0000  -0.0345   5.0063   0.0000   0.0000
18 ! Nr of off-diagonal terms; Ediss;Ro;gamma;rsigma;rpi;rpi2
 1  2   0.1239   1.4004   9.8467   1.1210  -1.0000  -1.0000
 2  3   0.0283   1.2885  10.9190   0.9215  -1.0000  -1.0000
 1  3   0.1156   1.8520   9.8317   1.2854   1.1352   1.0706
 2  4   0.0100   1.6000  13.2979  -1.0000  -1.0000  -1.0000
 3  4   0.1054   1.7539  12.0932   1.8770  -1.0000  -1.0000
 2  5   0.2000   1.5207  12.9535   1.2125  -1.0000  -1.0000
 3  5   0.1836   1.9157  10.9070   1.7073   1.2375  -1.0000
 4  5   0.1000   1.9000  11.0000  -1.0000  -1.0000  -1.0000
 1  6   0.2000   1.9000  12.0000  -1.0000  -1.0000  -1.0000
 2  6   0.0564   1.4937  12.0744   1.7276  -1.0000  -1.0000
 3  6   0.1745   1.8928  11.2476   1.5382  -1.0000  -1.0000
 5  6   0.0295   1.5025  11.8687  -1.0000  -1.0000  -1.0000
 1  7   0.1408   1.8161   9.9393   1.7986   1.3021   1.4031
 2  7   0.0895   1.6239  10.0104   1.4640  -1.0000  -1.0000
 3  7   0.2047   1.7931  10.2391   1.4608   1.3987  -1.0000
 2  8   0.1100   1.8410   9.1430   1.7735  -1.0000  -1.0000
 3  8   0.1497   1.5719  13.3058   1.6111  -1.0000  -1.0000
 5  8   0.1174   1.9434  17.1734  -1.0000  -1.0000  -1.0000
65 ! Nr of angles;at1;at2;at3;Thetao,o;ka;kb;pv1;pv2
 1  1  1  59.0573   30.7029   0.7606   0.0000   0.7180   6.2933   1.1244
 1  1  2  65.7758   14.5234   6.2481   0.0000   0.5665   0.0000   1.6255
 2  1  2  70.2607   25.2202   3.7312   0.0000   0.0050   0.0000   2.7500
 1  2  2   0.0000    0.0000   6.0000   0.0000   0.0000   0.0000   1.0400
 1  2  1   0.0000    3.4110   7.7350   0.0000   0.0000   0.0000   1.0400
 2  2  2   0.0000   27.9213   5.8635   0.0000   0.0000   0.0000   1.0400
 1  1  3   49.6811   7.1713   4.3889   0.0000   0.7171  10.2661   1.0463
 3  1  3   77.7473  40.1718   2.9802 -25.3063   1.6170 -46.1315   2.2503
 2  1  3   65.0000  13.8815   5.0583   0.0000   0.4985   0.0000   1.4900
 1  3  1   73.5312  44.7275   0.7354   0.0000   3.0000   0.0000   1.0684
 1  3  3   79.4761  36.3701   1.8943   0.0000   0.7351  67.6777   3.0000
 3  3  3   80.7324  30.4554   0.9953   0.0000   1.6310  50.0000   1.0783
 1  3  2   70.1880  20.9562   0.3864   0.0000   0.0050   0.0000   1.6924
 2  3  3   75.6935  50.0000   2.0000   0.0000   1.0000   0.0000   1.1680
 2  3  2   85.8000   9.8453   2.2720   0.0000   2.8635   0.0000   1.5800
 1  2  3   0.0000   25.0000   3.0000   0.0000   1.0000   0.0000   1.0400
 3  2  3   0.0000   15.0000   2.8900   0.0000   0.0000   0.0000   2.8774
 2  2  3   0.0000    8.5744   3.0000   0.0000   0.0000   0.0000   1.0421
```

```
 3  4  3  1.1001    4.9610   2.2118   0.0000   0.7118   0.0000   1.2337
 4  3  4  2.8736    5.1092   1.8311   0.0000   1.5359   0.0000   1.8829
 2  3  4  42.2769   2.8497   0.2663   0.0000   0.4192   0.0000   1.0000
 3  3  4  70.0000  25.0000   1.0000   0.0000   1.0000   0.0000   1.2500
 5  5  5  78.5339  36.4328   1.0067   0.0000   0.1694   0.0000   1.6608
 2  5  5  77.2616   5.0190   7.8944   0.0000   4.0000   0.0000   1.0400
 2  5  2  75.7983  14.4132   2.8640   0.0000   4.0000   0.0000   1.0400
 3  5  5  86.3294  18.3879   5.8529   0.0000   1.7361   0.0000   1.2310
 2  5  3  73.6998  40.0000   1.8782   0.0000   4.0000   0.0000   1.1290
 3  5  3  79.5581  34.9140   1.0801   0.0000   0.1632   0.0000   2.2206
 5  3  5  82.3364   4.7350   1.3544   0.0000   1.4627   0.0000   1.0400
 2  3  5  90.0000   6.6857   1.6689   0.0000   2.5771   0.0000   1.0400
 3  3  5  92.1207  24.3937   0.5000   0.0000   1.7208   0.0000   3.0000
 2  2  5   0.0000  47.1300   6.0000   0.0000   1.6371   0.0000   1.0400
 5  2  5   0.0000  27.4206   6.0000   0.0000   1.6371   0.0000   1.0400
 3  2  5   0.0000   5.0000   1.0000   0.0000   1.0000   0.0000   1.2500
 3  2  6   0.0000   4.2750   1.0250   0.0000   1.3750   0.0000   1.4750
 2  2  6   0.0000   3.0000   1.0000   0.0000   1.0000   0.0000   1.2500
 6  2  6   0.0000  20.2391   0.1328   0.0000   2.9860   0.0000   1.0870
 2  3  6  90.0000  19.7491   1.8227   0.0000   1.0000   0.0000   2.5337
 3  3  6  34.4326  25.9544   5.1239   0.0000   2.7500   0.0000   1.7141
 6  3  6  23.7270  19.5973   4.0000   0.0000   0.6619   0.0000   1.9380
 2  6  2  67.4229   4.5148   5.9702   0.0000   3.0000   0.0000   2.6879
 2  6  3  41.8108  17.3800   2.6618   0.0000   0.7372   0.0000   1.0100
 3  6  3  54.0864   9.7594   1.9476   0.0000   3.0000   0.0000   1.4400
 2  6  6  78.2279  37.6504   0.4809   0.0000   1.0000   0.0000   2.9475
 5  3  6  15.7093   0.0100   2.7033   0.0000   1.0000   0.0000   1.0000
 3  5  6  88.2703   0.3954   0.2500   0.0000   0.5000   0.0000   2.1060
 3  6  5  83.8306   0.3712   0.2500   0.0000   0.5000   0.0000   2.1153
 1  1  7  74.4180  33.4273   1.7018   0.1463   0.5000   0.0000   1.6178
 1  7  1  79.7037  28.2036   1.7073   0.1463   0.5000   0.0000   1.6453
 2  1  7  63.3289  29.4225   2.1326   0.0000   0.5000   0.0000   3.0000
 1  7  2  85.9449  38.3109   1.2492   0.0000   0.5000   0.0000   1.1000
 1  7  7  85.6645  40.0000   2.9274   0.1463   0.5000   0.0000   1.3830
 2  7  2  83.8555   5.1317   0.4377   0.0000   0.5000   0.0000   3.0000
 2  7  7  97.0064  32.1121   2.0242   0.0000   0.5000   0.0000   2.8568
 3  7  3  81.7931  31.2043   6.5492  -4.4116   2.6067   0.0000   3.0000
 1  7  3  70.0000  35.0000   3.4223   0.0000   1.3550   0.0000   1.2002
 1  3  7  57.3353  41.0012   1.0609   0.0000   1.3000   0.0000   3.0000
 3  3  7  83.9753  31.0715   3.5590   0.0000   0.8161   0.0000   1.1776
 2  3  7  90.0000  17.5000   3.5000   0.0000   2.0000   0.0000   2.2501
 4  3  6  74.9672  11.7556   5.0000   0.0000   0.3509   0.0000   2.0116
 4  3  7  114.2370 19.7117   0.5240   0.0000   3.0000   0.0000   0.8335
 3  8  3  100.0000 45.9627   3.0941   0.0000   3.2848   0.0000   2.0000
 2  3  8  87.9313   7.1387   3.0639   0.0000   1.5000   0.0000   1.5554
 8  3  8  84.9984   6.4965   1.5553   0.0000   1.0368   0.0000   2.0000
 5  3  8  95.9867   2.0000   5.0000   0.0000   0.8452   0.0000   1.0000
28 ! Nr of torsions;at1;at2;at3;at4;;V1;V2;V3;V2(BO);vconj;n.u;n
 1  1  1  1     -0.2500   34.7453   0.0288  -6.3507  -1.6000   0.0000   0.0000
 1  1  1  2     -0.2500   29.2131   0.2945  -4.9581  -2.1802   0.0000   0.0000
```

```
 2  1  1  2    -0.2500   31.2081    0.4539   -4.8923   -2.2677   0.0000   0.0000
 1  1  1  3    -0.3495   22.2142   -0.2959   -2.5000   -1.9066   0.0000   0.0000
 2  1  1  3     0.0646   24.3195    0.6259   -3.9603   -1.0000   0.0000   0.0000
 3  1  1  3    -0.5456    5.5756    0.8433   -5.1924   -1.0180   0.0000   0.0000
 1  1  3  1     1.7555   27.9267    0.0072   -2.6533   -1.0000   0.0000   0.0000
 1  1  3  2    -1.4358   36.7830   -1.0000   -8.1821   -1.0000   0.0000   0.0000
 2  1  3  1    -1.3959   34.5053    0.7200   -2.5714   -2.1641   0.0000   0.0000
 2  1  3  2    -2.5000   70.0597    1.0000   -3.5539   -2.9929   0.0000   0.0000
 1  1  3  3     0.6852   11.2819   -0.4784   -2.5000   -2.1085   0.0000   0.0000
 2  1  3  3     0.1933   80.0000    1.0000   -4.0590   -3.0000   0.0000   0.0000
 3  1  3  1    -1.9889   76.4820   -0.1796   -3.8301   -3.0000   0.0000   0.0000
 3  1  3  2     0.2160   72.7707   -0.7087   -4.2100   -3.0000   0.0000   0.0000
 3  1  3  3    -2.5000   71.0772    0.2542   -3.1631   -3.0000   0.0000   0.0000
 1  3  3  1     2.5000   -0.6002    1.0000   -3.4297   -2.8858   0.0000   0.0000
 1  3  3  2    -2.5000   -3.3822    0.7004   -5.4467   -2.9586   0.0000   0.0000
 2  3  3  2     2.5000   -4.0000    0.9000   -2.5000   -1.0000   0.0000   0.0000
 1  3  3  3     1.2329   -4.0000    1.0000   -2.5000   -1.7479   0.0000   0.0000
 2  3  3  3     0.8302   -4.0000   -0.7763   -2.5000   -1.0000   0.0000   0.0000
 3  3  3  3    -2.5000   -4.0000    1.0000   -2.5000   -1.0000   0.0000   0.0000
 0  1  2  0     0.0000    0.0000    0.0000    0.0000    0.0000   0.0000   0.0000
 0  2  2  0     0.0000    0.0000    0.0000    0.0000    0.0000   0.0000   0.0000
 0  2  3  0     0.0000    0.1000    0.0200   -2.5415    0.0000   0.0000   0.0000
 0  1  1  0     0.0000   50.0000    0.3000   -4.0000   -2.0000   0.0000   0.0000
 0  3  3  0     0.5511   25.4150    1.1330   -5.1903   -1.0000   0.0000   0.0000
 2  3  7  3     2.5000    2.5000    0.2237  -10.0000   -1.0000   0.0000   0.0000
 0  3  7  0     0.1000   50.0000    0.0100  -10.0000    0.0000   0.0000   0.0000
4    ! Nr of hydrogen bonds;at1;at2;at3;Rhb;Dehb;vhb1
 3  2  3   2.1200  -3.5800   1.4500  19.5000
 3  2  7   1.5000  -2.0000   3.0582  19.1627
 7  2  3   1.5000  -2.0000   3.0582  19.1627
 7  2  7   1.5000  -2.0000   3.0582  19.1627
```

I.b. ClayFF force field

Table I.2 Nonbond parameters for ClayFF force field

Species	**Charge (e)**	D_o **(kcal/mol)**	R_o **(Å)**
Si	2.10	1.8402×10^{-6}	3.3019
O (bridge)	-1.05	0.1554	3.1655
O (water)	-0.82	0.1554	3.1655
Al	1.575	1.8402×10^{-6}	3.3019
O (hydroxyl)	-0.95	0.1554	3.1655
H (water)	0.41	-	-
H (hydroxyl)	0.425	-	-
Na ions	1.0	0.1301	2.3500

Table I.3 Bond parameters for ClayFF force field

Bond stretch		k_1 **(kcal/mol Å^2)**	r_0 **(Å)**
Species *i*	**Species *j***		
O (water)	H (water)	553.9359	1.0000
O (hydroxyl)	H (hydroxyl)	553.9359	1.0000

Table I.4 Angle parameters for ClayFF force field

Angle bend			k_2 **(kcal/mol rad^2)**	θ_0 **(deg)**
Species *i*	**Species *j***	**Species *k***		
H (water)	O (water)	H (water)	45.7530	109.47

I.c. OPLS force field

Table I.5 Nonbond parameters for OPLS force field

Species	Charge (e)	D_o (kcal/mol)	R_o (Å)
C3	-0.30	0.1050	3.8510
C2	-0.20	0.1050	3.8510
H	0.10	0.0030	2.5000

Table I.6 Bond parameters for OPLS force field

Bond stretch		k_1 (kcal/mol Å^2)	r_0 (Å)
Species *i*	Species *j*		
H	C3	340.00	1.0900
C3	C2	268.00	1.5290
H	C2	340.00	1.0900
C2	C2	268.00	1.5290

Table I.7 Angle parameters for OPLS force field

Angle bend			k_2 (kcal/mol rad^2)	θ_0 (deg)
Species *i*	Species *j*	Species *k*		
H	C3	C2	37.50	110.70
H	C3	H	33.00	107.80
H	C2	C3	37.50	110.70
C3	C2	C2	58.35	112.70
H	C2	H	33.00	107.80
H	C2	C2	37.50	110.70
C2	C2	C2	58.35	112.70

Table I.8 Dihedral parameters for OPLS force field

Dihedral				K_1	K_2	K_3	K_4
Species *i*	Species *j*	Species *k*	Species *l*	(kcal/mol)	(kcal/mol)	(kcal/mol)	(kcal/mol)
H	C3	C2	C2	0.0	0.0	0.3	0.0
H	C3	C2	C2	0.0	0.0	0.3	0.0
C3	C2	C2	C2	1.3	-0.2	0.2	0.0
H	C2	C2	C3	0.0	0.0	0.3	0.0
H	C2	C2	C2	0.0	0.0	0.3	0.0
H	C2	C2	H	0.0	0.0	0.3	0.0
C2	C2	C2	C2	1.3	-0.2	0.2	0.0

Appendix II

Computed Properties of NASH Gels

II.a. Bond angles distribution

As shown by **Figure II.1**, negligible impact on bond angles is found from the oligomers' configurations. At the Si/Al ratio of 3, the bond distribution curves are very close to each other between linear and cyclic structures.

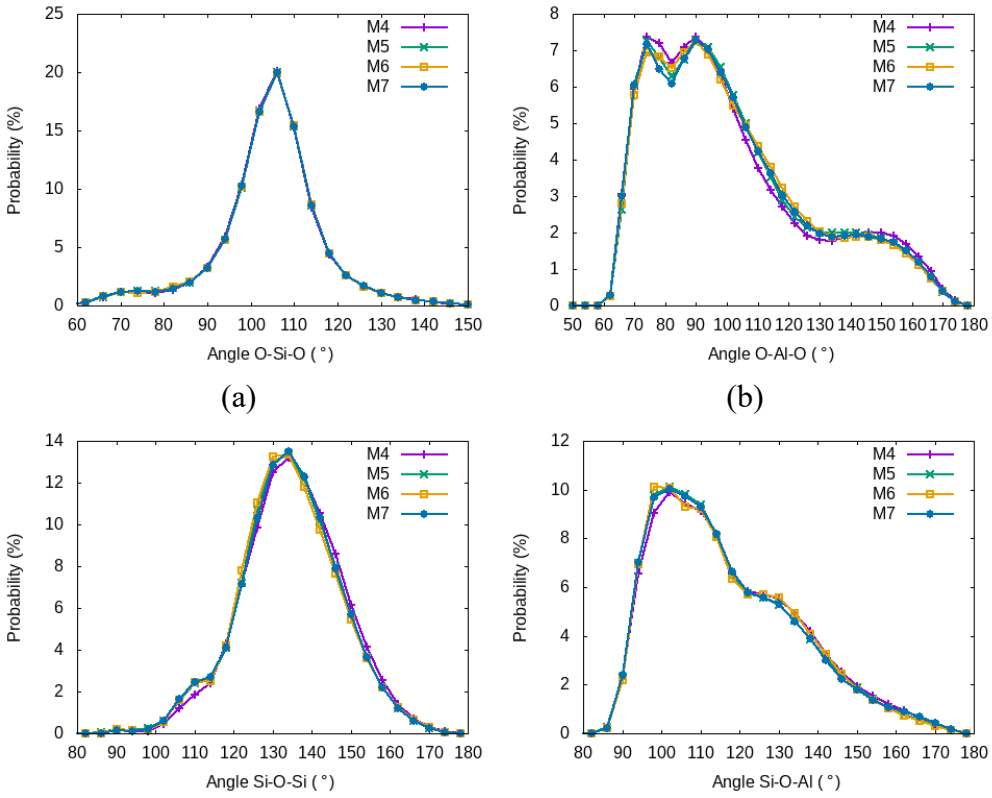

Figure II.1 Bond angle distributions of O-T-O and T-O-T bonds in NASH gels: M4, M5, M6 and M7 (Si/Al=3)

II.b. Dynamic properties of NASH gels

Figure II.2 displayed the MSD comparison of different atoms in the NASH gel models with various Si/Al ratios from 1 to 3. From the MSD curves of skeleton atoms of Si and Al (i.e. **Figure II.2(a)** and **Figure II.2(b)**, respectively), it is readily discovered that the structures of NASH gels are stable. Moreover, the structural stability is improved with the increase of Si/Al ratio, as the MSD of M2 and M4 are lower than M1 in **Figure II.2(b)**. The MSD of O atoms in M2 and M4 are higher than that in M1, which is because of that water mobility increases significantly with the Si/Al ratio, as discussed in Section 4.4.2.3. The MSD of Na ion increase with the increase of Si/Al ratio, as shown in **Figure II.2(d)**. This is due to the less Al element in the NASH gel decreases the restriction of Na ions in the system, which consequently enhance its mobility.

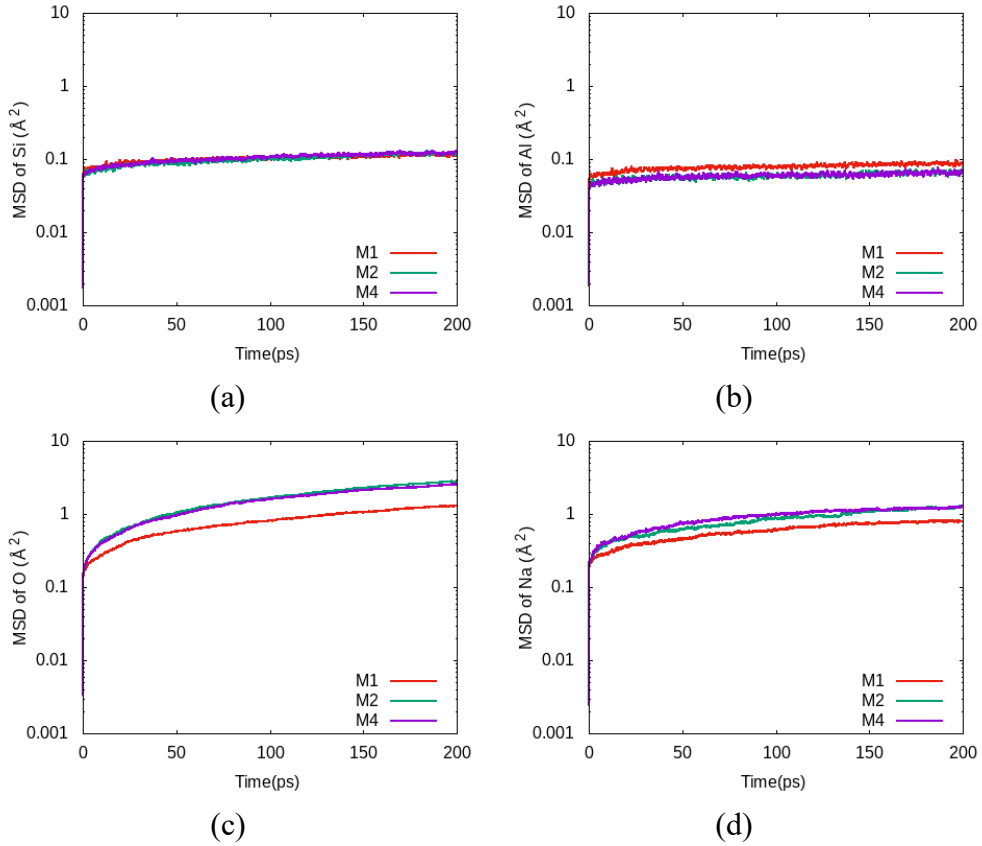

Figure II.2 Mean square displacement for M1(Si/Al=1), M2(Si/Al=2) and M4(Si/Al=3) NASH gels: (a) curves of Si; (b) curves of Al; (c) curves of O; (d) curves of Na.

II.c. Stiffness tensors of NASH gels

All the calculated stiffness tensors of NASH gels of M1 to M7 are listed in **Table II.1**.

Table II.1 Computed full stiffness tensors (C_{ij}) of NASH gels

Stiffness tensors of M1 (GPa)							
C_{11}	40.81	C_{44}	12.70	C_{24}	0.59	C_{45}	-0.27
C_{22}	41.77	C_{55}	13.50	C_{25}	0.37	C_{46}	-0.18
C_{33}	43.79	C_{66}	12.20	C_{26}	-0.77	C_{56}	-0.41
C_{12}	16.18	C_{14}	-0.02	C_{34}	0.02		
C_{13}	20.32	C_{15}	1.15	C_{35}	1.36		
C_{23}	19.29	C_{16}	-0.27	C_{36}	-0.27		
Stiffness tensors of M2 (GPa)							
C_{11}	52.90	C_{44}	15.10	C_{24}	0.71	C_{45}	0.42
C_{22}	57.45	C_{55}	13.83	C_{25}	-0.66	C_{46}	0.33
C_{33}	51.75	C_{66}	15.25	C_{26}	0.15	C_{56}	0.68
C_{12}	25.75	C_{14}	-0.60	C_{34}	1.03		
C_{13}	23.43	C_{15}	1.10	C_{35}	-1.19		
C_{23}	23.99	C_{16}	-0.13	C_{36}	0.38		
Stiffness tensors of M3 (GPa)							
C_{11}	54.47	C_{44}	16.52	C_{24}	0.30	C_{45}	-0.28
C_{22}	54.88	C_{55}	14.53	C_{25}	0.09	C_{46}	-0.23
C_{33}	52.01	C_{66}	14.80	C_{26}	0.24	C_{56}	0.09
C_{12}	23.41	C_{14}	0.26	C_{34}	-1.36		
C_{13}	22.98	C_{15}	0.68	C_{35}	0.38		
C_{23}	23.24	C_{16}	0.32	C_{36}	-0.06		
Stiffness tensors of M4 (GPa)							
C_{11}	47.02	C_{44}	14.84	C_{24}	0.28	C_{45}	0.92
C_{22}	43.69	C_{55}	12.92	C_{25}	-0.43	C_{46}	0.38
C_{33}	47.65	C_{66}	13.38	C_{26}	0.68	C_{56}	0.50
C_{12}	19.35	C_{14}	0.50	C_{34}	-0.19		
C_{13}	20.46	C_{15}	0.67	C_{35}	0.18		

C_{23}	17.30	C_{16}	-0.02	C_{36}	0.36		
Stiffness tensors of M5 (GPa)							
C_{11}	54.98	C_{44}	16.61	C_{24}	-0.61	C_{45}	0.18
C_{22}	55.51	C_{55}	15.44	C_{25}	-0.02	C_{46}	0.40
C_{33}	56/33	C_{66}	15.91	C_{26}	0.24	C_{56}	0.55
C_{12}	24.11	C_{14}	-0.15	C_{34}	-0.33		
C_{13}	21.56	C_{15}	1.21	C_{35}	0.35		
C_{23}	23.78	C_{16}	-0.20	C_{36}	-0.05		
Stiffness tensors of M6 (GPa)							
C_{11}	57.75	C_{44}	14.61	C_{24}	-0.90	C_{45}	-1.06
C_{22}	54.96	C_{55}	17.19	C_{25}	-0.49	C_{46}	-0.92
C_{33}	58.83	C_{66}	15.04	C_{26}	0.50	C_{56}	0.60
C_{12}	25.30	C_{14}	-1.02	C_{34}	-0.22		
C_{13}	26.60	C_{15}	-0.48	C_{35}	0.19		
C_{23}	26.39	C_{16}	-0.83	C_{36}	0.39		
Stiffness tensors of M7 (GPa)							
C_{11}	46.35	C_{44}	14.31	C_{24}	0.57	C_{45}	-0.73
C_{22}	50.89	C_{55}	15.74	C_{25}	1.00	C_{46}	0.20
C_{33}	48.63	C_{66}	15.19	C_{26}	-1.71	C_{56}	-0.36
C_{12}	20.10	C_{14}	1.13	C_{34}	0.47		
C_{13}	19.39	C_{15}	1.47	C_{35}	0.69		
C_{23}	21.49	C_{16}	0.00	C_{36}	-1.62		